

Thesis

Non-Hermitian Aspect  
of  
Strongly-Correlated Electron Systems

Yoshihiro Michishita

Department of Physics, Kyoto University

January, 2022



# Abstract

Recently, studies of non-Hermitian Hamiltonians about how they change conventional phenomena have been extensively conducted, especially in the context of open systems. For example, non-Hermiticity triggers the unidirectional visibility [1–3], enhances the sensitivity[4–8], and induces unusual critical phenomena[9, 10]. On the other hand, one of the oldest works about non-Hermitian physics was done by Hatano and Nelson, in which they map the pinning problems in type-II superconductors into effective non-Hermitian Hamiltonian. Therefore, non-Hermitian physics is closely related to strongly-correlated electron materials (SCES). However, the connection between the effective non-Hermitian Hamiltonian of open systems and SCES was utterly unknown. Moreover, it is also unknown what non-Hermitian phenomena we can observe in equilibrium SCES and, of course, in non-equilibrium SCES.

Stimulated by the above situation, we elucidate the relationship between SCES and open quantum systems (OQS), and explore non-Hermitian phenomena in equilibrium and non-equilibrium SCES. Summaries of the study are shown below:

*1. Non-Hermitian Physics in strongly-correlated electron materials* [11, 12]. — In this study, we unveil the equivalence of effective non-Hermitian Hamiltonians in the context of SCES and OQS by describing the model, which is originally a SCES, as OQS. We also analyze when the non-Markovian effect in the context of OQS becomes dominant in SCES. Next, we show that the Kondo effect, which is one of the central and basic problems in SCES, can be understood from the point of view of non-Hermitian physics.

*2. Nonlinear responses in strongly-correlated electron materials* [13]. — Motivated by the recent experimental results about the nonlinear response in SCES, we analyze the correlation effect on nonlinear response in SCES. Here, we discover the non-Hermitian effect on nonlinear responses, or to say, in non-equilibrium SCES. We also elucidate that the renormalization effect of mass and the non-Hermitian effect greatly enhance the nonlinear responses.



# Contents

<b>Abstract</b>	<b>i</b>
<b>List of publications</b>	<b>v</b>
<b>1 Introduction</b>	<b>1</b>
1.1 How to introduce the effective non-Hermitian Hamiltonian . . . . .	2
1.2 Unique properties of non-Hermitian matrix . . . . .	8
1.3 Unique phenomena in non-Hermitian system . . . . .	13
1.4 Motivation of this thesis . . . . .	15
1.5 Organization of this thesis . . . . .	15
<b>2 Equivalence of the effective non-hermitian Hamiltonians in the context of open quantum systems and strongly-correlated electron systems</b>	<b>17</b>
2.1 Quantum Master equation for the Hubbard model . . . . .	17
2.2 Dynamics of the Hubbard model in the quantum Master equation . . . . .	22
2.3 Quantum master equation in the periodic Anderson model . . . . .	24
2.4 Dynamics of the PAM in the quantum Master equation . . . . .	25
<b>3 The relationship between the nonhermitian property and the Kondo effect in <math>f</math>-electron materials</b>	<b>29</b>
3.1 Models and Non-Hermitian properties in SCES . . . . .	30
3.2 Relation between Kondo temperature and $T_{EP}$ in $f$ -electron materials . . . . .	34
3.3 Extension of the exceptional manifolds to $\omega$ -space . . . . .	36
<b>4 Effects of renormalization and non-Hermiticity on nonlinear responses in strongly-correlated electron systems</b>	<b>41</b>
4.1 Background . . . . .	41
4.2 Nonlinear response using the Green function method . . . . .	43
4.3 Diagrammatic formalism for nonlinear response at finite temperature . . . . .	46
4.4 Models used in this Chapter . . . . .	49
4.5 Difficulties describing dissipation effects in the reduced density matrix formalism .	50

4.6	Extension of the reduced density matrix formalism to interacting system . . . . .	56
4.7	Correlation effects on the nonlinear response . . . . .	58
<b>5</b>	<b>Conclusion</b>	<b>65</b>
<b>A</b>	<b>Appendix for the Chapter.2</b>	<b>69</b>
A.1	Correspondence between the perturbation approach in Nakajima-Zwanzig equation and the diagram approach in the Green function method . . . . .	69
A.2	Self-energy in density matrix representation . . . . .	71
A.3	Spectral function in the case of larger system . . . . .	72
A.4	Spectral function in the steady state of open quantum systems . . . . .	73
<b>B</b>	<b>Appendix for the Chapter.3</b>	<b>77</b>
B.1	definition of the vorticity in momentum-frequency space . . . . .	77
<b>C</b>	<b>Appendix for the Chapter.4</b>	<b>79</b>
C.1	Derivation of the Matsubara formalism . . . . .	79
C.2	Analytic continuation of the nonlinear response function . . . . .	80
C.3	DC-limit . . . . .	83
C.4	Weak-scattering limit in the Green's function method . . . . .	86
C.5	Semi-classical Boltzmann equation . . . . .	87
C.6	Details of the numerical calculations . . . . .	90
C.7	Proof that $\gamma_{NH} \geq 1$ . . . . .	91
	<b>Bibliography</b>	<b>93</b>
	<b>Acknowledgment</b>	<b>100</b>

# List of publications

## Papers related to the thesis

1. Yoshihiro Michishita, Tsuneya Yoshida, and Robert Peters,  
*Relationship between exceptional points and the Kondo effect in  $f$ -electron materials*,  
Physical Review B **101**, 085122 (2020).  
© 2020 American Physical Society
2. Yoshihiro Michishita and Robert Peters,  
*Equivalence of effective non-Hermitian Hamiltonian in the context of open quantum systems  
and strongly-correlated electron systems*,  
Physical Review Letters **124**, 196401 (2020).  
© 2020 American Physical Society
3. Yoshihiro Michishita and Robert Peters,  
*Effects of renormalization and non-Hermiticity on nonlinear responses in strongly-correlated  
electron systems*,  
Physical Review B **103**, 195133 (2021).  
© 2021 American Physical Society

## Published papers not included in the thesis

1. Akira Kofuji, Yoshihiro Michishita and Robert Peters,  
*Effects of strong correlation on the nonlinear response in Weyl-Kondo semimetals*,  
Physical Review B **104**, 085151 (2021).  
© 2021 American Physical Society





# Chapter 1

## Introduction

Interaction creates the nonlinearity of systems, materials, and the world and gives scale-interference and mode-coupling. The scale-interference and the mode-coupling show the decadent behavior of materials and the world, depending on the time-scale, length-scale, and temperature. Due to the limit of human capability or computer power, we cannot understand the whole behavior of interacting many-body systems, which has many modes coupling with each other. However, we can effectively understand its behavior by focusing on a few dominant modes on a certain scale. The unfocused modes behave as noise or dissipation, giving fluctuations to the focused modes. When the dominant modes change, the critical phenomena emerge, and the fluctuations become large.

In strongly-correlated electron systems (SCES), the modes, or to say, the various freedoms, such as orbitals, spins, and phonons, interfere with each other and show us the rich phases and functionality. Due to the nonlinearity, in SCES, the phases, functionality, and dominant modes change depending on temperature and become versatile. On the other hand, many-body systems with nonlinearity also highly enlarge the Hilbert space of the system, which practically cannot be block-diagonalized, and annoys theoretical researchers due to its ridiculous complexity. However, by using a kind of contraction, such as tracing out into the single-particle Hilbert space or time-scale separation, or using perturbation treatment in an appropriate frame, we can understand much of the rich phases in SCES. One of the most common ways to understand the physics of SCES is the single-particle Green functions. The single-particle Green functions fragmentarily hold the information of the original nonlinearity through the self-energy. The frequency dependence of self-energy represents the memory effect of the traced-out modes or the difficulty to separate the time-scale between the focused modes and the traced-out modes. Self-energy also holds non-Hermiticity, which represents the dissipation of the focused modes, and it is also the vestiges of the original nonlinearity.

The physics induced by the effective Hamiltonian including non-Hermiticity is now paid a lot of attention, especially in open systems, such as cold atoms[9, 15–17], photonic crystals[1–8, 18–25], mechanical systems[26], electrical circuits[27–29], and active matters[30–33]. In open systems, we trace out the bath which holds large Hilbert space and dissipations, and therefore the system which

holds the reduced Hilbert space has the non-Hermiticity. Non-Hermiticity triggers the unidirectional visibility[1–3], enhances the sensitivity[4–8], and induces unusual critical phenomena[9, 10]. On the other hand, one of the oldest works about non-Hermitian physics was done by Hatano and Nelson[34, 35], in which they map the pinning problems in type-II superconductors into effective non-Hermitian Hamiltonian. Moreover, the origin of the recent intensive studies on non-Hermitian physics is the work by H. Shen and L. Fu, which originally tried to approach the topological phase transition at finite temperature in SCES. Therefore non-Hermitian physics is closely related to strongly-correlated electron materials (SCES). However, the connection between the effective non-Hermitian Hamiltonian of open systems and of SCES was completely unknown. Moreover, it is also unknown what is the non-Hermitian phenomena we can observe both in equilibrium SCES and , of course in non-equilibrium SCES.

In this thesis, we first prove that the equivalence of the effective non-Hermitian Hamiltonian in the context of OQS and SCES. Then we show that the Kondo effect seems related to the emergence of exceptional points at the Fermi surface. Finally, we analyze the non-Hermitian effect on the nonlinear conductivity in SCES. We show the example for the non-Hermitian phenomena in equilibrium SCES and in non-equilibrium SCES.

In the following, we briefly explain how we can derive the non-Hermitian Hamiltonian in open systems. (Sec. 1.1). Then we introduce the linear algebra about the non-Hermitian matrices and the notion of exceptional points, which is unique in non-Hermitian matrices. (Sec. 1.2). Finally the organization of this thesis is represented in Sec. 1.5.

## 1.1 How to introduce the effective non-Hermitian Hamiltonian

In this section, we explain how the effective non-Hermitian Hamiltonian is introduced especially in OQS.

### 1.1.1 Open quantum systems

An open system is a system that holds gain and(or) loss of particles and energy and has the bath, which is unfocused and coupled to the system. All of the phenomena we see in this world are the phenomena of the open system because we cannot see everything in the world, and this truth demonstrates the importance of open systems. We first introduce the Nakajima-Zwanzig equation in open quantum systems[36–39] and derive the quantum master equation and the Lindblad equation under some approximation.[40, 41] Here, we review the exact master equation of the dynamics of open quantum systems by using the projection operator  $\mathcal{P}$  and  $\mathcal{Q}$ .  $\mathcal{P}$  is the projection operator on the Hilbert space, where the system and the bath are disentangled,  $\mathcal{P}\rho = \text{tr}_B[\rho] \otimes \rho_B = \rho_S \otimes \rho_B$ , and  $\mathcal{Q} = 1 - \mathcal{P}$ . We consider the total system which is an isolated system and includes the system

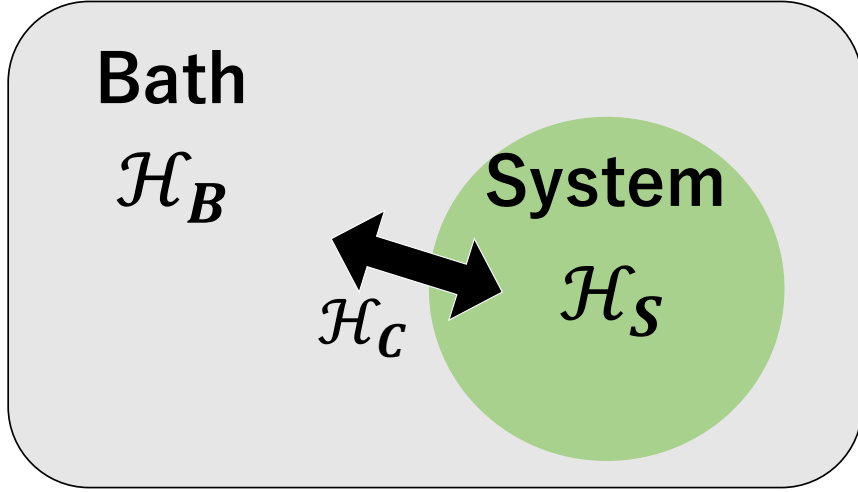


Figure 1.1: Schematic picture of open quantum systems.

and the bath. We can describes as

$$\mathcal{H}_{tot} = \mathcal{H}_S + \mathcal{H}_B + \mathcal{H}_c \quad (1.1.1)$$

$$\mathcal{H}_S = \sum_{\alpha} \epsilon_{\alpha} \mathcal{S}_{\alpha}^{\dagger} \mathcal{S}_{\alpha} \quad (1.1.2)$$

$$\mathcal{H}_B = \sum_{\beta} \epsilon_{\beta} \mathcal{B}_{\beta}^{\dagger} \mathcal{B}_{\beta} \quad (1.1.3)$$

$$\mathcal{H}_c = \sum_{\alpha\beta} \lambda_{\alpha\beta} (\mathcal{S}_{\alpha}^{\dagger} \mathcal{B}_{\beta} + h.c.), \quad (1.1.4)$$

where  $\mathcal{S}_{\alpha}^{(\dagger)}$  are the operators acting on the system and  $\mathcal{B}_{\beta}^{(\dagger)}$  are the operators acting on the bath.

We suppose that the odd moments of the system-bath coupling,  $\mathcal{H}_c$ , which describes the coupling between bath and system, vanish. This assumption is justified when the bath operator in the system-bath coupling changes the particle number or the energy of the bath, because the bath is under equilibrium and the odd moment of the system-bath coupling, which changes the bath state, becomes zero. Thus,

$$\text{tr}_B \left[ \underbrace{\mathcal{H}_c^I(t_1) \dots \mathcal{H}_c^I(t_{2n+1})}_{\text{odd power}} \rho_B^I \right] = 0, \quad (1.1.5)$$

where  $\mathcal{O}^I(t) = \exp[i(\mathcal{H}_S \otimes \mathcal{H}_B)t] \mathcal{O} \exp[-i(\mathcal{H}_S \otimes \mathcal{H}_B)t]$  is the interaction representation. We usually suppose the bath is under the thermal equilibrium, which results in  $\rho_B^I(t) = \rho_B$ . Eq. (1.1.5) leads to the relation

$$\mathcal{P} \mathcal{L}(t_1) \dots \mathcal{L}(t_{2n+1}) \mathcal{P} = 0, \quad (1.1.6)$$

where

$$\mathcal{L}(t_n)\rho = -i[\mathcal{H}_c^I(t_n), \rho]. \quad (1.1.7)$$

The dynamics of the disentangled system and its complement can be written as

$$\frac{\partial}{\partial t}\mathcal{P}\rho(t) = \mathcal{P}\frac{\partial}{\partial t}\rho(t) = \mathcal{P}\mathcal{L}(t)(\mathcal{P} + \mathcal{Q})\rho(t), \quad (1.1.8)$$

$$\frac{\partial}{\partial t}\mathcal{Q}\rho(t) = \mathcal{Q}\frac{\partial}{\partial t}\rho(t) = \mathcal{Q}\mathcal{L}(t)(\mathcal{P} + \mathcal{Q})\rho(t). \quad (1.1.9)$$

Using Eq. (1.1.8), Eq. (1.1.9), and Eq. (1.1.6), we can derive

$$\mathcal{Q}\rho(t) = \mathcal{Q}\rho(t_0) + \int_{t_0}^t ds \mathcal{Q}\mathcal{L}(s)(\mathcal{P} + \mathcal{Q})\rho(s) \quad (1.1.10)$$

$$= \mathcal{Q}\rho(t_0) + \int_{t_0}^t ds \mathcal{Q}\mathcal{L}(s)\mathcal{Q}\rho(t_0) \quad (1.1.11)$$

$$+ \int_{t_0}^t ds \mathcal{Q}\mathcal{L}(s)\mathcal{P}\rho(s)$$

$$+ \int_{t_0}^t dt_1 \mathcal{Q}\mathcal{L}(t_1) \int_{t_0}^{t_1} dt_2 \mathcal{Q}\mathcal{L}(t_2)(\mathcal{P} + \mathcal{Q})\rho(t_2)$$

$$= \mathcal{G}(t, t_0)\mathcal{Q}\rho(t_0) + \int_{t_0}^t ds \mathcal{G}(t, s)\mathcal{Q}\mathcal{L}(s)\mathcal{P}\rho(s),$$

where we introduce the forward propagator

$$\mathcal{G}(t, s) = \text{T exp} \left[ \int_s^t ds' \mathcal{Q}\mathcal{L}(s') \right]. \quad (1.1.12)$$

T describes the chronological time ordering. By inserting Eq.(1.1.11) into Eq.(1.1.8), we can derive the dynamics of the system, which reads

$$\frac{\partial}{\partial t}\mathcal{P}\rho(t) = \mathcal{I}(t, t_0)\mathcal{Q}\rho(t_0) + \int_{t_0}^t ds \mathcal{K}(t, s)\mathcal{P}\rho(s) \quad (1.1.13)$$

$$\mathcal{I}(t, t_0) = \mathcal{P}\mathcal{L}(t)\mathcal{G}(t, t_0)\mathcal{Q} \quad (1.1.14)$$

$$\mathcal{K}(t, s) = \mathcal{P}\mathcal{L}(t)\mathcal{G}(t, s)\mathcal{Q}\mathcal{L}(s)\mathcal{P}. \quad (1.1.15)$$

Eq.(1.1.13) is the exact quantum Master equation by using the projection operator, which is known as Nakajima-Zwanzig equation.[36–39]

The first term in Eq. (1.1.13) disappears when we assume that the system and the bath are not entangled in the initial state. When the system-bath coupling  $\mathcal{H}_c$  is enough smaller than  $\mathcal{H}_S$ , it is enough to consider up to the second-order of  $\mathcal{L}$  and then we can derive the quantum Master equation,

$$\frac{\partial}{\partial t}\rho_S^I(t) = - \int_{t_0}^t d\text{str}_B \left[ \mathcal{H}_c^I(t), [\mathcal{H}_c^I(s), \rho_S^I(s) \otimes \rho_B] \right], \quad (1.1.16)$$

Furthermore, if we approximate  $\mathcal{P}\rho(s) \rightarrow \mathcal{P}\rho(t)$  in Eq. (1.1.13), the dynamics of the system is determined only by the current state of the system, which is known as the Markov approximation. The Markov approximation is justified in the limit where the relaxation of the system is much slower than the relaxation of the bath and the memory of the bath does not matter in the focused time scale of the system. This limit is realized when the system-bath coupling is enough small or in the long-time limit when the system almost reaches the steady state. Therefore, we usually take the long-time limit  $t_0 \rightarrow -\infty$  in the Markov approximation. Then, we can get the Redfield master equation[39], which is written as,

$$\frac{\partial}{\partial t} \rho_S^I(t) \simeq - \int_{-\infty}^t d\text{str}_B \left[ \mathcal{H}_c^I(t), [\mathcal{H}_c^I(s), \rho_S^I(t) \otimes \rho_B] \right] \quad (1.1.17)$$

$$= - \int_0^{\infty} d\tau \text{tr}_B \left[ \mathcal{H}_c^I(t), [\mathcal{H}_c^I(t - \tau), \rho_S^I(t) \otimes \rho_B] \right] \quad (1.1.18)$$

$$= - \int_0^{\infty} d\tau \sum_{\alpha\beta} \left\{ C_{\alpha\beta}(\tau) [S_\alpha^I(t), S_\beta^I(t - \tau) \rho_S^I(t)] - C_{\alpha\beta}^*(\tau) [S_\alpha^I(t), \rho_S^I(t) S_\beta^I(t - \tau)] \right\}, \quad (1.1.19)$$

$$\frac{\partial}{\partial t} \rho_S(t) \simeq -i[\mathcal{H}_S, \rho_S(t)] - \sum_{\alpha} \left[ S_\alpha^I, (\Lambda_\alpha \rho_S(t) - \rho_S(t) \Lambda_\alpha^\dagger) \right], \quad (1.1.20)$$

where

$$C_{\alpha\beta}(\tau) = \text{tr}_B [B_\alpha^I(t) B_\beta^I(t - \tau) \rho_B] \quad (1.1.21)$$

$$\Lambda_\alpha = \int_0^{\infty} d\tau C_{\alpha\beta}(\tau) S_\beta^I(-\tau). \quad (1.1.22)$$

By using the eigenstate of the system Hamiltonian  $\mathcal{H}_S |n\rangle_S = \epsilon_n |n\rangle_S$ , we can rewrite Eq.(1.1.19) as follows:

$$\frac{\partial}{\partial t} \rho_{S;mn}^I(t) = -i\epsilon_{mn} \rho_{S;mn}^I(t) - \sum_{pq} \mathcal{R}_{mn;pq} \rho_{S;pq}^I(t) \quad (1.1.23)$$

$$\Leftrightarrow \frac{\partial}{\partial t} \rho_{S;mn}^I(t) = - \sum_{pq} \mathcal{R}_{mn;pq} \exp[-i(\epsilon_{mn} - \epsilon_{pq})t] \rho_{S;pq}^I(t) \quad (1.1.24)$$

$$\Rightarrow \rho_{S;mn}^I(t) \simeq \rho_{S;mn}^I(0) - \sum_{pq} \mathcal{R}_{mn;pq} \frac{\exp[-i(\epsilon_{mn} - \epsilon_{pq})t] - 1}{i(\epsilon_{mn} - \epsilon_{pq})} \rho_{S;pq}^I(t), \quad (1.1.25)$$

where  $\epsilon_{nm} = \epsilon_n - \epsilon_m$ . We note that  $\mathcal{R}_{mn;pq}$  can be derived by describing Eq. (1.1.20) in the eigenstate of the system Hamiltonian. The approximation in Eq.(1.1.25) is justified when  $\mathcal{R}$  (system-bath coupling) is small. The second term in Eq.(1.1.25) becomes large when  $\epsilon_{mn} = \epsilon_{pq}$  and therefore we can just focus on  $m = p, n = q$  and  $m = n, p = q$ , which is called as "the secular approximation" ,

and we can write the equation in the Lindblad master equation form as[39],

$$\frac{\partial}{\partial t}\rho_S(t) \simeq -i[\mathcal{H}_S, \rho_S(t)] - \frac{1}{2} \sum_m \gamma_m \left( \{\mathcal{S}_m^\dagger \mathcal{S}_m, \rho_S(t)\} - 2\mathcal{S}_m \rho_S(t) \mathcal{S}_m^\dagger \right). \quad (1.1.26)$$

$$= -i(\mathcal{H}_{eff} \rho_S(t) - \rho_S(t) \mathcal{H}_{eff}^\dagger) + \sum_m \gamma_m \mathcal{S}_m \rho_S(t) \mathcal{S}_m^\dagger, \quad (1.1.27)$$

where  $\gamma_m$  is the strength of dissipation. In this form, the second term in Eq.(1.1.26) is the dissipation and the third term is gain and loss. In Eq.(1.1.27), except for the second term, the dynamics of the density matrix can be described by the effective non-Hermitian Hamiltonian  $\mathcal{H}_{eff} = \mathcal{H}_S - i \sum_m \gamma_m \mathcal{L}_m^\dagger \mathcal{L}_m$ . One prescription to describe the dynamics with the effective non-Hermitian Hamiltonian is postselection.[42] In postselection, we do the measurement on the bath and just focus on the particular results. In the context of non-Hermitian physics, we usually measure the number of particle of the bath and focus on the results in which the number does not change during the dynamics. In this case, the projection operator effectively act on the system in which the number of particle does not change during the dynamics because the number of particle in the total system is conserved. This procedure can be described by a projection operator as follows:

$$\rho_S \rightarrow \rho'_S = \mathcal{P}_M \rho_S \mathcal{P}_M / \text{tr}[\mathcal{P}_M \rho_S \mathcal{P}_M] \quad (1.1.28)$$

where  $\rho_S$  is the density matrix of the system and  $\mathcal{P}_M$  is the projection operator on the result of the measurement,  $M$ . The dynamics of the projected density matrix of the system under postselection becomes

$$\rho'_S(t + \delta t) = \rho'_S(t) - i \left( H'_{eff} \rho'_S(t) - \rho'_S(t) H'_{eff}{}^\dagger \right) \quad (1.1.29)$$

$$- \sum_m \gamma_m \mathcal{L}'_m \rho'_S(t) \mathcal{L}'_m{}^\dagger \quad (1.1.30)$$

$$\rho'_S(t + \delta t) = \mathcal{P}_N \rho_S(t + \delta t) \mathcal{P}_N / \text{tr}[\mathcal{P}_N \rho_S \mathcal{P}_N] \quad (1.1.31)$$

$$O' = \mathcal{P}_N O \mathcal{P}_M. \quad (1.1.32)$$

where  $O$  is an arbitrary operator acting on the system,  $N$  is the measurement result at the time  $t + \delta t$ , and  $\gamma_m \mathcal{L}'_m \rho'_S(t) \mathcal{L}'_m{}^\dagger$  describes the gain or loss, resulting in a change of the particle number of the system. When the repeated measurement of the system is performed in a way so that we only focus on the results where the particle number of the system does not change, the gain and loss modes disappear due to the projection operators. Thus, the dynamics of the open quantum system under postselection is described by an effective non-Hermitian Hamiltonian.

## 1.1.2 Other open systems

In this subsection, we introduce the effective non-Hermitian matrix describing the dynamics in several system.

- Photonics

In photonics systems, such as photonic crystal systems, the light (the photon) is sometimes scattered out of the crystal, which can be thought as loss. (gain is also possible.) The effect of loss(gain) can be taken into account as the complexity of refractive index  $n$  in the Maxwell equation.[43, 44] After that, by considering the propagating equation as a kind of Schrödinger equation, we can derive the effective non-Hermitian Hamiltonian which describes the mode of the light in photonic crystal.[1–8, 18–25]

- Mechanical systems

In mechanical systems, the friction behaves as the loss. We can construct the Schrödinger-like equation by focusing on the dynamics of the state vector  $\Psi(t) = (p(t), q(t))$ , where  $p(t)$  is the momentum and  $q(t)$  is the position. At this time, the matrix describing the dynamics of  $\Psi(t)$  becomes a non-Hermitian matrix due to the friction.[26, 45, 46] We note that, in this procedure, the effective non-Hermitian matrix has the emergent chiral symmetry due to the relation  $dq(t)/dt = p(t)$ .[26]

- Active matters

Active matters are the physics of the particles who have self-propelled force( and usually interact with each other). Because the self-propelled force is a kind of gain of energy, active matters is also a kind of open system. The dynamics of active matters are often analyzed with the Toner-Tu equation.[47–50] Although this equation is a non-linear equation, we can linearize it near the steady state[47] and the dynamics near the steady state is described by an effective non-Hermitian matrix.[30, 32]

### 1.1.3 Strongly-correlated electron systems

In SCES, we usually understand the physics through the behavior of a single-particle in an effective potential describing the many-body interacting system. This philosophy is represented in a self-energy in the single-particle Green function in SCES. Actually, the single-particle Green functions determine the measurable physics in SCES. For examples, the imaginary part of the (retarded) Green functions is the spectral function and can be measured by the angular-resolved photo-emission spectroscopy(ARPES). Furthermore, we can calculate the response function by using the Green functions when ignoring the vertex corrections, such as the magnetic susceptibility and conductivity, which are also measurable quantities. Therefore, under some approximation, the physics of strongly-correlated electron systems can be understood through the single-particle Green function.

Moreover, the single-particle Green function  $G^R(\omega, \mathbf{k}) = 1/(\omega - (\mathcal{H}_0(\mathbf{k}) + \Sigma^R(\omega, \mathbf{k})))$ , where  $\mathcal{H}_0$  is the non-interacting Hamiltonian and  $\Sigma^R(\omega, \mathbf{k})$  is the retarded self-energy, is described by the effective Hamiltonian,  $\mathcal{H}_{ef}^R(\omega, \mathbf{k}) = \mathcal{H}_0(\mathbf{k}) + \Sigma^R(\omega, \mathbf{k})$ , which is non-Hermitian because the

self-energy is usually non-Hermitian due to electron-electron, electron-phonon, impurity scattering and so on. [51–54]

## 1.2 Unique properties of non-Hermitian matrix

In this section, we explain the difference of the matrix properties from the conventional Hermitian case. Important thing is that the left and right eigenvectors are different and they themselves are non-orthogonal, and there can be non-diagonalizable points, which are called “exceptional point.”

### 1.2.1 Spectral decomposition of non-Hermitian matrices

Here we focus on the generic square matrices with complex entries,  $\hat{M} \in \mathbb{C}^{n \times n}$ . Eigenvectors and eigenvalues satisfies the following equation as:

$$\hat{M}\mathbf{v} = \omega\mathbf{v} \Leftrightarrow (\omega\hat{1} - \hat{M})\mathbf{v} = 0 \quad (1.2.1)$$

where  $\hat{1}$  is the unit matrix  $\hat{1} = \underbrace{diag(1, 1, \dots, 1)}_n$ ,  $\omega$  is an eigenvalue and  $\mathbf{v} \in \mathbb{C}^n$  is an eigenvector.

Therefore, all the possible eigenvalues can be determined from the characteristic polynomial,

$$p_M(\omega) \equiv \det(\omega\hat{1} - \hat{M}) = 0. \quad (1.2.2)$$

It is known that, by using the eigenvalues, we can decompose  $p_M(\omega)$  into

$$p_M(\omega) = \prod_{j=1}^J (\omega - \omega_j)^{m_j^a}, \quad (1.2.3)$$

where  $\omega_j \neq \omega_{j'}$  for  $j \neq j'$  and  $m_j^a$  is called “algebraic multiplicities”, which represent the multiplicity of the eigenvalues and satisfies  $\sum_j m_j^a = n$ .

We also consider the eigenspace of  $\hat{M}$ , which can be defined as

$$V_M(\omega_j) \equiv Ker(\hat{M} - \omega_j\hat{1}) \equiv span\{\mathbf{v}_j : \hat{M}\mathbf{v}_j = \omega_j\mathbf{v}_j, \mathbf{v}_j \in \mathbb{C}^n\}. \quad (1.2.4)$$

Then its dimension  $m_j^g \equiv dimV_M(\omega_j)$  is called “geometric multiplicity” and satisfies  $m_j^g \leq m_j^a$ . If  $M$  is Hermitian,  $m_j^g = m_j^a$  is satisfied which is equivalent to that  $\hat{M}$  can be diagonalized with  $\{\mathbf{v}_j\}$ . On the other hand, if  $M$  is non-Hermitian, it is not ensured. For example, let us consider the following  $2 \times 2$  matrix as,

$$\hat{M} = \begin{pmatrix} \omega & 1 \\ 0 & \omega \end{pmatrix}. \quad (1.2.5)$$

This matrix has the degenerate eigenvalue  $\omega$ , and the eigenvectors are also doubly degenerate because  $V_M(\omega) \equiv Ker(\hat{M} - \omega\hat{1}) = (1, 0)^T$ . In this case,  $m_j^g = 1 < m_j^a = 2$ , and  $M$  cannot be



diagonalized.  $M$  is called  $2 \times 2$  ‘‘Jordan block’’. We can also generalize Jordan block to arbitrary  $n(\geq 1)$  as,

$$\hat{J}_n(\omega) = \begin{pmatrix} \omega & 1 & 0 & \dots & \dots & 0 \\ 0 & \omega & 1 & 0 & \dots & 0 \\ 0 & 0 & \omega & 1 & \dots & 0 \\ \vdots & \vdots & \vdots & \ddots & \vdots & \vdots \\ 0 & 0 & \dots & \dots & \omega & 1 \\ 0 & 0 & \dots & \dots & \dots & \omega \end{pmatrix}_{n \times n}. \quad (1.2.6)$$

$\hat{J}_n(\omega)$  has the  $n$ -th degenerate eigenvalue  $\omega$  and the eigenvector is also  $n$  times degenerate because  $V_M(\omega) \equiv \text{Ker}(\hat{J}_n(\omega) - \omega \hat{1}) = (1, 0, \dots, 0)^T$ . It is known that an arbitrary square matrix  $\hat{M} \in \mathbb{C}^{n \times n}$  can be transformed by using an invertible matrix  $\hat{X} \in \mathbb{C}^{n \times n}$  into ‘‘Jordan normal form’’, which is the direct sum of the Jordan block as,

$$\hat{X}^{-1} \hat{M} \hat{X} = \begin{pmatrix} \hat{J}_{k_1, 1}(\omega_1) & & O \\ & \ddots & \\ O & & \hat{J}_{k_J, m_J^g}(\omega_J) \end{pmatrix}_{n \times n}, \quad (1.2.7)$$

where  $\sum_{j=1}^J \sum_{p=1}^{m_j^g} k_{j,p} = n$  is satisfied. We note that we can uniquely determine  $\hat{X}$  and Jordan normal form in Eq.(1.2.7) except for the order of the Jordan blocks. By decomposing the Jordan blocks into the diagonal part and non-diagonal part as

$$\hat{J}_{k_j, p}(\omega_j) = \omega_j \hat{1}_{k_j, p} + \hat{J}'_{k_j, p}, \quad (1.2.8)$$

where  $(\hat{J}'_{k_j, p})_{ab} = \delta_{a, b-1}$ . Therefore we finally obtain the spectral decomposition of matrix  $\hat{M}$  as,

$$\hat{X}^{-1} \hat{M} \hat{X} = \hat{D} + \hat{N}, \quad \hat{D} = \bigoplus_{j=1}^J \bigoplus_{p=1}^{m_j^g} \omega_j \hat{1}_{k_j, p}, \quad \hat{N} = \bigoplus_{j=1}^J \bigoplus_{p=1}^{m_j^g} \hat{J}'_{k_j, p} \quad (1.2.9)$$

$$\Leftrightarrow \hat{M} = \hat{D}' + \hat{N}', \quad \hat{D}' = \bigoplus_{j=1}^J \bigoplus_{p=1}^{m_j^g} \omega_j \hat{P}_{k_j, p}, \quad \hat{N}' = \bigoplus_{j=1}^J \bigoplus_{p=1}^{m_j^g} \hat{N}_{k_j, p} \quad (1.2.10)$$

$$\hat{P}_{k_j, p} = \hat{X} \hat{1}_{k_j, p} \hat{X}^{-1}, \quad \hat{N}_{k_j, p} = \hat{X} \hat{J}'_{k_j, p} \hat{X}^{-1}. \quad (1.2.11)$$

We can also easily derive the following relations as

$$\hat{P}_{k_j, p} \hat{P}_{k_j, p'} = \delta_{j, j'} \delta_{p, p'} \hat{P}_{k_j, p}, \quad \hat{N}_{k_j, p} \hat{P}_{k_j, p'} = \hat{P}_{k_j, p'} \hat{N}_{k_j, p} = \delta_{j, j'} \delta_{p, p'} \hat{N}_{k_j, p} \quad (1.2.12)$$

$$\hat{N}_{k_j, p}^{(k_j, p-1)} \neq 0, \quad \hat{N}_{k_j, p}^{k_j, p} = 0. \quad (1.2.13)$$

Eq.(1.2.12) represent that  $\hat{P}$  is the projection operator and Eq.(1.2.13) shows  $\hat{N}$  is a nilpotent.

## 1.2.2 Function of non-Hermitian matrix

After the spectral decomposition, we easily calculate the polynomial of matrix, because it almost behaves as  $c$ -number on its eigenvectors. When the matrix can be diagonalized, it completely behaves as  $c$ -number on its eigenvectors, while the things become a bit complicated when the Jordan normal form holds Jordan blocks  $J_n(\omega)$  ( $n \geq 2$ ).

First, we consider a general complex analytic function  $f(z)$ . Its Taylor expansion is

$$f(z) = \sum_{l=0}^{\infty} c_l z^l. \quad (1.2.14)$$

Then we can get  $f(\hat{M})$  by utilizing the spectral decomposition as,

$$f(\hat{M}) = \sum_{j=1}^J \left( f(\omega_j) \hat{P}_j + \sum_{p=1}^{m_j^s} \sum_{l=1}^{k_{j,p}-1} \frac{f^{(l)}(\omega_j)}{l!} \hat{N}_{j,p}^l \right), \quad (1.2.15)$$

where  $\hat{P}_j = \sum_{p=1}^{m_j^s} \hat{P}_{k_{j,p}}$  and  $f^{(l)}(z) = d^l f(z)/dz^l$ . Especially we are interested in the case  $f(z) = e^{zt}$ , because it appears when we consider the time evolution of the system as  $d\mathbf{v}(t)/dt = \hat{M}\mathbf{v} \Rightarrow \mathbf{v}(t) = e^{\hat{M}t}\mathbf{v}(0)$ . In that case, remembering  $f^{(l)}(z) = t^l e^{zt}$ , we can obtain,

$$\exp[\hat{M}t] = \sum_{j=1}^J \exp[\omega_j t] \left( \hat{P}_j + \sum_{p=1}^{m_j^s} \sum_{l=1}^{k_{j,p}-1} \frac{t^l (\omega_j)}{l!} \hat{N}_{j,p}^l \right). \quad (1.2.16)$$

This results tell us that when a non-Hermitian Hamiltonian cannot be diagonalized, which means its Jordan normal form include Jordan blocks  $J_n(\omega)$  ( $n \geq 2$ ), the dynamics hold the linear-time growth represented in the second term in Eq.(1.2.16).

## 1.2.3 Eigenvectors of non-Hermitian matrices

In this subsection, we consider the properties of eigenvectors of general non-Hermitian matrices, especially about non-orthogonality, and introduce the notion of left and right eigenvectors. First, we check the orthogonality of eigenvectors of Hermitian matrix. When there are two eigenvector with the different eigenvalues as  $\hat{M}\mathbf{v}_j = \omega_j \mathbf{v}_j$ ,  $\hat{M}\mathbf{v}_{j'} = \omega_{j'} \mathbf{v}_{j'}$ ,  $\omega_j \neq \omega_{j'}$ , then  $\mathbf{v}_{j'}^\dagger \mathbf{v}_j = 0$ . This is because

$$\mathbf{v}_{j'}^\dagger \hat{M} \mathbf{v}_j = \omega_j \mathbf{v}_{j'}^\dagger \mathbf{v}_j = \omega_{j'} \mathbf{v}_{j'}^\dagger \mathbf{v}_j \Rightarrow (\omega_j - \omega_{j'}) \mathbf{v}_{j'}^\dagger \mathbf{v}_j = 0, \quad (1.2.17)$$

where we used the Hermiticity of  $\hat{M}$  as  $\mathbf{v}_{j'}^\dagger \hat{M} = (\hat{M}^\dagger \mathbf{v}_{j'})^\dagger = (\hat{M} \mathbf{v}_{j'})^\dagger = \omega_{j'} \mathbf{v}_{j'}^\dagger$ . Moreover, even if two eigenvectors have the same eigenvalue and they are not orthogonal as  $\omega_j = \omega_{j'} (\mathbf{v}_j \neq \mathbf{v}_{j'})$ ,  $\mathbf{v}_{j'}^\dagger \mathbf{v}_j = a (|a| < 1)$ , we can construct the new orthogonal basis  $\mathbf{v}'_{j'} = (\mathbf{v}_{j'} - a^* \mathbf{v}_j) / |\mathbf{v}_{j'} - a^* \mathbf{v}_j|$ , which satisfies

$\hat{M}\mathbf{v}'_{j'} = \omega_{j'}\mathbf{v}'_{j'}$ ,  $\mathbf{v}'_{j'}\mathbf{v}_j = 0$ . Therefore, in the Hermitian case, we can construct a orthogonal basis using the eigenvectors of  $\hat{M}$ .

On the other hand, when  $\hat{M}$  is non-Hermitian, we need to define the left eigenvectors to construct the orthogonal basis. It means we need also the eigenvectors of  $\hat{M}^\dagger$  as,

$$\hat{M}\tilde{\mathbf{v}}_j = \omega_j^*\tilde{\mathbf{v}}_j \Leftrightarrow \tilde{\mathbf{v}}_j^\dagger\hat{M} = \omega_j\tilde{\mathbf{v}}_j^\dagger\hat{M}^\dagger. \quad (1.2.18)$$

By using this left eigenvectors, we can construct non-Hermitian version in Eq.(1.2.17) as,

$$\tilde{\mathbf{v}}_j^\dagger\hat{M}\mathbf{v}_j = \omega_j\tilde{\mathbf{v}}_j^\dagger\mathbf{v}_j = \omega_{j'}\tilde{\mathbf{v}}_j^\dagger\mathbf{v}_j \Rightarrow (\omega_j - \omega_{j'})\tilde{\mathbf{v}}_j^\dagger\mathbf{v}_j = 0. \quad (1.2.19)$$

Then we can derive  $\tilde{\mathbf{v}}_j^\dagger\mathbf{v}_j = 0$  for  $\omega_j \neq \omega_{j'}$  cases, and for  $\omega_j = \omega_{j'}$  by using the same procedure as for the Hermitian case. We usually call  $\tilde{\mathbf{v}}_j$  as a left eigenvector and  $\mathbf{v}_j$  as a right eigenvector in non-Hermitian case. We note that, in general  $\tilde{\mathbf{v}}_j \neq \mathbf{v}_j$  while they are same in a Hermitian case. Here we construct the orthogonality with left and right eigenvectors, which is called ‘‘biorthogonality’’.

By using biorthogonal basis, we can concretely construct the spectral decomposition in Eq.(1.2.10) as,

$$\hat{M} = \sum_{j=1}^J \sum_{p=1}^{m_j^s} \left( \omega_j \sum_{l=1}^{k_{j,p}} \mathbf{r}_{jpl} \mathbf{l}_{jpl}^\dagger + \sum_{l=1}^{k_{j,p}-1} \mathbf{r}_{jpl} \mathbf{l}_{jpl}^\dagger \right), \quad (1.2.20)$$

where  $\mathbf{r}_{jpl}(\mathbf{l}_{jpl})$  is the right (left) eigenvector of  $\hat{M}$  for  $l = 1$  and otherwise it is not the eigenvector but it satisfies the orthogonality  $\mathbf{l}_{jpl}^\dagger \mathbf{r}_{j'p'l'} = \delta_{j,j'}\delta_{p,p'}\delta_{l,l'}$ , which is called as  $l$ -th generalized eigenvector in the  $p$ -th Jordan block with eigenvalue  $\omega_j$ . We note that in general  $\{\mathbf{r}_{jpl}\}(\{\mathbf{l}_{jpl}\})$  themselves are not orthogonal which means  $\mathbf{r}_{jpl}^\dagger \mathbf{r}_{j'p'l'} \neq \delta_{j,j'}\delta_{p,p'}\delta_{l,l'}$  ( $\mathbf{l}_{jpl}^\dagger \mathbf{l}_{j'p'l'} \neq \delta_{j,j'}\delta_{p,p'}\delta_{l,l'}$ ). We usually normalize  $\mathbf{l}_{jpl}^\dagger \mathbf{r}_{j'p'l'} = \delta_{j,j'}\delta_{p,p'}\delta_{l,l'}$  and  $\mathbf{r}_{jpl}^\dagger \mathbf{r}_{jpl} = 1$ , which means in general  $\mathbf{l}_{jpl}^\dagger \mathbf{l}_{jpl} \neq 1$  (Actually,  $\mathbf{l}_{jpl}^\dagger \mathbf{l}_{jpl} \geq 1$ ).

To the end of this subsection, we consider the resolvent of a non-Hermitian matrix. The resolvent of  $\hat{M}$  is a function  $\mathbb{C} \rightarrow \mathbb{C}^{n \times n}$  defined as,

$$\hat{R}_M(z) \equiv (z\hat{1} - \hat{M})^{-1} \quad (1.2.21)$$

By utilizing the spectral decomposition, we can derive the following expression:

$$\hat{R}_M(z) = \sum_{j=1}^J \left( \frac{\hat{P}_j}{z - \omega_j} + \sum_{p=1}^{m_j^s} \sum_{l=1}^{k_{j,p}-1} \frac{N_{jp}^l}{(z - \omega_j)^{l+1}} \right). \quad (1.2.22)$$

We note that we can derive inversely  $\hat{P}_j$  and  $\hat{N}_j = \sum_{p=1}^{m_j^s} \hat{N}_{jp}$  from the resolvent as,

$$\hat{P}_j = \oint_{C_j} \frac{dz}{2\pi i} \hat{R}(z), \quad \hat{N}_j = \oint_{C_j} \frac{dz}{2\pi i} (z - \omega_j) \hat{R}(z) \quad (1.2.23)$$

### 1.2.4 Exceptional points

Finally, we consider the non-Hermitian matrix on the parameter space. Although any non-Hermitian matrix can be written in Jordan normal form, there sometimes exist singular points about the spectral and nilpotent matrix  $\hat{N}$  in the parameter space, and we call such points as ‘‘exceptional points (EPs)’’. In the context of physics, EPs usually means the points where the non-Hermitian matrix cannot be diagonalized and two or more eigenvectors are coalescent while it can be diagonalized in the other area. Let us see a simple example shown as,

$$\hat{M}(\kappa) = \begin{pmatrix} i\kappa & g \\ g & -i\kappa \end{pmatrix}. \quad (1.2.24)$$

When  $\hat{M}(\kappa)$  can be diagonalized, the spectrum and the diagonalizing matrix  $\hat{X}$  is

$$\omega_{\pm}(\kappa) = \pm\Delta(\kappa), \quad \hat{X}(\kappa) = \begin{pmatrix} i\kappa/\Delta(\kappa) & -g/\Delta(\kappa) \\ g/\Delta(\kappa) & i\kappa/\Delta(\kappa) \end{pmatrix}, \quad \hat{X}^{-1}(\kappa) = \begin{pmatrix} i\kappa/\Delta(\kappa) & g/\Delta(\kappa) \\ -g/\Delta(\kappa) & i\kappa/\Delta(\kappa) \end{pmatrix} \quad (1.2.25)$$

where  $\Delta(\kappa) = \sqrt{g^2 - \kappa^2}$ . We can see that, at  $\kappa = g$ ,  $\omega_{\pm}(\kappa)$  are degenerate and  $\hat{X}(\kappa)$  ( $\hat{X}^{-1}(\kappa)$ ) diverges. This singular point is an exceptional points of  $\hat{M}(\kappa)$ . Actually, at this exceptional point, the eigenvectors are also coalescent.

In the first example, the parameter space is one-dimensional and the exceptional manifold is zero-dimensional (point). Here we focus on the  $2 \times 2$  non-Hermitian matrix and  $n$ -dimensional parameter space  $\kappa \in \mathbb{R}^n$ . In general,  $2 \times 2$  non-Hermitian matrix can be written in the following form:

$$\hat{M}(\kappa) = \omega_0(\kappa)\hat{1} + (\mathbf{a}(\kappa) + i\mathbf{b}(\kappa)) \cdot \hat{\sigma}, \quad \omega_{\pm}(\kappa) = \pm\sqrt{(|\mathbf{a}(\kappa)|^2 - |\mathbf{b}(\kappa)|^2) + i\mathbf{a}(\kappa) \cdot \mathbf{b}(\kappa)}, \quad (1.2.26)$$

where  $\mathbf{a}(\kappa)$  and  $\mathbf{b}(\kappa)$  are the real vectors and  $\hat{\sigma} = \{\hat{\sigma}^x, \hat{\sigma}^y, \hat{\sigma}^z\}$  is the vector of the Pauli matrix, and  $\omega_{\pm}$  is the eigenvalues of  $\hat{M}$ . As in the first example, when  $\kappa$  satisfies that  $\Delta = \sqrt{(|\mathbf{a}(\kappa)|^2 - |\mathbf{b}(\kappa)|^2) + i\mathbf{a}(\kappa) \cdot \mathbf{b}(\kappa)}$  is zero, the point on the parameter space is an exceptional point. Here  $\kappa$  must satisfies two conditions, which are  $|\mathbf{a}(\kappa)|^2 - |\mathbf{b}(\kappa)|^2 = 0$  and  $\mathbf{a}(\kappa) \cdot \mathbf{b}(\kappa) = 0$ . Therefore, if there are exceptional points, exceptional points should have a  $(n - 2)$  dimensional structure.[53] However, in the first example, the exceptional point has a zero dimensional structure while the parameter space dimension is one.

The reason is symmetry. It is known that, if the non-Hermitian matrix has the pseudo-Hermiticity, the eigenvalues must be real or the pairs of pure imaginary. The pseudo-Hermiticity can be written as[55–57]

$$\hat{M}^\dagger = \hat{\eta}\hat{M}\hat{\eta}^{-1}. \quad (1.2.27)$$

For the first example, we can derive  $\hat{\eta} = \hat{\sigma}^x$  and  $\hat{M}(\kappa)$  has the pseudo-Hermiticity. In that case, the second condition for the emergence of the exceptional points, which is  $\mathbf{a}(\kappa) \cdot \mathbf{b}(\kappa) = 0$ , is always satisfied due to the pseudo-Hermiticity.

Finally, we introduce the vorticity of exceptional points in the Brillouin zone. Here we consider  $\hat{M}(\boldsymbol{\kappa})$  as a Hamiltonian and the Brillouin zone as the periodic parameter space. For the one dimensional case, we can define the vorticity as[58]

$$w(\omega) \equiv \int_{-\pi}^{\pi} \frac{dk}{2\pi i} \partial_k \ln[\det(\hat{H}(k) - \omega \hat{1})]. \quad (1.2.28)$$

When we set  $\omega$  as the degenerate eigenvalue at an exceptional point, the vorticity can be non-zero. For the one dimensional case, it was shown that when the Hamiltonian has the time-reversal symmetry and the vorticity is nonzero, there is a skin effect, which means that eigenvectors and spectrum strongly depend on the boundary condition.

On the other hand, for the two dimensional case, the vorticity is usually defined as[51]

$$v(\omega) \equiv \oint_C \frac{d\mathbf{k}}{2\pi i} \cdot \nabla_{\mathbf{k}} \ln[\det(\hat{H}(\mathbf{k}) - \omega \hat{1})]. \quad (1.2.29)$$

We note that the phenomena related to this vorticity in two dimension has not been found yet while the vorticity is related to the skin effect in one dimension.[59, 60]

## 1.3 Unique phenomena in non-Hermitian system

In this section, we introduce several unique phenomena in non-Hermitian systems. Most phenomena are related to the exceptional points, and the other phenomena are usually related to the non-orthogonality of right and left eigenvectors themselves.

### 1.3.1 Phenomena related to exceptional points

Exceptional points have two distinct properties. One is the singular dispersion around exceptional points and the other is the coalescence of the eigenvectors. First, we list up the phenomena which stem from the singular dispersion, and then the phenomena which originate from the coalescence of the eigenvectors.

#### *Phenomena related to the singular dispersion at exceptional points*

- Enhancement of the sensitivity

For example, around the exceptional point of the matrix  $\hat{M}$  in Eq.(1.2.24), the eigenvalues are  $E_{\pm}(\kappa = g - \delta\kappa) = \pm\sqrt{2g\delta\kappa - \delta\kappa^2} \simeq \pm\sqrt{2g\delta\kappa}$ . Therefore, near the exceptional points, the eigenvalue has the square-root dependence of  $\delta\kappa$ . This square-root dispersion is unique near exceptional points, and gives the higher sensitivity to  $\delta\kappa$  than the linear dispersion. This sensitivity enhancement can be utilized for a micro-cavity sensor that detects nanometre-scale particles. The existence of nanometre-scale particles gives a small perturbation (as  $\delta\kappa$ ) to

the micro-cavity, resulting in the frequency splitting of the micro-cavity that can be detected. The square-root dispersion results in larger frequency splitting for a small perturbation and realizes the higher sensitivity. We note that, in general, around at  $n$ -fold exceptional points,  $(\delta\kappa)^{1/n}$  can be realized, and higher sensitivity is possible as  $n$  is large.[4–8] We note that, in general, around at  $n$ -fold exceptional points,  $(\delta\kappa)^{1/n}$  can be realized and higher sensitivity is possible as  $n$  is large.

*Phenomena related to the coalescence of eigenvectors at exceptional points*

- unidirectional transparent

When we consider the Bragg scatterer and solve the Helmholtz equation, the relation between the forward and backward light at one site and those at the other side can be described by the non-Hermitian Hamiltonian. At the exceptional points where the Hamiltonian is described by the size-2 Jordan block, the Hamiltonian becomes a triangular matrix, and therefore, reflectivity is completely asymmetric. This results in unidirectional transparency.[1, 3]

- asymmetric mode switching

Let us consider a periodically modulated two-mode waveguide. The dynamics of the two-mode light in the dissipative waveguide can be described by the two by two non-Hermitian matrix. Because of the space modulation of the waveguide, this non-Hermitian matrix depends on the position, which is equivalent to the non-Hermitian matrix depending on time for the light propagating in the waveguide. If the non-Hermitian matrix effectively and slowly changes in time, the modes of light also slowly change. When the parameter of the non-Hermitian matrix moves around the exceptional points in time evolution, the final state is only determined by the circling direction (clockwise or anti-clockwise) and independent from the initial state. Therefore, by changing the direction in which we insert the light, the circling direction changes, and the mode of the output light can be switched. [2]

*phenomena related to the non-orthogonality*

- slowing down of thermalization

When an open quantum system is described by the Lindblad equation and the steady state is the thermalized state, the relaxation time to the thermalized state is conventionally believed to be proportional to  $1/g$ , where  $g$  is the first Liouvillian gap which means the eigenvalue of the slowest relaxation mode. However, recently, it was shown that the relaxation time is not only decided by the first Liouvillian gap but also by the non-Hermitian factor  $\gamma_n^{NH} = \langle n_L | n_L \rangle \langle n_R | n_R \rangle / |\langle n_L | n_R \rangle|^2$ , which represents the non-orthogonality of left and right eigenvectors themselves.  $|n_R\rangle$  ( $|n_L\rangle$ ) is the  $n$ -th right (left) eigenvector of the Lindblad

dynamics.[61, 62] We note that the Lindblad equation can be described by the effective non-Hermitian matrix in the doubled-Hilbert space where the density matrix is considered as a vector.[63–66]

## 1.4 Motivation of this thesis

In 2019, when we started to study non-Hermitian physics, the non-Hermitian physics in strongly-correlated electron systems was poorly understood, and I had two questions:

- While the unique phenomena related to exceptional points and non-orthogonality were found in photonics systems, such phenomena had not been found in the condensed matter physics. Are there phenomena related to the unique properties of non-Hermitian matrices in strongly-correlated electron systems?
- The relationship between the effective non-Hermitian Hamiltonian in open quantum system and in strongly-correlated electron systems was not clear. Are they related or not? Moreover, the condition to derive the effective non-Hermitian Hamiltonian is also different in each context. Why is the postselection not necessary in strongly-correlated electron systems?

These two questions are the motivation of our works in my Ph.D course.

## 1.5 Organization of this thesis

In this thesis, we elucidate the relationship between the effective non-Hermitian Hamiltonian in open quantum systems and strongly-correlated electron systems and search for phenomena related to exceptional points and non-Hermiticity in strongly-correlated electron systems. In Chapter 2, we describe the Hubbard model, which is initially the model of strongly-correlated electron systems and is closed a system, as an open quantum system, and then derive the effective non-Hermitian Hamiltonian (NHH) in the context of open quantum systems. By performing this procedure, we elucidate the equivalence of the effective NHH in strongly-correlated electron systems and open quantum systems and why post-selection is not necessary to derive an effective NHH in the context of SCES. We also check the importance of non-Markovianity in the dynamics of SCES. In Chapter 3, we consider the Kondo crossover in  $f$ -electron materials from the non-Hermitian point of view. We give a simple picture of the Kondo crossover with eigenvalues of the effective NHH and numerically show that the temperature at which exceptional points emerge at the Fermi surface is closely related to the Kondo temperature. Moreover, we point out that the emergence of exceptional points at the Fermi surface corresponds to the topological change of the exceptional manifolds in the frequency space. In Chapter 4, we construct the Green function formalism for the nonlinear response and analyze the interaction effects: the renormalization effect and the dissipation (non-Hermitian) effect.

We show that the renormalization effect enhances the nonlinear response much more as it is the higher-order response. Moreover, we construct the non-Hermitian band index for analyzing the (non)linear response under the dissipation and show that the non-Hermiticity effectively enhances lifetime and the new terms that stem from the non-orthogonality of the effective NHH.



# Chapter 2

## Equivalence of the effective non-hermitian Hamiltonians in the context of open quantum systems and strongly-correlated electron systems

In this Chapter, we prove that the equivalence of the effective non-Hermitian Hamiltonian in the context of open quantum systems and strongly-correlated electron systems. We demonstrate that the NHH describing the Green function is equal to the NHH describing a single particle coupled to the rest of particles acting as a bath under postselection. For this purpose, we analyze the dynamics of a single particle in the Hubbard model using the quantum master equation (QME) in the context of OQS. The equivalence of the NHH in the single-particle spectral function and in the QME makes it possible to study non-Hermitian phenomena in OQS by analyzing certain response functions without applied postselection. Our analysis furthermore reveals why postselection is not necessary to observe non-Hermitian phenomena in the context of single-particle Green functions.

### 2.1 Quantum Master equation for the Hubbard model

First, we derive the QME for the dynamics of a single particle in a strongly correlated material. Furthermore, we demonstrate that the effective NHH in the context of OQS under postselection corresponds to that in the single-particle Green function in the context of SCES. We here use the Hubbard model as a prototypical model describing SCES. In order to derive the effective NHH in the Hubbard model in the context of OQS, we divide the degrees of freedom into a system, describing a single particle,  $(\mathbf{k}_0, \sigma)$ , at momentum  $\mathbf{k}_0$  in spin-state  $\sigma$ , and a bath, which includes the rest of the electrons, see Fig. 2.1. Thus, the total Hubbard Hamiltonian is divided into the Hamiltonian of the system,  $\mathcal{H}_S$ , the Hamiltonian of the bath,  $\mathcal{H}_B$ , and the coupling between system and bath,  $\mathcal{H}_C$ . The

Hamiltonian becomes

$$\mathcal{H}_{tot} = \sum_{\mathbf{k}, \sigma} (\epsilon_{\mathbf{k}} + \mu_c) c_{\mathbf{k}\sigma}^\dagger c_{\mathbf{k}\sigma} + U \sum_i n_{i\uparrow} n_{i\downarrow} \quad (2.1.1)$$

$$= \mathcal{H}_S + \mathcal{H}_B + \mathcal{H}_c \quad (2.1.2)$$

$$\mathcal{H}_S = (\epsilon_{\mathbf{k}_0} + \mu_c + U n_{\bar{\sigma}}) c_{\mathbf{k}_0\sigma}^\dagger c_{\mathbf{k}_0\sigma} = \xi c_{\mathbf{k}_0\sigma}^\dagger c_{\mathbf{k}_0\sigma} \quad (2.1.3)$$

$$\mathcal{H}_B = \sum_{(\mathbf{k}, \sigma') \neq (\mathbf{k}_0, \sigma)} (\epsilon_{\mathbf{k}} + \mu_c) c_{\mathbf{k}\sigma'}^\dagger c_{\mathbf{k}\sigma'} \quad (2.1.4)$$

$$+ \frac{U}{N} \sum_{\sigma'} \sum_{\substack{\mathbf{k}_1, \mathbf{k}_2, \\ \mathbf{k}_3, \mathbf{k}_4 \\ \neq (\mathbf{k}_0, \sigma)}} \delta_{\mathbf{k}_1 + \mathbf{k}_3, \mathbf{k}_2 + \mathbf{k}_4} c_{\mathbf{k}_1\sigma'}^\dagger c_{\mathbf{k}_2\sigma'} c_{\mathbf{k}_3\bar{\sigma}'}^\dagger c_{\mathbf{k}_4\bar{\sigma}'}$$

$$\begin{aligned} \mathcal{H}_c &= \frac{U}{N} \sum_{\substack{\mathbf{k}_1, \mathbf{k}_2, \mathbf{k}_3 \\ \neq \mathbf{k}_0}} \delta_{\mathbf{k}_1 + \mathbf{k}_3, \mathbf{k}_0 + \mathbf{k}_2} \left( c_{\mathbf{k}_0\sigma}^\dagger c_{\mathbf{k}_1\sigma} c_{\mathbf{k}_2\bar{\sigma}}^\dagger c_{\mathbf{k}_3\bar{\sigma}} + h.c. \right) \\ &= \frac{U}{N} \left( C_\sigma^\dagger \otimes \mathcal{B}_\sigma + h.c. \right) \end{aligned} \quad (2.1.5)$$

$$C_\sigma = c_{\mathbf{k}_0\sigma} \quad (2.1.6)$$

$$\mathcal{B}_\sigma = \sum_{\substack{\mathbf{k}_1, \mathbf{k}_2, \mathbf{k}_3 \\ \neq \mathbf{k}_0}} \delta_{\mathbf{k}_1 + \mathbf{k}_3, \mathbf{k}_0 + \mathbf{k}_2} c_{\mathbf{k}_1\sigma} c_{\mathbf{k}_2\bar{\sigma}}^\dagger c_{\mathbf{k}_3\bar{\sigma}}, \quad (2.1.7)$$

where  $c_{\mathbf{k}\sigma}^{(\dagger)}$  is an annihilation(creation) operator of an electron in momentum  $\mathbf{k}$  and spin-direction  $\sigma$ .  $\epsilon_{\mathbf{k}}$  is the energy dispersion,  $\mu_c$  is the chemical potential,  $U$  is the Hubbard interaction, and  $N$  is the number of the lattice sites. Note that the coupling between the system and the bath corresponds to a part of the two-particle interaction and  $n_{\bar{\sigma}}$  behaves as the constant because it is the conservative quantity while it is originally the bath operator.

Starting from the von Neumann equation for the density matrix of the full system,  $\frac{d}{dt}\rho(t) = -i[H, \rho(t)]$ , we derive the QME for the density matrix of the system in second-order perturbation in  $\mathcal{H}_c$  as written in Eq.(1.1.16). Here  $\rho_S^I(t)$  is the density matrix of the system, i.e. the single particle.

The commutators in Eq. (1.1.16) include terms such as<sup>1</sup>

$$\begin{aligned} &C_\sigma^\dagger C_\sigma \rho_S(s) \otimes \text{Tr}_B \left[ \mathcal{B}_\sigma(t) \mathcal{B}_\sigma^\dagger(s) \rho_B \right] \\ &= C_\sigma^\dagger C_\sigma \rho_S(s) \otimes \text{Tr}_B \left[ \sum_{\mathbf{k}_1, \mathbf{k}_2, \mathbf{k}_3} \delta_{\mathbf{k}_1 + \mathbf{k}_3, \mathbf{k}_0 + \mathbf{k}_2} c_{\mathbf{k}_1\sigma}(t) c_{\mathbf{k}_2\bar{\sigma}}^\dagger(t) c_{\mathbf{k}_3\bar{\sigma}}(t) c_{\mathbf{k}_3\bar{\sigma}}^\dagger(s) c_{\mathbf{k}_2\bar{\sigma}}(s) c_{\mathbf{k}_1\sigma}^\dagger(s) \rho_B \right]. \end{aligned} \quad (2.1.8)$$

This trace over three creation and three annihilation operators including the time evolution by the full Hamiltonian, only missing the scattering via  $(\mathbf{k}_0, \sigma)$ , appears in the second-order diagram for the self-energy shown in Fig. 2.2.

<sup>1</sup>The detailed derivation is written in Appendix. A.

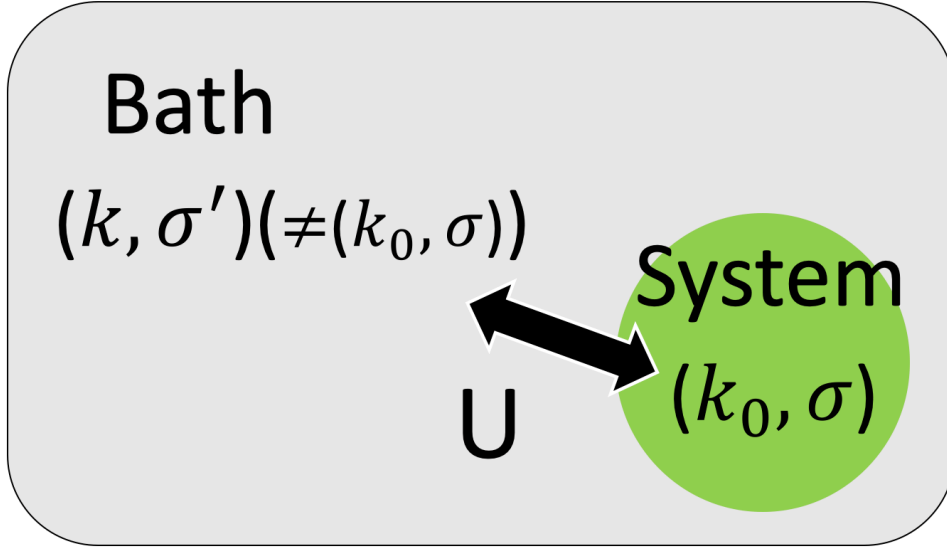


Figure 2.1: To derive an effective non-Hermitian Hamiltonian for the single-particle dynamics in the Hubbard model in the context of OQS, we divide the electrons into a system, including only one particle, and the rest of the particles, acting as bath.

Because the amplitude of a single scattering process via  $\mathbf{k}_0$  vanishes in the limit of an infinite large bath,  $N \rightarrow \infty$ , the self-energy shown in Fig. 2.2 becomes the exact self-energy in second-order perturbation in  $\mathcal{H}_c$  (not  $U$ ). Even when considering higher-order perturbations in  $\mathcal{H}_c$ , we find that the QME still can be described by the self-energy<sup>2</sup>. Collecting all terms in Eq.(1.1.16), we obtain

$$\begin{aligned}
\frac{\partial}{\partial t} \rho_S^I(t) = & \int_{t_0}^t ds \left[ -i\text{Re}(S_l(t-s)) [C_\sigma^\dagger C_\sigma, \rho_S^I(s)] + i\text{Re}(S_g(t-s)) [C_\sigma C_\sigma^\dagger, \rho_S^I(s)] \right. \\
& + \text{Im}(S_l(t-s)) \left( \{C_\sigma^\dagger C_\sigma, \rho_S^I(s)\} - 2C_\sigma \rho_S^I(s) C_\sigma^\dagger \right) \\
& \left. + \text{Im}(S_g(t-s)) \left( \{C_\sigma C_\sigma^\dagger, \rho_S^I(s)\} - 2C_\sigma^\dagger \rho_S^I(s) C_\sigma \right) \right] \quad (2.1.9)
\end{aligned}$$

with

$$\begin{aligned}
S_l(t) &= \Sigma_{\mathbf{k}_0}^T(t) e^{i\xi t} \\
S_g(t) &= (\Sigma_{\mathbf{k}_0}^R(t) - \Sigma_{\mathbf{k}_0}^T(t)) e^{i\xi t}
\end{aligned}$$

where  $\Sigma^T$  is the time-ordered self-energy,  $\Sigma^R$  is the retarded self-energy, and  $\xi = \epsilon_{\mathbf{k}_0} + \mu_c + U n_{\bar{\sigma}}$ .

<sup>2</sup>See Appendix. A for (i) brief explanation about the postselection; (ii) detail explanation for the reason why the quantum master equation can be described by the self-energy; (iii) proof that the gain and loss contribution to the Green function disappears in general open quantum systems; (iv) correspondence of the effective non-Hermitian Hamiltonians in the context of open quantum systems and strongly-correlated systems in the periodic Anderson model, which includes Refs. [11, 39]

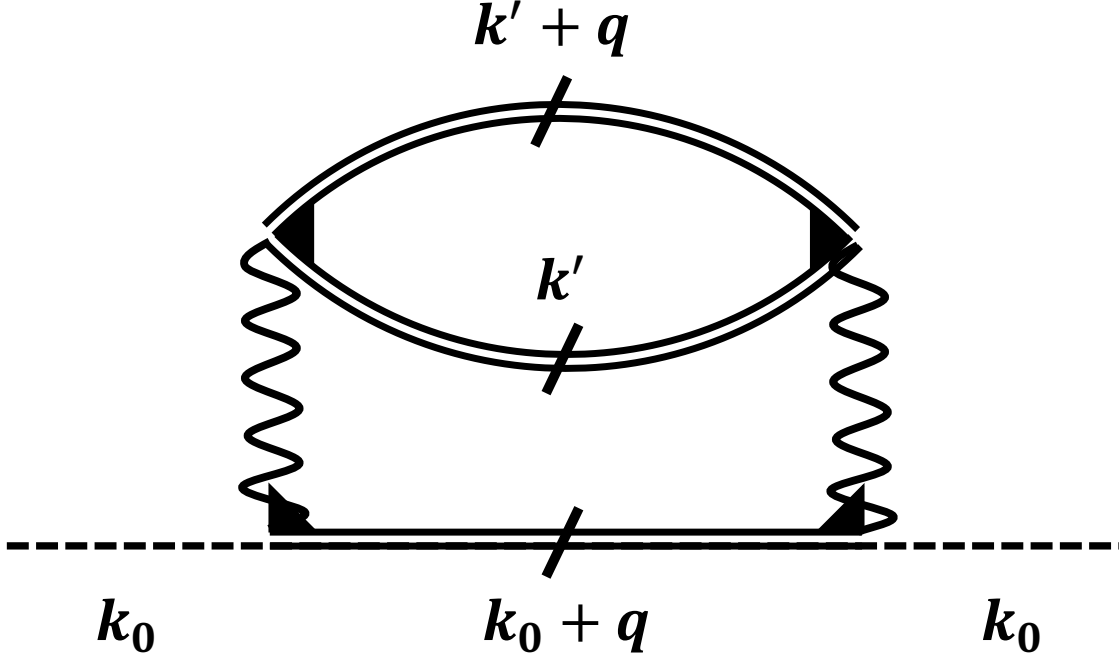


Figure 2.2: Feynman diagram which describes the dynamics of the QME in second-order. The slashed double lines correspond to full Green function which do not include the scattering to  $\mathbf{k}_0$ . The black triangle corresponds to the full two-particle vertex, which does not include scattering via  $\mathbf{k}_0$ .

We see that the time-evolution of the density-matrix of a single particle at  $(\mathbf{k}_0, \sigma)$  is governed by the self-energy  $\Sigma_{\mathbf{k}_0}^{R/T}(s)$ . However, because Eq. (2.1.9) includes gain and loss terms, i.e.  $2C_\sigma \rho_S^I(s) C_\sigma^\dagger$  and  $2C_\sigma^\dagger \rho_S^I(s) C_\sigma$ , the dynamics cannot be described by an effective NHH alone.

We next fix the particle number of the system, which corresponds to applying postselection. We restrict the Hilbert space to states where  $c_{\mathbf{k}_0\sigma}^\dagger c_{\mathbf{k}_0\sigma} + c_{\mathbf{k}_0\bar{\sigma}}^\dagger c_{\mathbf{k}_0\bar{\sigma}} = 1$ . We furthermore assume the absence of magnetism, which results in  $c_{\mathbf{k}_0\sigma}^\dagger c_{\mathbf{k}_0\sigma} = c_{\mathbf{k}_0\sigma} c_{\mathbf{k}_0\sigma}^\dagger$  in the restricted Hilbert space. Due to these restrictions, the gain and loss terms vanish in Eq. (2.1.9), and the commutators and anticommutators can be summed up

$$\frac{\partial}{\partial t} \rho_S^{I PS}(t) = -i \int_{t_0}^t ds \left( \mathcal{S}_{eff}(t-s) \rho_S^{I PS}(s) - \rho_S^{I PS}(s) \mathcal{S}_{eff}^\dagger(t-s) \right) \quad (2.1.10)$$

$$\mathcal{S}_{eff}(t-s) = \Sigma_{\mathbf{k}_0}^R(t-s) e^{i\xi(t-s)} c_{\mathbf{k}_0\sigma}^\dagger c_{\mathbf{k}_0\sigma}, \quad (2.1.11)$$

where  $\rho_S^{(I) PS}(t)$  is the density matrix with applied postselection. By using the Markov approximation, which means  $\rho_S(s) \rightarrow \rho_S(t)$  and  $t_0 \rightarrow -\infty$ , we find that the density matrix of a single particle

under postselection can be written as

$$\frac{\partial}{\partial t} \rho_S^{PS}(t) = -i \left( \mathcal{H}_{eff} \rho_S^{PS}(t) - \rho_S^{PS}(t) \mathcal{H}_{eff}^\dagger \right) \quad (2.1.12)$$

$$\mathcal{H}_{eff} = \mathcal{H}_0 + \sum_{\mathbf{k}_0}^R (\xi) c_{\mathbf{k}_0 \sigma}^\dagger c_{\mathbf{k}_0 \sigma}, \quad (2.1.13)$$

which corresponds to the von Neumann equation with an effective NHH. Thus, the time-evolution of the density-matrix of a single particle  $(\mathbf{k}_0, \sigma)$  is given by an effective NHH including the self-energy, if postselection is applied.<sup>3</sup> We note that the frequency dependence of the self-energy has vanished because of the Markov approximation.

However, in the context of SCES, the Green function is described by an effective NHH without postselection[11, 52, 53, 67–70]. To clarify the reason why postselection is not necessary in this context, we will now introduce the retarded Green function in the steady state using the density matrix form, which is given as  $G_{OQS}^R(t) = -i\Theta(t)\text{Tr} \left[ (C(t)C^\dagger(0) + C^\dagger(0)C(t)) \rho_S^{SS} \otimes \rho_B \right]$ . Here,  $\rho_S^{SS}$  is the density matrix of the system in the long-time limit (steady-state)<sup>4</sup> and  $C(t) = e^{i\mathcal{H}_{tot}t} C e^{-i\mathcal{H}_{tot}t}$ . Combining the density-matrix,  $\rho_S^{SS}$ , with the creation-operator,  $C^\dagger$ , we define the density-matrix describing the single-particle Green function,  $\rho_S^{RGF} = C^\dagger \rho_S^{SS} + \rho_S^{SS} C^\dagger$ . Thus, we can rewrite the Green function as

$$G_{OQS}^R(t) = -i\Theta(t)\text{Tr} [C \rho_S^{RGF}(t)],$$

where the time evolution of  $\rho_S^{RGF}(t)$  is given by the QME in Eq. (2.1.9).

When considering a system which includes only a single particle,  $(\mathbf{k}_0, \sigma)$ ,  $\rho_S^{RGF}(t)$  is given by the following matrix element,  $|\sigma\rangle \langle 0|$ , where  $|\sigma\rangle = c_{\mathbf{k}_0, \sigma}^\dagger |0\rangle$ . Gain and loss terms vanish in the time evolution for this matrix element, because  $C^\dagger |\sigma\rangle \langle 0| C = C |\sigma\rangle \langle 0| C^\dagger = 0$ . Therefore, the QME can be written as

$$\frac{\partial}{\partial t} \rho_S^{I, RGF}(t) = -i \int_{t_0}^t ds \left( \mathcal{S}_{eff}(t-s) \rho_S^{I, RGF}(s) - \rho_S^{I, RGF}(s) \mathcal{S}_{eff}^\dagger(t-s) \right) \quad (2.1.14)$$

---

<sup>3</sup>We have shown here that the dynamics of the single-particle Hilbert space is determined by the self-energy of the single-particle in the total system. The imaginary part of the effective Hamiltonian (corresponding to the imaginary part of the self-energy) is equivalent to the sum of the gain and loss terms, and it causes a decay of the norm of the density matrix,  $\rho_S^{PS}$ . This decay of the norm means that the possibility of obtaining results, in which gain or loss (electron-electron scattering) does not occur and the particle number does not change, decreases in time. Therefore, the imaginary part of the self-energy can be interpreted as the inverse of the lifetime of the quasi-particle, as it is well-known in the context of the strongly-correlated electron systems. On the other hand, the real part of the self-energy describes the correction of the energy levels due to the coupling with the bath. Thus, these kinds of two-particle interaction effects are included in the dynamics of the single-particle Hilbert space and the dynamics is determined by the self-energy.

<sup>4</sup>Because the total system is isolated, we here suppose that it reaches the equilibrium (steady-state) state. Therefore, if we consider the exact non-Markovian dynamics, the density matrix of the system is given as  $\rho_S^{SS} = \mathcal{P} \rho_{total}^{eq} \mathcal{P}$ , where  $\mathcal{P}$  is the projection operator on the Hilbert space of the system and  $\rho_{total}^{eq}$  is the density matrix of the equilibrium state of the total system.

$$\begin{aligned} \Rightarrow -i\omega\rho_S^{RGF}(\omega) - \rho_S^{RGF}(t_0) &= -i\left(\mathcal{H}_{eff}(\omega)\rho_S^{RGF}(\omega) - \rho_S^{RGF}(\omega)\mathcal{H}_{eff}^\dagger(\omega)\right) \\ &= -i\mathcal{H}_{eff}(\omega)\rho_S^{RGF}(\omega) \end{aligned} \quad (2.1.15)$$

$$\mathcal{H}_{eff}(\omega) = \mathcal{H}_0 + \sum_{\mathbf{k}_0}^R(\omega)c_{\mathbf{k}_0,\sigma}^\dagger c_{\mathbf{k}_0,\sigma}. \quad (2.1.16)$$

The equality in Eq. (2.1.15) holds because  $\rho_S^{RGF}$  is proportional to  $|\sigma\rangle\langle 0|$  and  $\rho_S^{RGF}\mathcal{H}_{eff}^\dagger$  becomes zero. Then, the Green function becomes

$$G_{OQS}^R(\omega) = -i\text{Tr}[C\rho_S^{RGF}(\omega)] = \frac{1}{\omega - \xi - \Sigma_{\mathbf{k}_0}^R(\omega)} \quad (2.1.17)$$

We here have demonstrated the following statements: First, the Green function of a single particle described as an OQS and its effective NHH is identical to the Green function and its NHH in closed equilibrium systems. Second, the dynamics of  $\rho_S^{PS}$  and  $\rho_S^{RGF}$  are described by the same equations, Eq. (2.1.10) and Eq. (2.1.14). We can conclude that the effective NHH describing the dynamics under postselection is identical to the effective NHH describing the Green function in SCES. Thus, we can analyze non-Hermitian phenomena, which are observable in OQSs under postselection, by studying the spectral function  $A(\omega) = -\frac{1}{\pi}\text{Im}G_{OQS}^R(\omega)$  in equilibrium or the nonequilibrium steady state. While postselection becomes increasingly difficult in large systems, the analysis of spectral properties remains feasible. We note that non-Hermitian properties may occur in different response functions than the single-particle spectral function and that the correspondence between the NHH in the density matrix under postselection and the NHH in the response function depends on the kind of the postselection. Third, because the density matrix describing the Green functions in the context of OQS is given by the off-diagonal matrix element, i.e.  $|\uparrow\rangle\langle 0|$ , gain and loss terms vanish in the QME, and postselection is unnecessary to derive an effective NHH. We note that, even if we consider larger systems, for example a system including  $(\mathbf{k}_0, \uparrow)$  and  $(\mathbf{k}_0, \downarrow)$ , gain and loss contributions in the QME for the Green function vanish <sup>5</sup>.

## 2.2 Dynamics of the Hubbard model in the quantum Master equation

Finally, we use the above-introduced QME to describe single-particle properties in the Hubbard model on a 2D square lattice. We furthermore show that the Markov approximation, which ignores the memory effect of the QME dynamics, fails to describe the full spectral function in the Mott phase of the Hubbard model in which non-Markovian dynamics plays an important role.

We have shown above that the time-evolution of the density matrix is determined by the self-energy in the QME. We here use the dynamical mean field theory (DMFT) combined with the numerical renormalization group (NRG) to calculate an approximate self-energy.[71–73] DMFT

---

<sup>5</sup>See the detail in Appendix.A.3

takes local fluctuations fully into account by self-consistently solving the mean field equations.[71] The lattice Hamiltonian is thereby mapped onto a quantum impurity model. DMFT neglects nonlocal fluctuations. To solve the quantum impurity model, we use the NRG, which calculates low energy properties by iteratively discarding high-energy states. It has been shown that NRG is a very reliable tool at low temperature.[72, 73]

Using the self-energy obtained by DMFT/NRG in the QME, Eq. (2.1.9), we show the relaxation dynamics of the density matrix into the steady state, and demonstrate that the spectral function calculated by the QME approach is identical with the spectral function directly obtained by DMFT/NRG.

In Fig. 2.3, we compare the spectral functions calculated by the QME and by DMFT/NRG for the weak-coupling regime (Fig. 2.3(a)) and the Mott insulator (Fig. 2.3(c)) for  $\mathbf{k}_0 = (0.4\pi, 0.4\pi)$ . We furthermore include a comparison between the QME approach using the Markov approximation and the full dynamics. In the weak-coupling regime, the spectral functions obtained by DMFT and the QME with and without Markov approximation agree with each other. Figure 2.3(b) shows the time-evolution of the diagonal elements of the density matrix with and without Markov approximation in the QME, Eq. (2.1.9). In the weak-coupling regime, memory effects are not important and therefore the Markov approximation works well. The dynamics without memory effects is given by an exponential decay as shown in Fig. 2.3(b). We conclude that the Markov approximation can describe the full dynamics of the system in the weak-coupling regime, Fig. 2.3(a-b).

In the Mott-insulating phase, shown in Fig. 2.3(c), the non-Markov spectral function does also agree with the spectral function obtained by DMFT/NRG. On the other hand, the spectral function calculated with the Markov approximation is nearly zero. In the Mott insulating regime, the Markov approximation describes strong dissipation due to the strong scattering with the bath electrons and the resulting spectral function has only a small and wide peak. We note, however, that the integral over the frequency is unity. Non-Markovian dynamics is essential to correctly describe the strongly interacting system. Both peaks in the spectral function are described by quasi-particles which follow non-Markovian dynamics. In Fig. 2.3(d), we show the dynamics of the diagonal elements of the density matrix comparing between Markovian and non-Markovian dynamics. Both approaches show a strong decay into the same steady state. Additional to the strong decay of the matrix element of the density-matrix, the non-Markovian dynamics show a strong oscillatory behavior of the occupation number.

In the next section, we perform a similar analysis for the periodic Anderson model, showing that also in this model the spectral function of a small system described as an OQS and its effective NHH are identical to the Green function and its NHH in closed equilibrium systems.

## 2.3 Quantum master equation in the periodic Anderson model

In the previous sections, we have proven in the Hubbard model that the non-Hermitian Hamiltonian describing the spectral functions is identical to the non-Hermitian Hamiltonian in the quantum master equation under postselection. Here, we extend our considerations to the periodic Anderson model(PAM) reading

$$\mathcal{H}_{\text{PAM}} = \sum_{\mathbf{k}\sigma} \left( (\epsilon_{\mathbf{k}} + \mu_c) c_{\mathbf{k}\sigma}^\dagger c_{\mathbf{k}\sigma} + (\epsilon_{f\mathbf{k}} + \mu_f) f_{\mathbf{k}\sigma}^\dagger f_{\mathbf{k}\sigma} + V(f_{\mathbf{k}\sigma}^\dagger c_{\mathbf{k}\sigma} + h.c.) \right) + U \sum_i n_{i\uparrow}^f n_{i\downarrow}^f \quad (2.3.1)$$

where  $c_{\mathbf{k}\sigma}^{(\dagger)}, f_{\mathbf{k}\sigma}^{(\dagger)}$  are annihilation (creation) operators of the  $c$ - and the  $f$ -electrons for momentum  $\mathbf{k}$  and spin-direction  $\sigma$ .  $\epsilon_{c,f}$  is the kinetic energy for the  $c$ - and the  $f$ -electrons,  $\mu_{c,f}$  the chemical potentials for the  $c$ - and  $f$ -electron band,  $V$  a local hybridization, and  $U$  a density-density interaction for the  $f$  electrons.

As in the Hubbard model, when fixing the particle number and the magnetization of the system by postselection, we find that the dynamics of the density matrix (under postselection) in the limit of  $t_0 \rightarrow -\infty$  and using the Markov approximation is given by an effective non-Hermitian Hamiltonian as

$$\frac{\partial}{\partial t} \rho_S^{PS}(t) = -i \left( \mathcal{H}_{eff} \rho_S^{PS}(t) - \rho_S^{PS}(t) \mathcal{H}_{eff}^\dagger \right) \quad (2.3.2)$$

where the effective non-Hermitian Hamiltonian is given as

$$\mathcal{H}_{eff} = \epsilon_c(\mathbf{k}_0) c_\sigma^\dagger c_\sigma + V(c_\sigma^\dagger f_\sigma + h.c.) + \left( \epsilon_f(\mathbf{k}_0) + \Sigma^R \right) f_\sigma^\dagger f_\sigma \quad (2.3.3)$$

$$\Sigma^R = \frac{\Sigma^R(\xi_+) + \Sigma^R(\xi_-)}{2} + \frac{h_1(\Sigma^R(\xi_+) - \Sigma^R(\xi_-))}{2\sqrt{h_1^2 + V^2}}. \quad (2.3.4)$$

We here have used postselection as  $(\xi_{\pm\uparrow}^\dagger \xi_{\pm\uparrow} = \xi_{\pm\downarrow}^\dagger \xi_{\pm\downarrow} = 0.5 \leftrightarrow \xi_{\pm\uparrow}^\dagger \xi_{\pm\uparrow} = \xi_{\pm\uparrow}^\dagger \xi_{\pm\uparrow}^\dagger)$  to derive Eq. (2.3.3). We suppose that the observation under postselection leads to  $\xi_{\pm\uparrow}^\dagger \xi_{\pm\uparrow} + \xi_{\pm\downarrow}^\dagger \xi_{\pm\downarrow} = 1$  and that there is no magnetization.

Here, we have derived the effective non-Hermitian Hamiltonian in the context of OQS. The dynamics is again described by the retarded self-energy. If we ignore the frequency dependence of the self-energy ( $\Sigma^R(\xi_+) = \Sigma^R(\xi_-) = \Sigma^R$ ), we see that the effective non-Hermitian Hamiltonian describing the dynamics in the quantum master equation and the effective non-Hermitian Hamiltonian of the spectral function agree with each other.

In the case of non-Markovian dynamics, the time-dependence of the self-energy must be considered, which makes an analytical comparison between the density matrix under postselection and the spectral function difficult. Therefore, we numerically compare the non-Markovian dynamics of the quantum master equation with those of the single-particle Green function calculated by the DMFT/NRG.



## 2.4 Dynamics of the PAM in the quantum Master equation

We here compare the Markovian dynamics and the non-Markovian dynamics in the PAM by numerical simulations in the metallic phase above the Kondo temperature and in the Kondo insulating phase below the Kondo temperature. We here use the self-energy as calculated by dynamical mean-field theory (DMFT) combined with the numerical renormalization group (NRG) and calculate the spectral function and the diagonal elements of the density matrix using the quantum master equation with and without Markov-approximation. Figure 2.4(a) and (c) show the spectral functions calculated by the DMFT/NRG and the spectral function calculated by the QME, where  $\mathbf{k}_0 = (0.5\pi, 0.5\pi)$ .

The spectral function calculated by the QME with non-Markovian dynamics agrees with the spectral function calculated directly from the Green function. We believe that the small discrepancies between the Green's function and the non-Markovian dynamics in Fig.2.4 are numerical errors. These numerical errors arise because of the two Fourier transformations (first, we calculate  $\Sigma(t-s)$  from  $\Sigma(\omega)$  and, second, we calculate  $G^R(\omega)$  from  $G^R(t)$ ) which is necessary to calculate  $G^R(\omega)$  and because of the finite time-interval of  $G^R(t)$ . This shows that the real time dynamics of the spectral function corresponds to the dynamics of the QME under postselection because gain and loss terms vanish in the spectral function. Therefore, the effective non-Hermitian Hamiltonian in the spectral function corresponds to the effective non-Hermitian Hamiltonian in the non-Markov QME under postselection. In Fig. 2.4(a) and (c), the spectral function by the QME using the Markov approximation in the limit of  $t_0 \rightarrow -\infty$  only includes the self-energy at  $\omega = \xi_{\pm}$  and neglects the frequency dependence of the self-energy around the Fermi energy. In this case, the effective Hamiltonian in the QME describes the scattering away from the Fermi energy. Thus, the spectral function calculated by the QME with Markov approximation includes the particle-hole excitations at  $\omega = \pm \frac{U}{2}$  but cannot describe the excitation near the Fermi energy. The peaks at high temperature in Fig. 2.4(a) are smeared out wider than those at low temperature due to the stronger scattering at high temperature.

Figures 2.4(b) and (d), show that the relaxation of the diagonal elements from the initial state  $\rho_i = \xi_{-}^{\dagger}|0\rangle\langle 0|\xi_{-}$  using Markovian and non-Markovian dynamics. In the metallic regime above the Kondo temperature, Fig. 2.4(b), these elements oscillate but are strongly damped. On the other hand, in the Kondo-insulating regime below the Kondo temperature, the oscillation persists for a long time. We believe that this change of the dynamics is related to the Kondo crossover. We note that the Markov dynamics in Fig. 2.4 does not significantly change between high-temperature metallic state and low-temperature insulating state. Therefore, we can conclude that the Kondo crossover from the metallic behavior at high temperature to the insulator at low temperature originates from the change in the non-Markovian dynamics. We note that the steady states as given by the Markovian dynamics and the non-Markovian dynamics are equivalent except for the case of the PAM above the Kondo temperature. This discrepancy might originate from the existence of exceptional manifolds in the spectral function in the case of the PAM above the Kondo temperature, as shown in [11],

while in the other cases there are no exceptional manifolds.

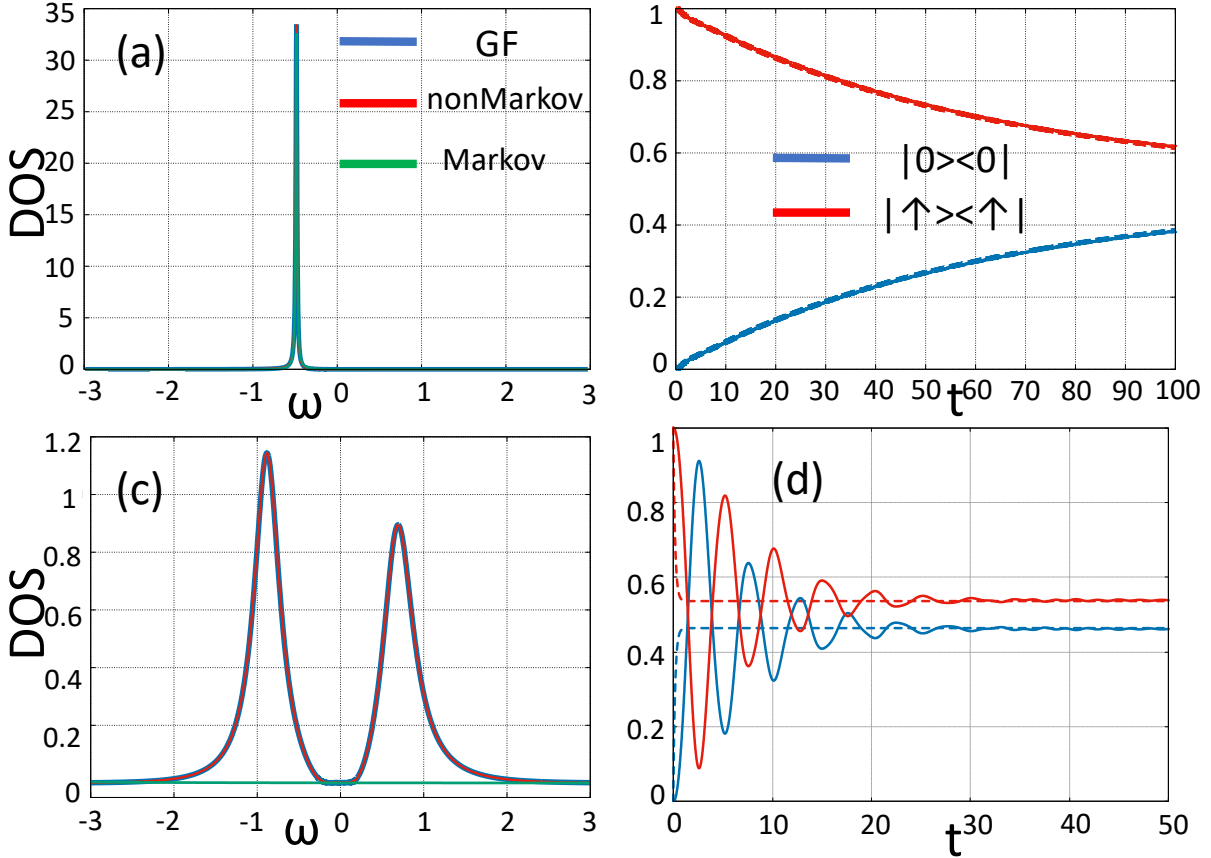


Figure 2.3: Spectral function and the time-evolution of the diagonal elements into the steady state in the weak-coupling regime and in the Mott insulating phase. The parameters in Fig. (a) and (b) are as follows:  $\epsilon_k = -0.49, \mu_c = -0.2, U = 0.4$ , and the temperature  $T = 0.001$ . The parameters in Fig. (c) and (d) are as follows;  $\epsilon_k = -0.12, t = 0.1, \mu_c = -0.8, U = 1.6, T = 0.00006$ . The blue, red and green lines in (a) and (c) show the spectral function as calculated by the Green function, non-Markov QME (Eq. (2.1.14)), and the Markov QME (Eq. (2.1.12)), respectively. The blue and the red lines in (b) and (d) show the dynamics of the diagonal elements  $|0\rangle\langle 0|$  and  $|\uparrow\rangle\langle \uparrow|$  from the initial state  $\rho_i = |\uparrow\rangle\langle \uparrow|$ . The full lines and the dashed lines correspond to the non-Markovian dynamics and the Markovian dynamics, respectively.

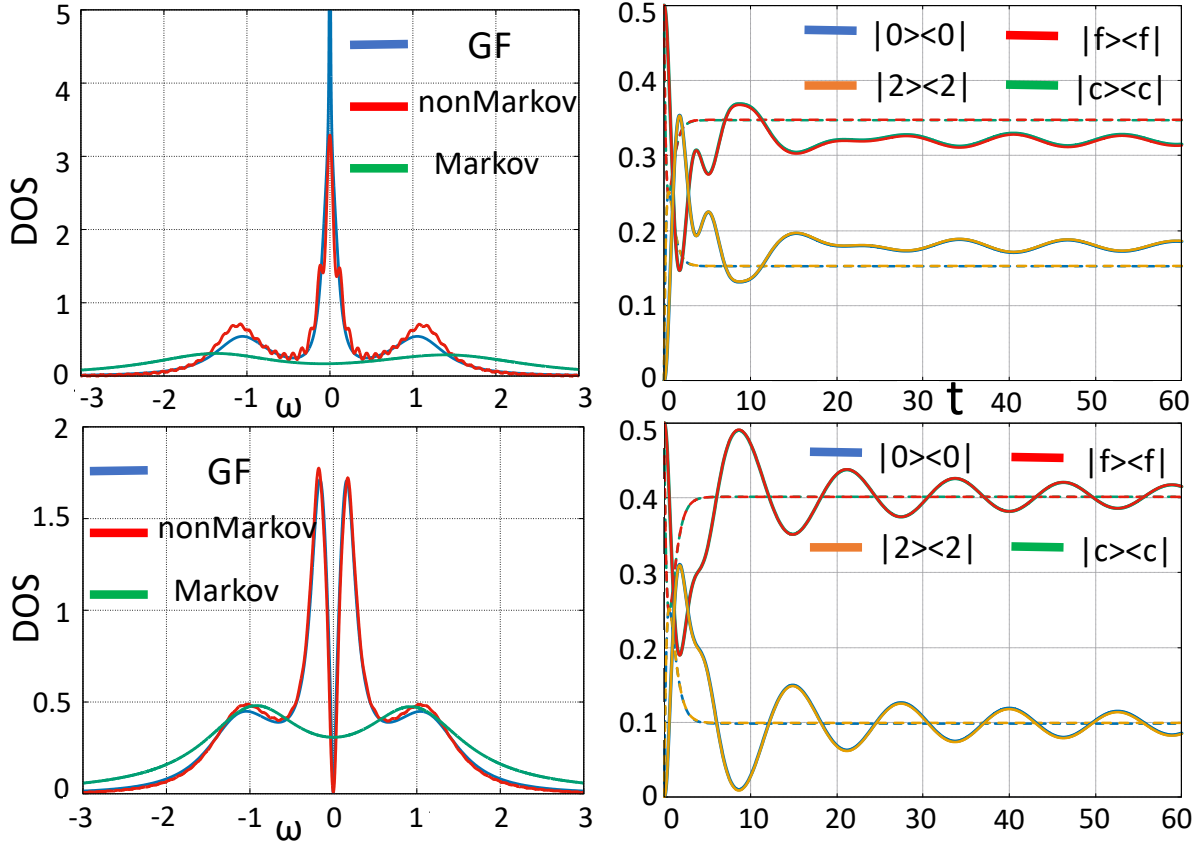


Figure 2.4: Spectral functions and matrix elements of the density matrix in the metallic regime at high temperature and the Kondo insulating phase at low temperature. The parameters in (a) and (b) are as follows:  $t_c = 1.0, t_f = -0.05, \mu_c = 0, \mu_f = -1.0, U = 2.0, V = 0.36$ , and the temperature is  $T = 0.13$ . The parameters in (c) and (d) are  $t_c = 1.0, t_f = -0.05, \mu_c = 0, \mu_f = -1.0, U = 2.0, V = 0.5$  and  $T = 0.0002$ . The blue, red and green lines in (a) and (c) show respectively the spectral functions calculated directly by the Green function, the spectral function using non-Markovian dynamics and the Markov dynamics. The dashed (full) lines in (b) and (d) show the Markovian dynamics (non-Markovian dynamics) of the diagonal elements of the density matrix from the initial state  $\rho_i = \xi_-^\dagger |0\rangle\langle 0| \xi_-$ .

## Chapter 3

# The relationship between the nonhermitian property and the Kondo effect in $f$ -electron materials

In this chapter, we study about the non-Hermitian effect of the self-energy in the Kondo regime in 2D  $f$ -electron materials by numerical calculation with DMFT/NRG. We show the relationship between the appearance of the exceptional points (or exceptional loop) and the transition from a metal to the Kondo insulator or the heavy fermions in 2D  $f$ -electron systems. This means that the appearance of the exceptional point denotes the transition of the  $f$ -electrons from the localized state to the itinerant state. Although we have found the physical phenomena relating to the exceptional points, we could not find any physical quantity or phenomena relating to their non-Hermitian topological number. This problem still remains as an open question.

The rest of this chapter is organized as follows. In Sec3.1, we introduce the models that we use in this work for 2D. Then we shortly explain about the exceptional points and their non-hermitian topological numbers in SCES. In Sec3.2, we show the numerical results by DMFT/NRG about the Kondo temperature and the temperature at which the exceptional points emerge at fermi surface for each case.

### 3.1 Models and Non-Hermitian properties in SCES

To analyze the emergence of exceptional points and the Kondo effect in  $f$ -electron materials, we use the periodic Anderson model,

$$\mathcal{H} = \sum_{\mathbf{k}} \left( (\epsilon_{\mathbf{k}} + \mu_c) c_{\mathbf{k}\sigma}^\dagger c_{\mathbf{k}\sigma} + (\epsilon_{f\mathbf{k}} + \mu_f) f_{\mathbf{k}\sigma}^\dagger f_{\mathbf{k}\sigma} + (V_{l/p})_{\sigma\sigma'} (f_{\mathbf{k}\sigma}^\dagger c_{\mathbf{k}\sigma'} + h.c.) \right) + U \sum_i n_{i\uparrow} n_{i\downarrow} \quad (3.1.1)$$

$$\epsilon_{c/f} = -2t_{c/f}(\cos k_x + \cos k_y) \quad (3.1.2)$$

$$V_l = V\delta_{\sigma\sigma'} \quad (3.1.3)$$

$$V_p = V(\boldsymbol{\sigma} \cdot \sin \mathbf{k}) \quad (\sin \mathbf{k} = (\sin k_x, \sin k_y)) \quad (3.1.4)$$

$$n_{i\sigma} = f_{i\sigma}^\dagger f_{i\sigma} \quad (3.1.5)$$

where  $c_{\mathbf{k}\sigma}^\dagger, f_{\mathbf{k}\sigma}^\dagger$  are annihilation (creation) operators of the  $c$ - and the  $f$ -electrons for momentum  $\mathbf{k}$  and spin-direction  $\sigma$ .  $t_{c,f}$  are the inter-site hopping strengths for the  $c$ - and the  $f$ -electrons. For simplicity, we assume a two-dimensional square lattice.  $\mu_{c/f}$  are the chemical potentials for the  $c$ - and  $f$ -orbitals.  $V_{l/p}$  describe a local and a nonlocal hybridization between the  $c$ - and  $f$ -orbitals, respectively. Throughout this chapter, we fix  $t_f = \pm 0.05t_c$ ,  $\mu_c = 0$ ,  $\mu_f = -1.0$ ,  $U = 2.0$  and use  $t_c = 0.8$ . Using this model, we analyze the relation between the Kondo effect and the emergence of exceptional points. We will focus on three different cases:  $t_f = -0.05t_c$  with a local hybridization ( $V_l \neq 0, V_p = 0$ ),  $t_f = 0.05t_c$  with a local hybridization ( $V_l \neq 0, V_p = 0$ ), and  $t_f = -0.05t_c$  with a  $p$ -wave hybridization ( $V_l = 0, V_p \neq 0$ ).

In Figs. 3.1 and 3.2, we show the momentum resolved spectral functions and the Fermi surfaces for all three states. At high temperature, the  $f$ -electrons are localized and do not hybridize with the  $c$ -electrons, as shown in Fig. 3.1(a) and Fig. 3.2(a). Below the Kondo temperature,  $f$ -electrons become itinerant and hybridize with the  $c$ -electrons, which results in strong changes in the spectral function. Figure 3.1(b) shows the spectral function of the Kondo insulator having a gap at the Fermi energy. Figure 3.1(c) shows the spectral function of the metallic regime with local hybridization, and Fig. 3.1(d) the spectral function of the  $p$ -wave hybridization. Corresponding to these spectral functions, we show the spectral weight at the Fermi energy in Fig. 3.2. At high temperatures, Fig. 3.2(a), we only find the  $c$  electrons at the Fermi energy. At low temperatures, all three states have very different Fermi surfaces. The Kondo insulating state, shown in Fig. 3.2(b), has no spectral weight at the Fermi energy. The heavy-Fermion state, Fig. 3.2(c), shows the Fermi surface corresponding to the metallic state. Finally, in Fig. 3.2(b), the point-like Fermi surface of the metallic state with  $p$ -wave hybridization is shown.

We employ the DMFT combined with the NRG to calculate the physical properties in these models. Even though nonlocal fluctuations might not be small in 2D systems and even crucial for the magnetic state, they might be less important for the Kondo effect and the emergence of

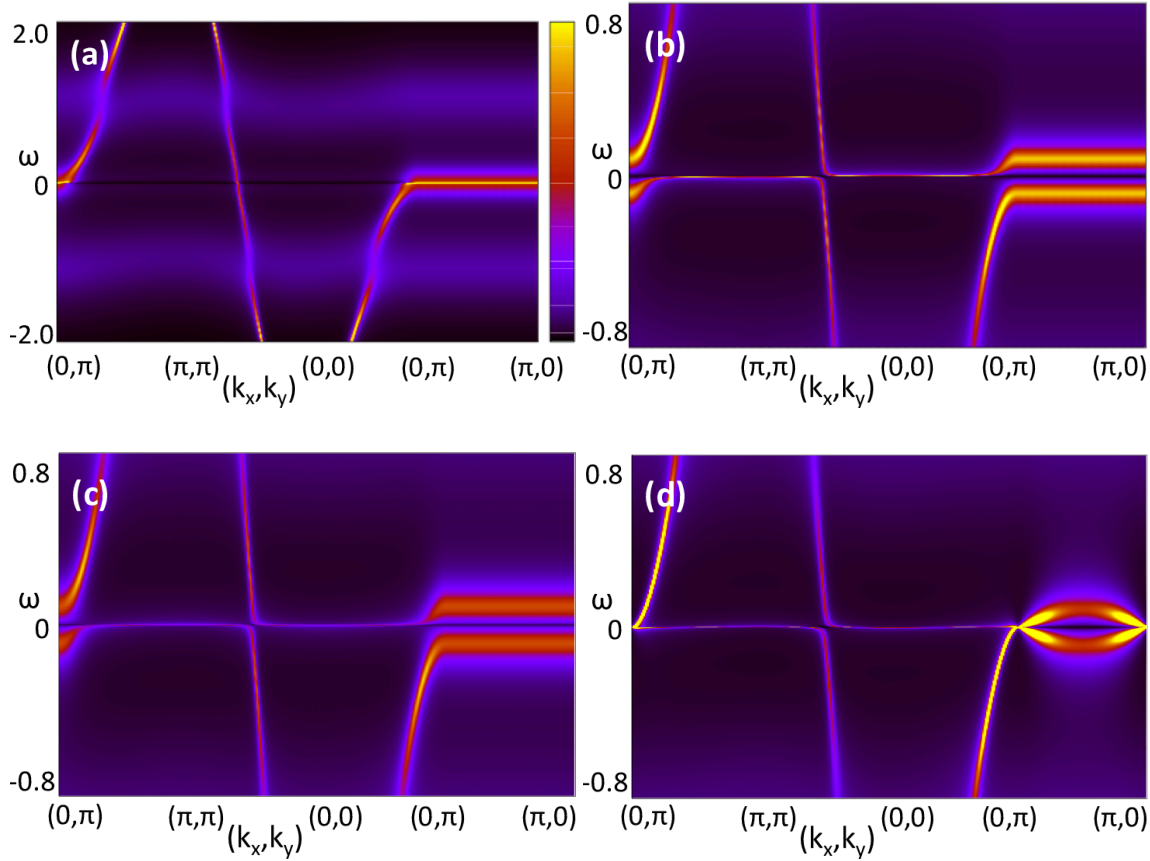


Figure 3.1: (a)-(d) : Momentum-resolved spectral functions for the Kondo insulator, the heavy-fermion state, and the metallic state with p-wave hybridization for  $V=0.4$ . Fig.3.1(a) shows a high temperature spectral function,  $T=0.13$  of the Kondo insulator. Fig.3.1(b)-(d) show spectral functions at low temperatures, for  $T=0.0005$ , for the Kondo insulator, the heavy-fermion state, and the nonlocal hybridization, respectively.

exceptional points. Furthermore, all shown results remain correct in three-dimensional systems, where nonlocal fluctuations are weaker compared to the 2D system.

Before showing the numerical results, we briefly introduce exceptional points in strongly correlated materials. As mentioned above, the periodic Anderson model is one of the minimal model for the emergence of the exceptional points. The effective non-Hermitian Hamiltonian which describes

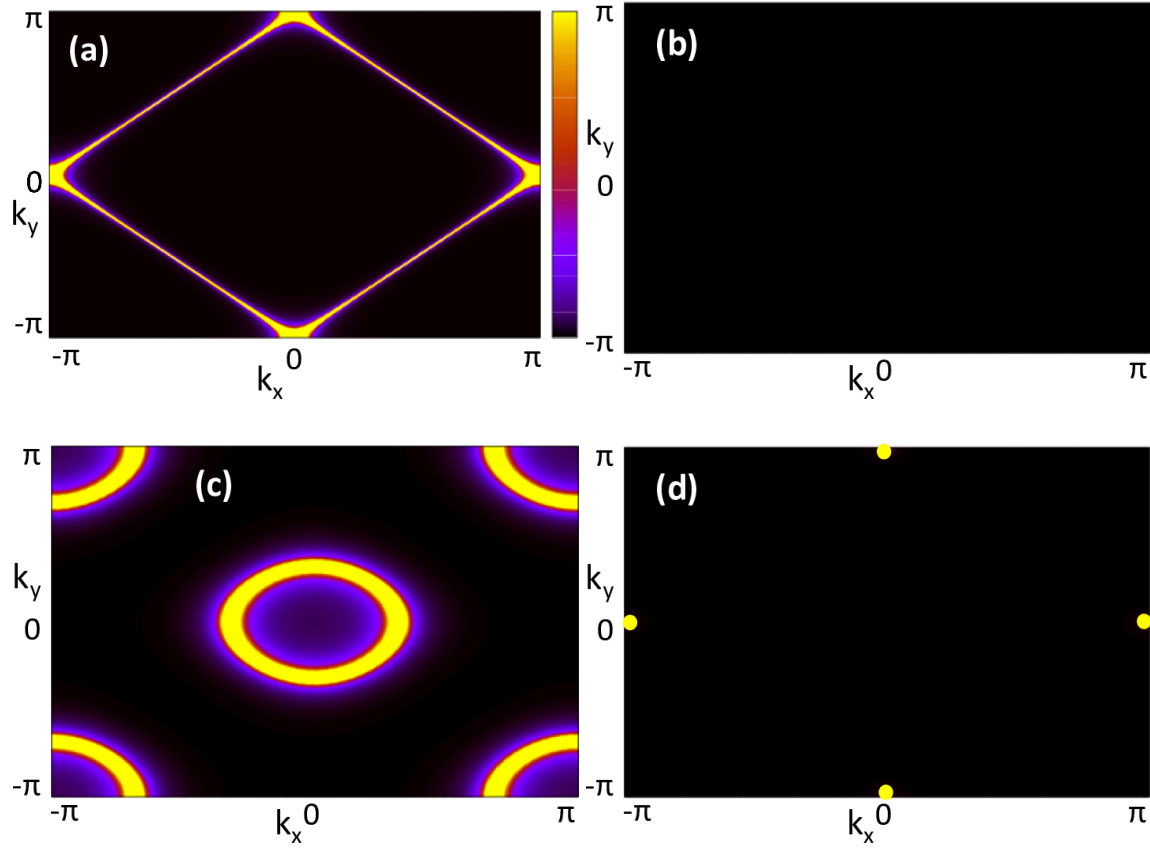


Figure 3.2: (a)-(d) : Momentum-resolved spectral functions at  $\omega = 0$  corresponding to the spectral functions shown in Fig.3.1. In (d), we have enhanced the visibility of the Fermi surface by changing the color.

the spectral function can be written by

$$\begin{aligned}
 \mathcal{H}_{eff}(\mathbf{k}, \omega) &= \mathcal{H}_0 + \Sigma(\omega) = \begin{pmatrix} \epsilon_c(\mathbf{k}) & V(\mathbf{k}) \\ V(\mathbf{k}) & \epsilon_f(\mathbf{k}) + \Sigma(\omega) \end{pmatrix} \\
 &= h_0 \mathbf{1} + h_1 \sigma^z + V(\mathbf{k}) \sigma^x
 \end{aligned} \tag{3.1.6}$$

$$h_0 = (\epsilon_c(\mathbf{k}) + \epsilon_f(\mathbf{k}) + \Sigma(\omega))/2 \tag{3.1.7}$$

$$h_1 = (\epsilon_c(\mathbf{k}) - \epsilon_f(\mathbf{k}) - \Sigma(\omega))/2 \tag{3.1.8}$$

$$E_{\pm} - h_0 = \pm \sqrt{h_1^2 + V^2(\mathbf{k})} \tag{3.1.9}$$

$$\begin{aligned}
 &= \pm \left\{ \left( \frac{(\epsilon_c(\mathbf{k}) - \epsilon_f(\mathbf{k}) - \text{Re}\Sigma(\omega))^2}{4} + V^2(\mathbf{k}) - \frac{(\text{Im}\Sigma(\omega))^2}{4} \right) \right. \\
 &\quad \left. + \frac{i}{2} \left( \text{Im}\Sigma(\omega) (\epsilon_c(\mathbf{k}) - \epsilon_f(\mathbf{k}) - \text{Re}\Sigma(\omega)) \right) \right\}^{\frac{1}{2}},
 \end{aligned} \tag{3.1.10}$$



where  $E_{\pm}$  are the eigenvalues of the effective Hamiltonian. For the system with  $p$ -wave hybridization, we use the helical basis, in which  $V(\mathbf{k}) = V_p \sqrt{\sin^2(k_x) + \sin^2(k_y)}$ . This effective non-Hermitian Hamiltonian becomes nondiagonalizable when the following conditions are satisfied:

$$\epsilon_c(\mathbf{k}) - \epsilon_f(\mathbf{k}) - \text{Re}\Sigma(\omega) = 0 \quad (3.1.11)$$

$$\text{Im}\Sigma(\omega)/2 = V(\mathbf{k}). \quad (3.1.12)$$

These points (sometimes loops) in the momentum space, for which the non-Hermitian Hamiltonian cannot be diagonalized, are called "exceptional points." Moreover, we can define a winding number on these points which reads[51],

$$W = \oint_{\text{EP}} \frac{d\mathbf{k}}{2\pi i} \cdot \nabla_{\mathbf{k}} \log \det \mathcal{H}_{\text{eff}}(\mathbf{k}, \omega). \quad (3.1.13)$$

Exceptional points with  $W \neq 0$  are topologically stable because  $W$  does not change unless the exceptional point is annihilated with another one. We note that, in strongly correlated materials, the effective non-Hermitian Hamiltonian is introduced for describing the spectral function[53]. Therefore, when  $(\omega - h_0)$  is not small, the spectral weight at the exceptional points is small and might only have a little effect on observable phenomena. We will thus distinguish exceptional points with  $\text{Re}(\omega - h_0) \simeq 0$  from the exceptional points where  $|\text{Re}(\omega - h_0)|$  is large. In this chapter, we call the former "exceptional points (EPs)" and the later "irrelevant exceptional point (iEP)." In short, iEPs have less spectral weight and therefore are less relevant to physical phenomena than EPs.

In Fig. 3.3, we show an example of the temperature dependence of the self-energy calculated by DMFT/NRG. The model with local hybridization,  $V=0.36$ , is shown in Fig. 3.3(a) and (b). Because Eq.(3.1.12) is independent of the momentum for a system with local hybridization, Eq.(3.1.12) can be satisfied for all  $\mathbf{k}$  in the BZ and therefore EPs and iEPs can emerge at  $\omega$  where the imaginary part of the self-energy crosses the black line. For the emergence of EPs which have strong spectral weight, additionally  $\text{Re}(\omega - h_0) \simeq 0$  must be fulfilled. Because  $\epsilon_f/\epsilon_c = \text{const}$  in our model, the momentum dependence vanishes in  $\text{Re}(w - h_0)=0$ . Thus, the condition for the emergence of an EP can be written as  $\epsilon_c w / (\epsilon_c + \epsilon_f) - \mu = \gamma w - \mu = \text{Re}\Sigma(\omega)$ , where  $\gamma$  is a constant. In Fig. 3(b) and (d), this condition is fulfilled when the black line intersects with  $\text{Re}\Sigma(\omega)$ . We note that even in a model where  $\epsilon_f/\epsilon_c$  is not constant, the momentum dependence of  $\text{Re}(\omega - h_0)$  is small, because usually  $\epsilon_f$  is much smaller than  $\epsilon_c$ . Thus, we see in Fig. 3 that the condition  $\text{Re}(w - h_0)=0$  can be fulfilled at the Fermi energy.

For the system with nonlocal hybridization, shown in Fig. 3.3(c) and (d), Eq.(3.1.12) can be satisfied at  $\omega$ , where the absolute value of the imaginary part of the self-energy is smaller than the black line, because the strength of the hybridization depends on the momentum. Therefore, EPs and iEPs can appear more easily in this case as we will show in the next section.

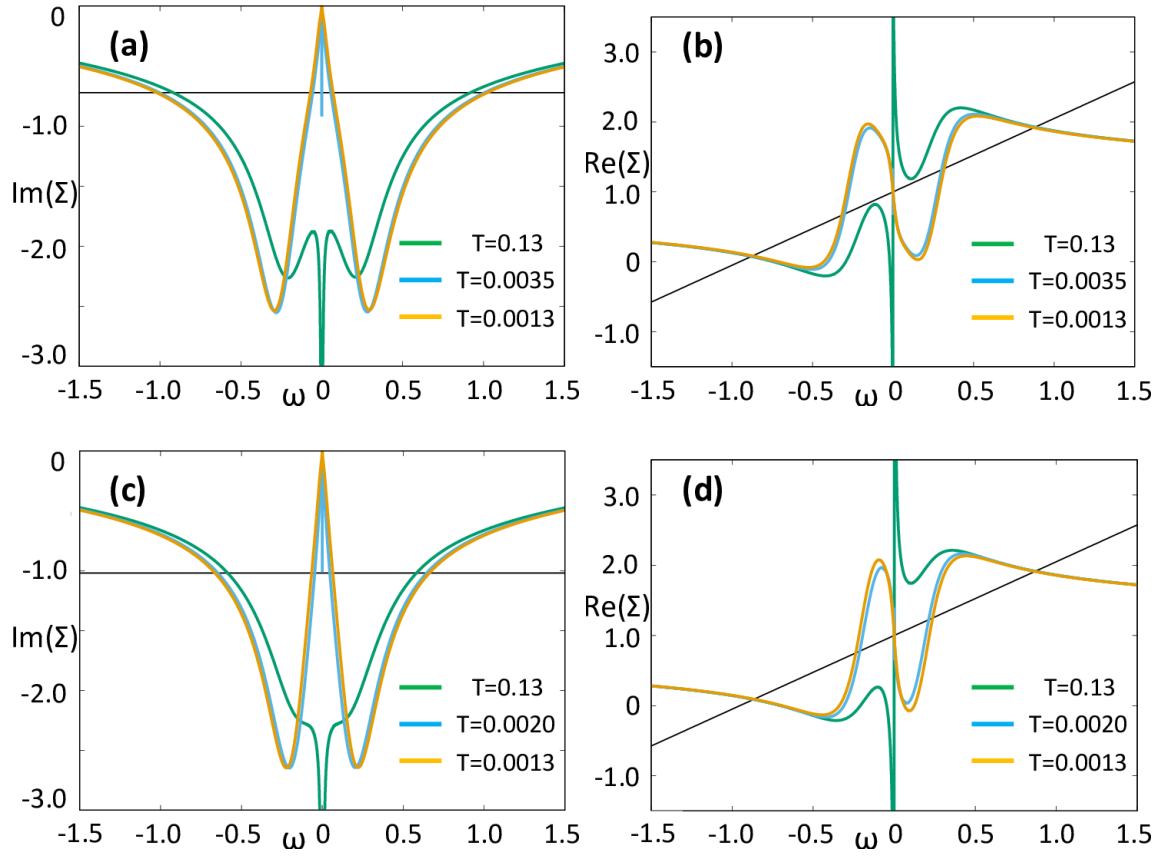


Figure 3.3: (a)-(d) : The temperature dependence of the imaginary and the real part of the self-energy calculated by DMFT/NRG. (a) and (b) show the results for the local hybridization with  $V=0.36$  and  $t_f = -0.05t_c$ . (c) and (d) show the results for the nonlocal hybridization with  $V=0.36$  and  $t_f = -0.05t_c$ . The black lines in (a) and (c) describe the condition  $\text{Im}\Sigma(\omega)/2 = \max|V(\mathbf{k})|$  and the black lines in (b) and (d) describe the conditions of Eq.(3.1.11) and  $\omega - \text{Re}(h_0) = 0$

## 3.2 Relation between Kondo temperature and $T_{EP}$ in $f$ -electron materials

In Fig. 3.4 (a)-(c), we show the magnetic moment of the  $f$ -electrons (contribution of the  $f$ -electron to the magnetic susceptibility,  $T\chi_f^z(T)$ ). Around the Kondo temperature, the magnetic moment changes from 0.25 at high temperatures to 0 at low temperatures, which corresponds to the Kondo screening. The magnetic susceptibility in Fig. 3.4 (a)-(c) is thereby calculated by applying a tiny magnetic field to the system and calculating the induced magnetic polarization of the  $f$ -electrons. We here estimate the Kondo temperature as the temperature where the magnetic moment crosses  $T\chi = 0.125$  in Fig. 3.4 (a)-(c) and include an arrow at these temperatures. We note that this screening is a crossover occurring over a finite temperature range. Thus, the Kondo temperature can also only be determined approximately within the temperature region where the magnetic moment is

screened. For the metallic system with local hybridization shown in Fig.3.4(b), the screening occurs more slowly compared to the other cases. In this system, the Fermi surface does not vanish below the Kondo temperature so that scattering around the Fermi surface can occur and the imaginary part of the self-energy at the Fermi energy, which prevent the screening of the  $f$ -electrons, decreases only slowly with lowering the temperature. Thus, the screening in Fig. 3.4(b) occurs slowly. Although the system with non-local hybridization shown in Fig. 3.4(c) and (f) also has a Fermi surface, it is almost point-like and therefore it induces much less scattering, resulting in a fast screening.

Besides analyzing the Kondo screening, we can use the self-energies obtained by DMFT/NRG, to analyze the emergence of EPs in the spectrum and the temperature at which the EPs appear at the Fermi energy. We show these EPs in Fig. 3.4 (g)-(i), where we plot iEPs with large eigenvalue  $\text{Re}(\omega - h_0)$  as black dots and EPs with  $\text{Re}(\omega - h_0) \simeq 0$  as colored dots corresponding to the colors of the hybridization shown in Fig. 3.4 (a)-(c). We see that EPs with  $\text{Re}(\omega - h_0) \simeq 0$  appear only in a narrow temperature region for the system with the local hybridization and below a certain temperature for the system with nonlocal hybridization. In Fig. 3.4(e), EPs appear in a wider temperature range than in Fig. 3.4(d) because the self-energy changes only slowly when lowering the temperature. Finally, in Fig. 3.4(f), EPs can emerge below a certain temperature, because of the momentum dependence of the hybridization, which makes it easier to satisfy Eq. (3.1.12). Furthermore, in Fig. 3.4(f), EPs appear also far from  $\omega = 0$ . This is possible because, for the system with the nonlocal hybridization, the conditions for the emergence of EPs can be satisfied more easily. However, the emergence of EPs far from  $\omega = 0$  seems to be irrelevant to the Kondo effect because the Kondo effect stems from the scattering around the Fermi surface.

Comparing the temperature at which EPs with  $\text{Re}(\omega - h_0) \simeq 0$  appear and the temperature in which the magnetic moment of the  $f$ -electron is screened, we see that both temperatures match very well. Thus, we conclude that the Kondo temperature is closely related to the temperature where EPs emerge at the Fermi energy. When lowering the temperature, the self-energy at the Fermi energy changes very strongly around the Kondo temperature, which results in a situation in which Eq. (3.1.11) and (3.1.12) can be easily fulfilled at the Fermi energy. For the system with the  $p$ -wave hybridization, the EPs start to emerge at the Kondo temperature when the absolute value of the imaginary part of the self energy becomes smaller than the hybridization strength.

In Fig. 3.4 (d)-(f), we can also see many iEPs with large  $\text{Re}(\omega - h_0)$ , which appear at almost all temperatures. These iEPs are mainly related to the imaginary part of the self-energy away from the Fermi energy, particularly in the Hubbard bands, which are nearly temperature independent and are irrelevant to the Kondo effect.

Figures 3.4 (g)-(i) show the Fermi surface at the temperature at which EPs appear at the Fermi energy for the systems with local hybridization and for the system with  $p$ -wave hybridization. For the system with the local hybridization, EPs appear only at  $T_{EP}$  and form a closed loop in the BZ. We note that it is not possible to define a vorticity at  $\omega = 0$  for this closed loop, which is different from the symmetry-protected exceptional ring in systems with chiral symmetry[26, 67, 74, 75]. Therefore, we believe that this loop of exceptional points will change into isolated EPs connected

by bulk Fermi arcs when taking into account a momentum-dependent self-energy. For the system with the  $p$ -wave hybridization, EPs appear as isolated points at the Fermi energy in the spectrum and have nonzero vorticity, and are thus topologically protected. These EPs change their position in the BZ satisfying Eq.(3.1.11) when changing the temperature, and finally merge and disappear at zero temperature.

### 3.3 Extension of the exceptional manifolds to $\omega$ -space

For the emergence of exceptional points, two equations (Eq.(3.1.11) and Eq.(3.1.12)) must be satisfied. Thus, in a  $d$ -dimensional model (2-dimensional momentum space in this chapter), exceptional points will generally form  $(d-2)$  dimensional manifolds. The dimension of the exceptional manifold might be higher, if additional symmetries do exist. For example, in 2D systems with chiral symmetry[67], one of the two conditions for EPs, such as Eq. (3.1.11) and (3.1.12), is always satisfied which leads to  $(d-1)$  dimensional exceptional manifolds. Besides the spatial dimension, the effective Hamiltonian in strongly-correlated systems also depends on the frequency,  $\omega$ , because the self-energy depends on the frequency. Thus, the inclusion of frequency will increase the dimension of the exceptional manifolds. Previous studies have only focused on the Fermi energy, ignoring the frequency dependence of the exceptional manifolds. We note that a frequency dependent effective Hamiltonian occurs in situations when focusing on a subsystem and integrating out the rest of the total system, even though the full system is described by a frequency-independent Hamiltonian[39, 76, 77]. Because we here focus on the one-particle Green function, the effective Hamiltonian depends on the frequency.

In Fig. 3.5, we show the exceptional manifolds for the local and the nonlocal hybridization and different temperatures in the  $(\mathbf{k}, \omega)$ -space. Until now, we have focused only on exceptional points close to the Fermi energy. Fig. 5(a) shows the exceptional loops in the system with local hybridization for a temperature above the Kondo temperature. As described above, in the system with local hybridization, Eq.(3.1.11) and Eq.(3.1.12) do not depend on the momentum and thus exceptional manifolds are loops in the momentum space. At temperatures above the Kondo temperature, we find one loop above the Fermi energy and one loop below the Fermi energy. Lowering the temperature towards the Kondo temperature, these exceptional loops move towards the Fermi energy. At the Kondo temperature, these exceptional loops merge at the Fermi energy.

We note that by extending our considerations to the  $(\mathbf{k}, \omega)$ -space, we are able to define and calculate the vorticity of these loops by

$$v = \oint_{\text{EP}} \frac{d\mathbf{k}'}{2\pi i} \cdot \nabla_{\mathbf{k}'} \log \det \mathcal{H}_{eff}(\mathbf{k}, \omega), \quad (3.3.1)$$

where  $\mathbf{k}'$  is defined on the plane which is perpendicular to the tangent vector of the exceptional loop. The line integral is done in mathematical positive direction. We then define the direction of the exceptional loops, shown in Fig. 3.5, so that the vorticities defined in Eq.(3.3.1) become  $1/2$ . Further

details are explained in Appendix B.1. We note that when considering a momentum dependent self-energy, these loops become distorted. Thus, looking at the Fermi energy, the exceptional manifold will appear as points.

Fig. 3.5(b)-(d) show the exceptional manifolds for the system with nonlocal hybridization. Fig. 3.5(b) and (c) show these exceptional points in  $(\mathbf{k}, \omega)$ -space at high temperatures. Including the  $\omega$ -space, these exceptional points form closed loops. Furthermore, we show in Fig. 3.5(c) a magnification of (b) around the Fermi energy, which demonstrates the absence of exceptional points at the Fermi energy for high temperatures. When lowering the temperature, one closed loop of EPs is formed above  $\omega = 0$  and one closed loop is formed below  $\omega = 0$ . At the Kondo temperature, these loops touch and merge at  $\omega = 0$  to a single 1D exceptional manifold as shown in Fig. 3.5(d).

We conclude that the crossover from localized to itinerant  $f$ -electrons in the system with local hybridization goes hand in hand with the merging and vanishing of two exceptional loops at the Fermi energy. In the system with nonlocal hybridization, different exceptional loops in the  $(\mathbf{k}, \omega)$ -space change their topology at the Kondo temperature and generate EPs at the Fermi energy.

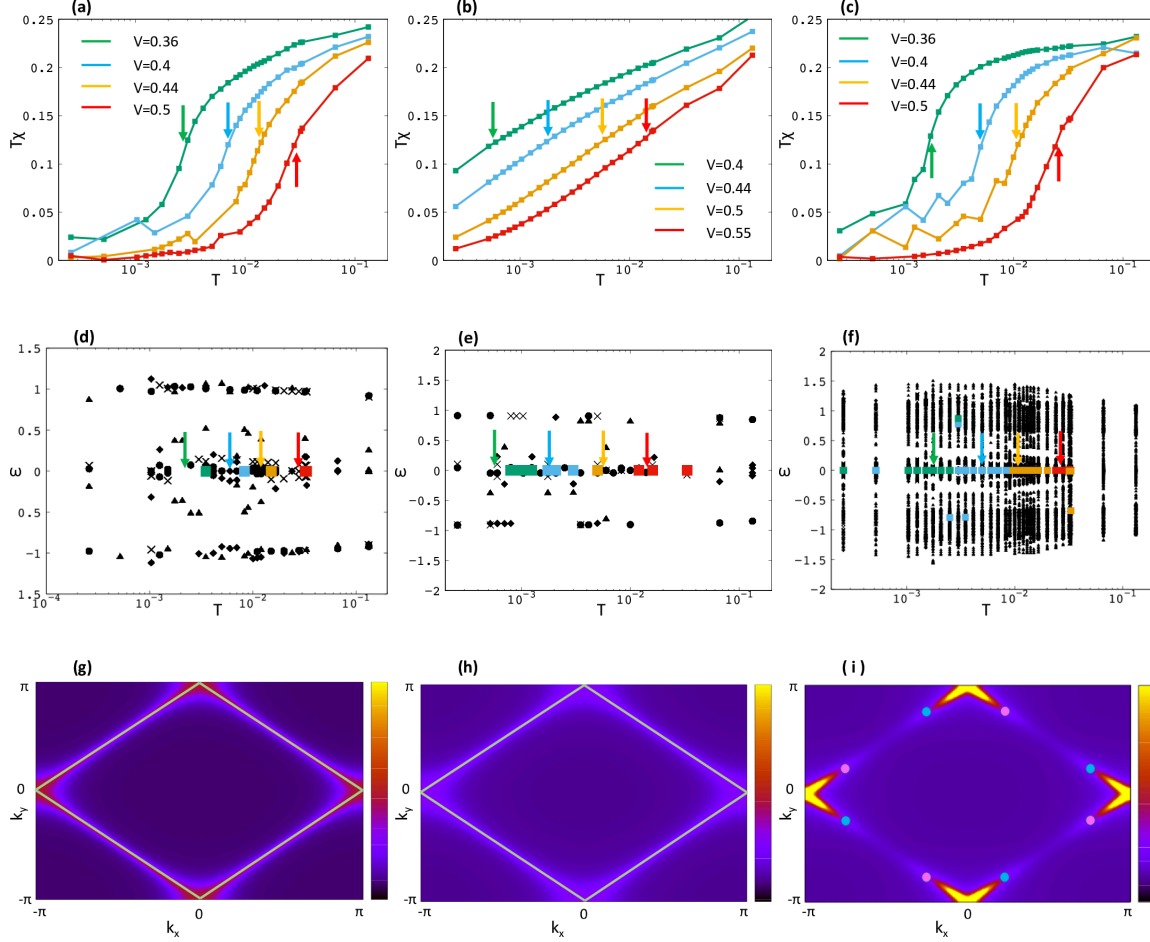


Figure 3.4: (a)-(f) : Comparison between the Kondo insulator, the heavy-fermion state, and the metallic state with p-wave hybridization for different strengths of  $V$ . (a)-(c) show the local susceptibility. The colors in (a)-(c) correspond to different  $V$ . The arrows describe the estimated Kondo temperature for each case. In (a) and (c), the green, skyblue, orange and red plot respectively correspond to  $V = 0.36, 0.4, 0.44, 0.5$ . In (b), the green, skyblue, orange and red plot respectively correspond to  $V = 0.4, 0.44, 0.5, 0.55$ . (d)-(f) show the temperature and the frequency dependence of the emergence of the iEPs and the EPs. The iEPs are drawn as black dots. In (d) and (f), the cross, point, triangle, and square dots are for  $V = 0.36, 0.4, 0.44, 0.5$ . In (e), the cross, point, triangle, and square dots correspond to  $V = 0.4, 0.44, 0.5, 0.55$ . The EPs are drawn as color plots. We use the same color as in (a)-(c). The arrows describe the Kondo temperature estimated from (a)-(c). (g)-(i) show momentum-resolved spectral functions at the Fermi energy around  $T_{EP}$ . (g) corresponds to  $V=0.36, T=0.0035$  shown in (a) and (d). (h) corresponds to  $V=0.4, T=0.0007$  shown in (b) and (e). (i) corresponds to  $V=0.36, T=0.0025$  shown in (c) and (f). The parameters are  $U=2, t_c=0.8, t_f=-0.04, \mu_c=0, \mu_f=-1.0$ . In (g) and (f), exceptional points form a closed loop in the BZ, highlighted as a green line. In (i), we included exceptional points with vorticity  $\pm 1/2$  as red and blue points.

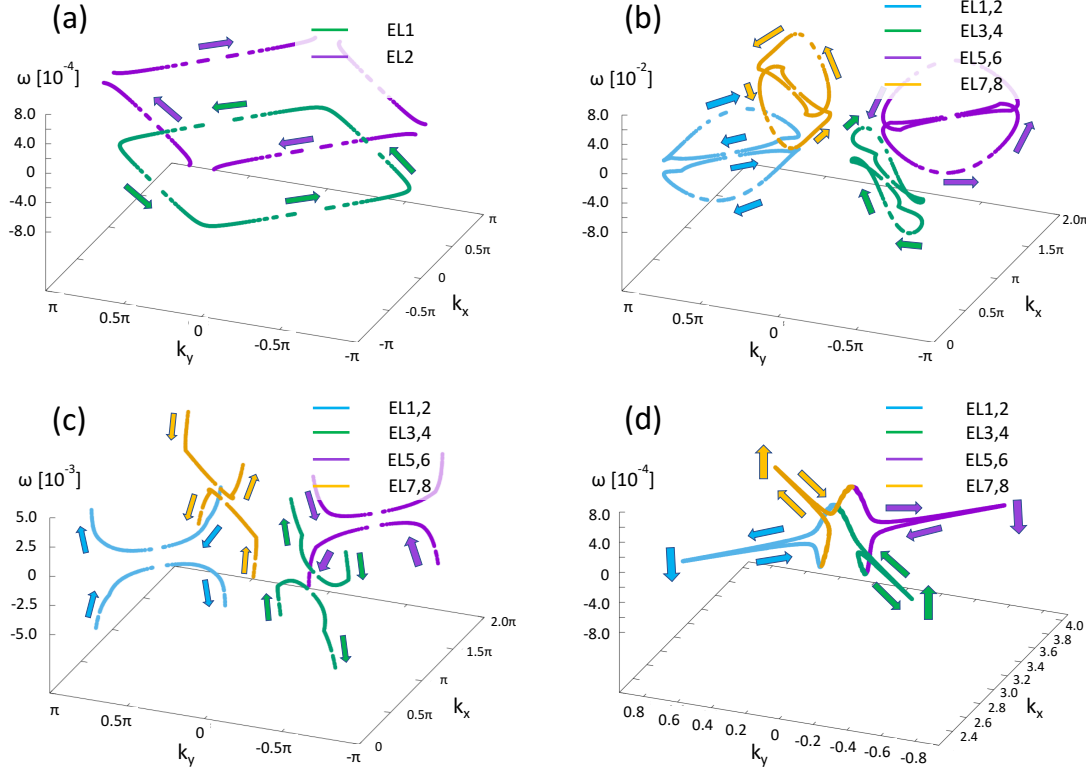


Figure 3.5: Exceptional points of  $\mathcal{H}_{eff}(k_x, k_y, \omega)$  in the system with local hybridization for (a) and with nonlocal hybridization for (b)-(d). The parameters are  $V_l = 0.4, t_f/t_c = -0.05, T = 0.016$  in (a),  $V_p = 0.4, t_f/t_c = -0.05, T = 0.016$  in (b) and (c), and  $V_l = 0.4, t_f/t_c = -0.05, T = 0.002$  in (d). (c) is a magnification of the exceptional manifold shown in (b) close to the Fermi energy. The vorticities in (a) are calculated by Eq.(3.3.1).





# Chapter 4

## Effects of renormalization and non-Hermiticity on nonlinear responses in strongly-correlated electron systems

In Chapter 4, we first give an analytical derivation of nonlinear responses using the Green function methods at finite temperature. Then, we discuss the difficulties of considering dissipation using conventional methods, such as the reduced density matrix method. We reveal that the relaxation time approximation leads to severe limitations when considering optical responses. Finally, we demonstrate that correlation effects, such as the renormalization of the band structure and different lifetimes in orbitals or sublattices, can significantly enhance nonlinear responses and even change the sign of the nonlinear conductivity.

### 4.1 Background

Nonlinear responses in condensed matter theory have attained great interest because of their rich information about the symmetries of materials and their various functionalities. For example, the breaking of the inversion symmetry in a material can be detected by measuring the second harmonic generation of the electric susceptibility[78–80]. Moreover, in non-centrosymmetric materials, the shift current and non-reciprocal(rectification) current can occur in nonlinear responses[81, 82]. It is extensively studied due to its application in solar cells, photodetectors, and high-frequency rectification devices[83–87].

Although nonlinear responses in condensed matter systems have many possible applications, the magnitude of the nonlinear response, which is usually small, poses a significant obstacle for most applications. Thus, much effort has been put into enhancing the amplitude of the nonlinear response. It has been proposed that the shift current can be magnified in Dirac systems[81, 84, 88, 89] and that superconducting fluctuations can enhance the nonreciprocity[90–92]. Another possibility to

enhance nonlinear responses might be correlation effects. A strong high-harmonic generation has been revealed in strongly-correlated electron systems both in experiments[93, 94] and numerical calculations[95–99]. A nonlinear Hall effect, which is almost  $10^3$  times as large as the ab-initio calculation result, has been measured in the Weyl-Kondo semimetal candidate  $\text{Ce}_3\text{Bi}_4\text{Pd}_3$ [100]. Moreover, it has been suggested from a Hartree-analysis that the strong Coulomb interaction may enhance nonreciprocity[101]. Although these works show that correlation effects give large nonlinear responses, a systematic analysis of strong correlation effects on nonlinear responses is still missing.

In this chapter, we first derive a formalism based on Green functions for calculating the nonlinear response at finite temperature and formulate a diagrammatic method to use them. We note that Parker *et al.*[102] have derived a similar diagrammatic method for nonlinear responses focusing on the zero dissipation limit and João *et al.*[103] have introduced a diagrammatic method based on Keldysh Green functions. Neglecting vertex corrections, we can derive equations based on the single-particle Green function, including correlation effects via the self-energy. Because there are many methods available to calculate the self-energy of correlated materials, the here derived formalism makes it easy to analyze correlation effects on nonlinear responses. Next, we discuss difficulties of including the dissipation effect in conventional methods, such as the reduced density matrix(RDM) method[104–108]. In these methods, dissipation is often introduced phenomenologically by using the relaxation time approximation(RTA). We reveal that the RTA breaks the gauge invariance and is only justified in the DC limit, the high-frequency limit, and at high-temperatures, while dissipation is appropriately included in the Green function method.

Furthermore, while the RDM method for nonlinear responses mainly focuses on noninteracting systems, we demonstrate that it is possible to include correlation effects into the RDM using Green functions. By including correlation effects into the RDM, we are able to retrieve the equations of the Green function method in the DC limit. Finally, we use our Green function formalism to analyze correlation effects on nonlinear responses. Notably, we look at the impact of the renormalization of the band structure and the effect of different lifetimes on the nonlinear response functions. We show that renormalization effects can enormously enhance the nonlinear response. Considering a renormalization uniform in all orbitals, the renormalization factor  $z(< 1)$  enhances the  $n$ -th order response by a factor of  $z^{-(n-1)}$ . Furthermore, we study the effect of different lifetimes in different orbitals using the non-Hermitian band-index of the effective non-Hermitian Hamiltonian describing the single-particle Green function. We show that the occurrence of different lifetimes can not only enhance terms already existing in the Hermitian case but also creates novel non-Hermitian terms in the nonlinear response function originating in the coalescence of several bands. Our framework can be applied to most correlated electron systems, such as heavy fermions, magnetic systems, Mott insulators, etc. However, we note that it cannot be directly used for systems with strong spatial fluctuations because we ignore vertex corrections and the momentum dependence of the self-energy. On the other hand, by using the Nambu formalism, we can also expand our framework to superconducting systems.

The rest of this chapter is organized as follows: In Section 4.2, we derive the Green function formalism for the nonlinear response at finite temperature. Next, we discuss the difficulties of including the dissipation in the RDM method in Section 4.5. We reveal that the RTA under an AC electric field is a severe approximation, although it is often used in previous works. In Section 4.6, we extend the RDM method to interacting systems by using Green functions. Finally, we analyze correlation effects, such as the renormalization of the band structure and the occurrence of different lifetimes in different orbitals, on the nonlinear response in Section 4.7.

## 4.2 Nonlinear response using the Green function method

In this section, we introduce the Matsubara formalism to express nonlinear response functions by Green functions, which are common and easy to handle in the context of correlated systems at finite temperature. Throughout this chapter, we set the Planck constant and the lattice constant to unity,  $\hbar = a = 1$ . We also set the electron charge  $q = 1$  in the numerical calculations.

We here use the velocity gauge, in which the effect of electric fields is described in the Hamiltonian as

$$\mathcal{H}(\mathbf{k}) \rightarrow \mathcal{H}(\mathbf{k} - q\mathbf{A}(t)) = \mathcal{H}(\mathbf{k}) + \sum_{n=1}^{\infty} \frac{1}{n!} \prod_{i=1}^n \left( -qA^{\alpha_i}(t) \partial_{\alpha_i} \right) \mathcal{H}(\mathbf{k}), \quad (4.2.1)$$

where  $q$  is the charge of the electron and  $\alpha_i$  is a direction in the momentum space. In this chapter, we suppose that there is no magnetic field and we use the Coulomb gauge  $\mathbf{A}(\mathbf{x}, t) = \mathbf{A}(t)$ . We note that there is another choice of gauge, namely the length gauge. Under the length gauge, electric fields can be described by the dipole Hamiltonian, and it is often used in the semi-classical Boltzmann equation and the RDM. It is known that both gauges give the same results for noninteracting systems when calculating exactly[106].

The action of the system in the imaginary time is given as

$$S[\mathbf{A}] = \int_0^{\beta} d\tau \left[ \sum_{\mathbf{k}, a} \left\{ \bar{\psi}_{a,\mathbf{k}} \partial_{\tau} \psi_{a,\mathbf{k}} + \mathcal{H}(\mathbf{k} - q\mathbf{A}(-i\tau)) \right\} + H_{int} \right] \quad (4.2.2)$$

$$= \int_0^{\beta} d\tau \left[ \sum_{\mathbf{k}, a} \left\{ \bar{\psi}_{a,\mathbf{k}} \partial_{\tau} \psi_{a,\mathbf{k}} + \mathcal{H}(\mathbf{k}) + \sum_{n=1}^{\infty} \frac{(-1)^n}{n!} \prod_{i=1}^n \left( A^{\alpha_i}(-i\tau) \right) \hat{\mathcal{J}}_{\alpha_1 \dots \alpha_n}(\mathbf{k}) \right\} + H_{int} \right] \quad (4.2.3)$$

$$\hat{\mathcal{J}}_{\alpha_1 \dots \alpha_n}(\mathbf{k}) = q^n \partial_{\alpha_1} \dots \partial_{\alpha_n} \mathcal{H}(\mathbf{k}) \quad (4.2.4)$$

where  $\bar{\psi}_a, \psi_a$  are fermionic creation and annihilation operators which construct the Hamiltonian  $\mathcal{H}$ ,  $a$  is the orbital index,  $\mathbf{A}(t)$  is the vector potential,  $\hat{\mathcal{J}}_{\alpha_1 \dots \alpha_n}(\mathbf{k}) = q^n \partial_{\alpha_1} \dots \partial_{\alpha_n} \mathcal{H}(\mathbf{k})$  and  $H_{int}$  is the interaction part of the Hamiltonian. In this chapter, we suppose that there is only a local interaction. We note that for general nonlocal interactions, the interaction part of the Hamiltonian also depends on the vector potential.

The partition function with applied electric field is written in the path integral formalism as

$$Z[A] = \int \mathcal{D}\bar{\psi} \mathcal{D}\psi \exp[-S[A]]. \quad (4.2.5)$$

The expectation value of the current is

$$\langle J_\alpha(\tau) \rangle = \frac{\delta}{Z[A] \delta A^\alpha(-i\tau)} Z[A], \quad (4.2.6)$$

which can be written using response functions as

$$\begin{aligned} \langle J_\alpha(\tau) \rangle &= \int d\tau' \mathcal{K}_{\alpha\beta}^1(\tau, \tau') A^\beta(-i\tau') \\ &+ \int d\tau' \int d\tau'' \mathcal{K}_{\alpha\beta\gamma}^2(\tau, \tau', \tau'') A^\beta(-i\tau') A^\gamma(-i\tau'') \\ &+ \dots, \end{aligned} \quad (4.2.7)$$

where

$$\mathcal{K}_{\alpha\alpha_1\dots\alpha_n}^n(\tau_1, \dots, \tau_n) = \frac{1}{Z[A]} \left( \prod_{i=1}^n \frac{\delta}{\delta A^{\alpha_i}(-i\tau_i)} \right) \frac{\delta}{\delta A^\alpha(-i\tau)} Z[A] \Big|_{A=0}. \quad (4.2.8)$$

The results for the response functions in imaginary time are explicitly written in the Appendix C.1.

After Fourier transformation to Matsubara frequencies, the current is given as

$$\begin{aligned} \langle J_\alpha(i\omega_n) \rangle &= K_{\alpha\beta}^{(1)}(i\omega_n; i\omega_n) A^\beta(i\omega_n) \\ &+ \sum_{\omega_m, \omega_l} K_{\alpha\beta\gamma}^{(2)}(i\omega_n; i\omega_m, i\omega_l) A^\beta(\omega_m) A^\gamma(\omega_l) \delta(\omega_n - \omega_m - \omega_l) \\ &+ \dots \end{aligned} \quad (4.2.9)$$

The frequency before the semicolon in the response function  $K_{\alpha\beta}^{(n)}(i\omega_n; i\omega_n, \dots)$  represents the frequency of the output response, and the frequencies after the semicolon represent the frequencies of the input forces, i.e. of the vector potentials.

Analytical continuation and using  $\mathbf{E}(\omega_i) = i\omega_i \mathbf{A}(\omega_i)$  finally yields

$$\begin{aligned} \langle J_\alpha(\omega) \rangle &= K_{\alpha\beta}^{(1)}(\omega; \omega) A^\beta(\omega) \\ &+ \int d\omega_1 \int d\omega_2 K_{\alpha\beta\gamma}^{(2)}(\omega; \omega_1, \omega_2) A^\beta(\omega_1) A^\gamma(\omega_2) \delta(\omega - \omega_{12}) \\ &+ \dots \end{aligned} \quad (4.2.10)$$

$$\begin{aligned} &= \sigma_{\alpha\beta}^{(1)}(\omega) E^\beta(\omega) \\ &+ \int d\omega_1 \sigma_{\alpha\beta\gamma}^{(2)}(\omega; \omega_1, \omega_2) E^\beta(\omega_1) E^\gamma(\omega_2) \delta(\omega - \omega_{12}) \\ &+ \dots \end{aligned} \quad (4.2.11)$$

$$\sigma_{\alpha\beta\dots}^{(n)}(\omega; \{\omega_s\}) = K_{\alpha\beta\dots}^{(n)}(\omega; \{\omega_i\}) / \left( \prod_{s=1}^n i\omega_i \right), \quad (4.2.12)$$

where  $\omega_{12} = \omega_1 + \omega_2$ . The first- and second-order conductivities can be expressed via single-particle Green functions as

$$\begin{aligned} & \sigma_{\alpha\beta}^{(1)}(\omega_1; \omega_1) \\ &= -\frac{1}{\omega_1} \int_{-\infty}^{\infty} \frac{d\omega}{2\pi} f(\omega) \sum_{\mathbf{k}} \left\{ \text{Tr} \left[ \mathcal{J}_{\alpha\beta}(\mathbf{k}) (G^R(\omega, \mathbf{k}) - G^A(\omega, \mathbf{k})) \right] \right. \\ & \quad + \text{Tr} \left[ \mathcal{J}_{\alpha}(\mathbf{k}) G^R(\omega + \omega_1, \mathbf{k}) \mathcal{J}_{\beta}(\mathbf{k}) (G^R(\omega, \mathbf{k}) - G^A(\omega, \mathbf{k})) \right. \\ & \quad \left. \left. + \mathcal{J}_{\alpha}(\mathbf{k}) (G^R(\omega, \mathbf{k}) - G^A(\omega, \mathbf{k})) \mathcal{J}_{\beta}(\mathbf{k}) G^A(\omega - \omega_1, \mathbf{k}) \right] \right\} \quad (4.2.13) \end{aligned}$$

$$\begin{aligned} & \sigma_{\alpha\beta\gamma}^{(2)}(\omega_1 + \omega_2; \omega_1, \omega_2) \\ &= \frac{1}{\omega_1 \omega_2} \int_{-\infty}^{\infty} \frac{d\omega}{2\pi i} f(\omega) \sum_{\mathbf{k}} \left\{ \frac{1}{2} \text{Tr} \left[ \mathcal{J}_{\alpha\beta\gamma} (G^R(\omega) - G^A(\omega)) \right] \right. \\ & \quad + \text{Tr} \left[ \mathcal{J}_{\alpha\beta} G^R(\omega + \omega_2) \mathcal{J}_{\gamma} (G^R(\omega) - G^A(\omega)) + \mathcal{J}_{\alpha\beta} (G^R(\omega) - G^A(\omega)) \mathcal{J}_{\gamma} G^A(\omega - \omega_2) \right] \\ & \quad + \frac{1}{2} \text{Tr} \left[ \mathcal{J}_{\alpha} G^R(\omega + \omega_{12}) \mathcal{J}_{\beta\gamma} (G^R(\omega) - G^A(\omega)) + \mathcal{J}_{\alpha} (G^R(\omega) - G^A(\omega)) \mathcal{J}_{\beta\gamma} G^A(\omega - \omega_{12}) \right] \\ & \quad + \text{Tr} \left[ \mathcal{J}_{\alpha} G^R(\omega + \omega_{12}) \mathcal{J}_{\beta} G^R(\omega + \omega_2) \mathcal{J}_{\gamma} (G^R(\omega) - G^A(\omega)) \right. \\ & \quad \quad + \mathcal{J}_{\alpha} G^R(\omega + \omega_1) \mathcal{J}_{\beta} (G^R(\omega) - G^A(\omega)) \mathcal{J}_{\gamma} G^A(\omega - \omega_2) \\ & \quad \quad \left. + \mathcal{J}_{\alpha} (G^R(\omega) - G^A(\omega)) \mathcal{J}_{\beta} G^A(\omega - \omega_1) \mathcal{J}_{\gamma} G^A(\omega - \omega_{12}) \right] \\ & \quad \left. + [(\beta, \omega_1) \leftrightarrow (\gamma, \omega_2)] \right\}, \quad (4.2.14) \end{aligned}$$

where  $\mathcal{J}_{\alpha\beta\dots}$  is the matrix representation of  $\hat{\mathcal{J}}_{\alpha\beta\dots}$ ,  $G^{R/A}(\omega, \mathbf{k})$  is the retarded/advanced Green function, and  $f(\omega)$  is the Fermi distribution function.  $[(\beta, \omega_1) \leftrightarrow (\gamma, \omega_2)]$  means a term in which the index and the variable have been replaced by the other set. Further details of the derivation are given in the Appendix C.1 and C.2. Throughout this chapter, we omit the  $\mathbf{k}$ -index of the Green function and the velocity operator,  $\mathcal{J}_{\alpha\beta\dots}$ . Furthermore, we ignore vertex corrections in the many-particle Green functions, which allows us to express the conductivity as a product of single-particle Green functions. This approximation is also commonly used in the semi-classical Boltzmann equation and the RDM formalism. The results above are consistent with the results in [102], and [103]. Especially, in the dissipationless limit, the results are consistent with<sup>1</sup> Eqs.(26)

<sup>1</sup>We note that the results in [102] seem to include a typo in Eq. (B18) where  $1/(\omega - \epsilon_{ab})$  should be changed to  $1/(\omega - \epsilon_{ba})$  in the third term in Eq. (43).

and (43) in ref. [102]. The detail is written in Appendix C.4. The here presented procedure to derive the nonlinear optical conductivity can be summarized into a diagrammatic method, which is written in the next section in Chapter. 4.3. We note that this diagrammatic method is a generalization of the diagrammatic method at zero temperature in Parker *et al.*[102] to nonlinear response functions using real-frequencies at finite temperature.

If we take the DC limit  $\omega_1, \omega_2 \rightarrow 0$ , the first and second-order conductivities become

$$\sigma_{DC;\alpha\beta}^{(1)} = \int_{-\infty}^{\infty} \frac{d\omega}{2\pi} \left\{ \left( -\frac{\partial f(\omega)}{\partial \omega} \right) \text{ReTr} \left[ \mathcal{J}_\alpha G^R(\omega) \mathcal{J}_\beta G^A(\omega) \right] - 2f(\omega) \text{ReTr} \left[ \mathcal{J}_\alpha \frac{\partial G^R(\omega)}{\partial \omega} \mathcal{J}_\beta G^R(\omega) \right] \right\} \quad (4.2.15)$$

$$\begin{aligned} \sigma_{DC;\alpha\beta\gamma}^{(2)} &= -2 \int_{-\infty}^{\infty} \frac{d\omega}{2\pi} \left\{ \left( -\frac{\partial f(\omega)}{\partial \omega} \right) \text{Im} \left( \text{Tr} \left[ \mathcal{J}_\alpha \frac{\partial G^R(\omega)}{\partial \omega} \mathcal{J}_\beta G^R(\omega) \mathcal{J}_\gamma G^A(\omega) \right] + \frac{1}{2} \text{Tr} \left[ \mathcal{J}_\alpha \frac{\partial G^R(\omega)}{\partial \omega} \mathcal{J}_{\beta\gamma} G^A(\omega) \right] \right) \right. \\ &\quad \left. - f(\omega) \text{Im} \left( \text{Tr} \left[ \mathcal{J}_\alpha \frac{\partial}{\partial \omega} \left( \frac{\partial G^R(\omega)}{\partial \omega} \mathcal{J}_\beta G^R(\omega) \right) \mathcal{J}_\gamma G^R(\omega) \right] + \frac{1}{2} \text{Tr} \left[ \mathcal{J}_\alpha \frac{\partial^2 G^R(\omega)}{\partial \omega^2} \mathcal{J}_{\beta\gamma} G^R(\omega) \right] \right) \right\} \\ &\quad + (\beta \leftrightarrow \gamma) \end{aligned} \quad (4.2.16)$$

Interaction effects can be taken into account by including the retarded/advanced self-energy  $\Sigma^{R/A}(\omega)$  into the Green function,  $G^R(\omega) = 1/(\omega - \mathcal{H} - \Sigma^{R/A}(\omega))$ . Throughout this chapter, we ignore the momentum dependence of the self-energy. Including the momentum dependence of the self-energy, we should also consider vertex corrections in order to satisfy the Ward-Takahashi identities. We note that the momentum-dependence of the self-energy can become significant for certain phenomena in strongly correlated materials and, in these cases, must be included in the considerations about nonlinear responses. We also note that we can recover the physical unit by substituting  $\omega \rightarrow \hbar\omega$  and multiply  $a^n$  for  $n$ -th order nonlinear conductivity.

Finally, setting  $\Sigma(\omega) = i\gamma/2$  and taking the limit  $\gamma \rightarrow 0$ , we can perform the frequency integrals and further simplify the results which are summarized in the Appendix C.4 .

### 4.3 Diagrammatic formalism for nonlinear response at finite temperature

Parker *et al.* have introduced a diagrammatic method for nonlinear responses in Ref. [102], and João *et al.*[103] introduced a diagrammatic method using Keldysh Green functions. In this section, with the results from the previous section in mind, we construct an extension to this diagrammatic method for finite temperatures using real frequencies, which is summarized in table 4.1. Each diagram for the  $N$ -th order response function includes  $N$  incoming photons and one vertex for an


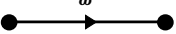

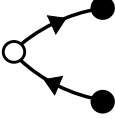
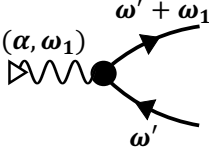
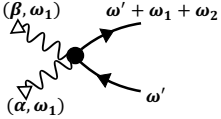
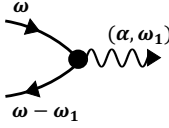
Component	Diagram	Value
(Classical) Photon Propagator	$(\alpha, \omega_1)$ 	1
Electron Propagator (Retarded)		$G^R(\omega)$
Electron Propagator (Advanced)		$G^A(\omega)$
Distribution Function		$(G^R(\omega) - G^A(\omega))f(\omega)$
One-Photon Input Vertex		$\frac{1}{i\omega_1} \mathcal{J}_\alpha$
Two-Photon Input Vertex		$\frac{1}{i\omega_1} \frac{1}{i\omega_2} \mathcal{J}_{\alpha\beta}$
One-Photon Output Ver- tex		$\mathcal{J}_\alpha$

Table 4.1: Objects to construct Feynman diagrams for nonlinear electromagnetic perturbations in a crystal at finite temperature – A new vertex with  $N$  incoming photons will appear in a diagram of the  $N$ -th order response function. The input vertex can appear with any number of photons with a coefficient  $(-i\omega_i)^{-1}$  for each photon. The right(left)-handed arrows represent retarded(advanced) Green functions. The direction of the arrow changes at the distribution function object and the output vertex, but not at the input vertices. We note that the input can occur at the same place as the output, such as in the first term of Eq. (4.3.1) and Eq. (4.3.2). In that case, the value for the  $n$ -th order vertex becomes  $\prod_i^{n-1} \frac{1}{i\omega_i} \mathcal{J}_{\alpha_1 \dots \alpha_n}$

outgoing photon. For each incoming photon a coefficient  $(i\omega_i)^{-1}$  is multiplied. The frequencies of the input vertices need to sum up to the output frequency. Furthermore, each diagram includes one object corresponding to the distribution function. Finally, retarded and advanced Green functions are used to connect all vertices in a single loop. The difference of our results to the results by Parker *et al.*[102] is the presence of the distribution function and the distinction between the retarded and advanced Green functions. For calculating the N-th order response, we construct all distinct diagrams using these rules. We then can easily evaluate the diagrams tracing the objects anticlockwise starting from the output vertex.

For example, the linear optical conductivity can be described using diagrams as

$$\begin{aligned}
& \sigma_{\alpha\beta}^{(1)}(\omega; \omega_1) \\
&= \text{Diagram 1} + \text{Diagram 2} + \text{Diagram 3} \\
&= -\frac{1}{\omega_1} \int_{-\infty}^{\infty} \frac{d\omega}{2\pi} f(\omega) \sum_{\mathbf{k}} \left\{ \text{Tr} \left[ \mathcal{J}_{\alpha\beta}(\mathbf{k}) (G^R(\omega, \mathbf{k}) - G^A(\omega, \mathbf{k})) \right] \right. \\
&\quad + \text{Tr} \left[ \mathcal{J}_{\alpha}(\mathbf{k}) G^R(\omega + \omega_1, \mathbf{k}) \mathcal{J}_{\beta}(\mathbf{k}) (G^R(\omega, \mathbf{k}) - G^A(\omega, \mathbf{k})) \right] \\
&\quad \left. + \mathcal{J}_{\alpha}(\mathbf{k}) (G^R(\omega, \mathbf{k}) - G^A(\omega, \mathbf{k})) \mathcal{J}_{\beta}(\mathbf{k}) G^A(\omega - \omega_1, \mathbf{k}) \right\}, \tag{4.3.1}
\end{aligned}$$



The diagrams for the second-order optical conductivity are given as

$$\begin{aligned}
& \sigma_{\alpha\beta\gamma}^{(2)}(\omega; \omega_1, \omega_2) \\
&= \text{Diagram 1} \\
&+ \text{Diagram 2} + \text{Diagram 3} \\
&+ \text{Diagram 4} + \text{Diagram 5} \\
&+ \text{Diagram 6} + \text{Diagram 7} \\
&+ ((\beta, \omega_1) \leftrightarrow (\gamma, \omega_2)).
\end{aligned} \tag{4.3.2}$$

## 4.4 Models used in this Chapter

In this chapter, we use the following two models to numerically confirm our general results. In this section, We introduce the effective Hamiltonian  $\mathcal{H}_{eff} = \mathcal{H}_0 + \Sigma^R$ , which includes the dissipation effect.

### 4.4.1 Monolayer TMD materials with a spin-dependent dissipation

This model is commonly used to describe transition metal dichalcogenide(TMD) monolayers. The effective non-Hermitian Hamiltonian, which can again be understood as the non-Hermitian matrix

describing the retarded single-particle Green function, can be written as[87, 119]

$$\begin{aligned} \mathcal{H}_{eff} = & \sum_{\mathbf{k},s} (\epsilon(\mathbf{k}) - \mu - i\eta - i\Gamma_s) c_{\mathbf{k},s}^\dagger c_{\mathbf{k},s} \\ & + \sum_{\mathbf{k},s,s'} \mathbf{g}(\mathbf{k}) \cdot \boldsymbol{\sigma}_{ss'} c_{\mathbf{k},s}^\dagger c_{\mathbf{k},s'} \end{aligned} \quad (4.4.1)$$

$$\epsilon(\mathbf{k}) = 2t \left( p \cos(\mathbf{k} \cdot \mathbf{a}_1) + \cos(\mathbf{k} \cdot \mathbf{a}_2) + \cos(\mathbf{k} \cdot (\mathbf{a}_1 + \mathbf{a}_2)) \right) \quad (4.4.2)$$

$$g^x(\mathbf{k}) = \frac{\alpha_1}{2} \left[ \sin(\mathbf{k} \cdot (\mathbf{a}_1 + \mathbf{a}_2)) + \sin(\mathbf{k} \cdot \mathbf{a}_2) \right] \quad (4.4.3)$$

$$g^y(\mathbf{k}) = -\frac{\alpha_1}{\sqrt{3}} \left[ \sin(\mathbf{k} \cdot \mathbf{a}_1) + \frac{\sin(\mathbf{k} \cdot (\mathbf{a}_1 + \mathbf{a}_2)) - \sin(\mathbf{k} \cdot \mathbf{a}_2)}{2} \right] \quad (4.4.4)$$

$$g^z(\mathbf{k}) = \frac{2\alpha_2}{3\sqrt{3}} \left[ \sin(\mathbf{k} \cdot \mathbf{a}_1) + \sin(\mathbf{k} \cdot \mathbf{a}_2) - \sin(\mathbf{k} \cdot (\mathbf{a}_1 + \mathbf{a}_2)) \right] \quad (4.4.5)$$

where  $c_{\mathbf{k},s}^{(\dagger)}$  is the annihilation(creation) operator for a conduction electron whose momentum is  $\mathbf{k}$  and spin is  $s$ .  $\mu$  is the chemical potential,  $\Gamma_{\uparrow/\downarrow} = \pm\Gamma$  is the spin-dependent dissipation,  $p$  is the effect of the strain[87] and  $\boldsymbol{\sigma}$  are the Pauli matrices and  $\mathbf{g}$  represents the spin-orbit coupling. The lattice vectors are  $\mathbf{a}_1 = (1, 0)$  and  $\mathbf{a}_2 = (-1/2, \sqrt{3}/2)$ . We set  $\Gamma_s = 0$  except for Chapter. 4.7.2.

#### 4.4.2 One-dimensional Rice-Mele model with sublattice-dependent dissipation

We start from the Hermitian 1D Rice-Mele model, but assume that the dissipation depends on the sublattice. Such an effective non-Hermitian Hamiltonian can also be derived from the non-Hermitian matrix describing the single-particle Green function. The effective non-Hermitian Hamiltonian reads[101]

$$\mathcal{H}_{eff}(\mathbf{k}) = \sum_{a,b} \psi_a^\dagger \left( \tau^0 i\eta + \tau^x t \cos k + \tau^y \delta t \sin k + \tau^z (\Delta + i\Gamma) \right)_{ab} \psi_b, \quad (4.4.6)$$

where  $\psi_{A/B}^{(\dagger)}$  describes the annihilation (creation) operator in sublattice A/B,  $\tau$  represents the Pauli matrices,  $\eta$  is the average of the dissipation strength at each sublattice,  $t$  is an intra-lattice hopping,  $\delta t$  is an inter-lattice hopping,  $\Delta$  is the difference of the chemical potential between the sublattices, and  $\Gamma$  is the difference of the dissipation strength at each sublattice.

### 4.5 Difficulties describing dissipation effects in the reduced density matrix formalism

Having introduced the Green function technique based on a path integral derivation to calculate nonlinear transport, we can compare with different approaches and approximations made to calculate

the nonlinear response. The semi-classical Boltzmann equation and the RDM method are often used to calculate nonlinear responses. In these methods, the dissipation is usually introduced by the relaxation time approximation(RTA). In this section, we briefly introduce the RDM method. Being able to compare it with the Green function method, we can pinpoint the problems accompanying the RTA and explain in what situation RTA is justified. We note that the results by the semi-classical Boltzmann equation can also be obtained by the RDM results[102] so that we here consider only the RDM method. We briefly introduce the Boltzmann equation approach to nonlinear transport in the Appendix C.5.

### 4.5.1 Reduced Density Matrix Formalism

When ignoring two-body correlations, we can write the total density matrix of the lattice system as the tensor product of the reduced density matrices  $\rho_{tot}(t) = \prod_{\mathbf{k}} \otimes \rho_{\mathbf{k}}(t)$ . We can now describe the dynamics of the density matrix for each momentum  $\mathbf{k}$  under the electric field by using the von-Neumann equation, which reads

$$\frac{d}{dt}\rho_{\mathbf{k}}(t) = -i[\mathcal{H}, \rho_{\mathbf{k}}(t)] - (\rho(t) - \rho^{(0)})/\tau \quad (4.5.1)$$

$$\mathcal{H} = \mathcal{H}_0 + \mathcal{H}_E \quad (4.5.2)$$

$$\mathcal{H}_E = -q\mathbf{E} \cdot \mathbf{r}, \quad \mathbf{r} = -i\nabla_{\mathbf{k}}, \quad (4.5.3)$$

where we introduce the effect of dissipation by using the RTA,  $-(\rho(t) - \rho^{(0)})/\tau$ , and  $\rho^{(0)}$  describes the equilibrium state without the electric field. In the RDM formalism, we use the length gauge and describe the dynamics with the dipole Hamiltonian in Eq. (4.5.3). The density matrix under the velocity gauge can be obtained by using the transformation  $\rho_E = U\rho_A U^\dagger$ ,  $U = \exp[-iq\mathbf{A}(t) \cdot \mathbf{r}]$ , where  $\rho_{E/A}$  is the density matrix under the length/velocity gauge. We note again that results obtained by the length gauge are equivalent to those obtained under the velocity gauge without dissipation[106]. The recurrence equation of the  $n$ -th order density matrix  $\rho^{(n)}(t)$  about the electric field can be written as

$$\begin{aligned} \frac{d\rho^{(n)}(t)}{dt} &= -i[\mathcal{H}_0, \rho^{(n)}(t)] - i[\mathcal{H}_E, \rho^{(n-1)}(t)] - \gamma\rho^{(n)}(t) \\ &= -i\mathcal{L}\rho^{(n)}(t) + q\mathbf{E}(t) \cdot \nabla\rho^{(n-1)}(t) - \gamma\rho^{(n)}(t) \end{aligned} \quad (4.5.4)$$

$$F.T. \Leftrightarrow \rho_{\mathbf{k}}^{(n)}(\omega) = \frac{iqE^\mu(\omega_n)}{\omega - \mathcal{L} + i\gamma} \nabla_\mu \rho_{\mathbf{k}}^{(n-1)}(\omega - \omega_n), \quad (4.5.5)$$

where  $-i\mathcal{L}\rho = -i[\mathcal{H}_0, \rho]$ ,  $\gamma = 1/\tau$ ,  $\omega_n$  describes the frequency of the electric field which leads to the  $n$ -th order density matrix  $\rho^{(n)}$ ,  $E(\omega_n)$  is the Fourier component of  $E(t)$  and *F.T.* means Fourier transformation. In the length gauge, the current operator  $\mathcal{J}$  can be written as,

$$\mathcal{J} = q\dot{\mathbf{r}} = -iq[\mathbf{r}, \mathcal{H}] = q\nabla_{\mathbf{k}}\mathcal{H}, \quad (4.5.6)$$

and, therefore, the  $n$ -th order conductivity can be calculated by

$$\sigma_{\alpha;\{\alpha_i\}}^{(n)}(\omega; \{\omega_i\}) = \sum_{\mathbf{k}} \text{Tr} \left[ \mathcal{J}_{\alpha} \rho_{\mathbf{k}}^{(n)}(\omega) / \left( \prod_i E^{\alpha_i}(\omega_i) \right) \right]. \quad (4.5.7)$$

Detailed expressions can be found in Ref. [105, 109]. We note that the equations of the RDM method using RTA can be derived from the Green function technique in the DC-limit and in the dissipation-free limit for  $\omega_i \gg \epsilon_{nm}, \gamma$ . Details about this correspondence are given in the Appendix C.4. The RDM method introduced here is exact except for the RTA, and therefore, the necessary conditions we have listed above are caused by the RTA.

## 4.5.2 Velocity gauge vs Length gauge under the relaxation time approximation

In an isolated system without dissipation, physical quantities calculated by the velocity and length gauge are the same, which has been shown in Ref. [106]. In this subsection, we show that this correspondence between both gauges breaks down when using the RTA. The density matrix in each gauge can be written as [106]

$$\rho_E(t) = U \rho_A(t) U^\dagger, \quad U = \exp[-i\mathbf{A}(t) \cdot \mathbf{r}] \quad (4.5.8)$$

$$\begin{aligned} \rho_E^{(n)}(t) &= \rho_A^{(n)}(t) + \sum_{l=1}^n \left( \prod_{m=1}^l -iA^{\alpha_m}(t) \right) [r_{\alpha_l}, [r_{\alpha_{l-1}}, \dots [r_{\alpha_1}, \rho^{(n-l)}]]] \\ &= \rho_A^{(n)}(t) - i\mathbf{A}(t) \cdot [\mathbf{r}, \rho_A^{(n-1)}(t)] - \dots, \end{aligned} \quad (4.5.9)$$

where  $\rho_E(t)$  is the density matrix under the length gauge,  $\rho_A(t)$  is the density matrix under the velocity gauge, and  $\rho^{(n)}(t)$  represent the density matrix with the  $n$ -th order perturbation by the electric fields. By applying the RTA, the density matrices under both gauges change as  $\rho_{E/A}^{(n)}(t) \rightarrow \rho_{E/A}^{(n)}(t)e^{-\gamma t}$  when  $n \geq 1$ . The equality in Eq. (4.5.9) for the  $n = 1$ -order density matrix using the RTA becomes

$$\rho_E^1(t)e^{-\gamma t} \stackrel{?}{=} \rho_A^1(t)e^{-\gamma t} - i\mathbf{A}(t) \cdot [\mathbf{r}, \rho_A^{(0)}] \quad (4.5.10)$$

However, because  $\rho_A^{(0)}$  does not include dissipation, the equality in Eq. (4.5.10) has to break down.

One possible strategy to avoid this breakdown is to ignore the dissipation in the system and instead include photon dissipation or adiabatic switching as  $\mathbf{A}(t) \rightarrow \mathbf{A}(t)e^{-\gamma t}$ . In this case, the equality in Eq. (4.5.9) holds true. However, it gives different results from the RTA, especially in the regime  $\omega_i \ll \gamma$  [107]. When substituting  $\mathbf{A}(t) \rightarrow \mathbf{A}(t)e^{-\gamma t}$ , we do not consider the dissipation and scattering of electrons in the system. Thus, a current must not occur because there is no mechanism to change the momentum of electrons,  $\mathbf{k} \rightarrow \mathbf{k}'$ , and to induce a non-equilibrium steady-state

state. Therefore, when including dissipation of electrons by applying the RTA, a breakdown of the equality between the velocity gauge and the length gauge is inevitable. We note that, in the Green function method, this breakdown does not occur when we use  $G^R(\omega) = 1/(\omega - \mathcal{H} + i\gamma/2)$  and  $G^A(\omega) = 1/(\omega - \mathcal{H} - i\gamma/2)$  because it just supposes that the dissipation is constant in the absence of an electric field.

### 4.5.3 Problems of the relaxation time approximation in an AC electric field

In this part, we introduce the dissipation into the RDM method without using the RTA and show under which conditions the RTA is a good approximation. This analysis reveals the problems of using the RTA in an AC electric field. Finally, we compare the RDM using the RTA with the Green function formalism numerically.

The easiest way to introduce the dissipation microscopically is to couple the system with a dissipative bath. For the sake of simplicity, we consider the single-band case and the coupling Hamiltonian  $\mathcal{H}_c = \lambda(\psi_k^\dagger \mathcal{B} + h.c.)$ , where  $\mathcal{B}^{(\dagger)}$  is the annihilation(creation) operator in the dissipative bath. In that case, the dynamics of the system can be described by the quantum master equation, which reads

$$\frac{d}{dt}\rho_k^I(t) = -\int_{t_0}^t ds Tr_B \left( [\mathcal{H}_c^I(t), [\mathcal{H}_c^I(s), \rho_k^I(s) \otimes \rho_B]] \right) \quad (4.5.11)$$

where  $\rho_B$  is the density matrix of the bath and  $Tr_B$  corresponds to the trace over the bath degrees of freedom. The operators are in the interaction representation,

$$O^I(t) = T_{\leftarrow} \exp[i \int_{t_0}^t dt' \mathcal{H}(t')] O T_{\rightarrow} \exp[-i \int_{t_0}^t dt' \mathcal{H}(t')], \quad (4.5.12)$$

where  $\mathcal{H}(t) = \mathcal{H}_S(t) \otimes \mathcal{H}_B$ ,  $\mathcal{H}_S(t) = \mathcal{H}_0 - q\mathbf{E}(t) \cdot \mathbf{r}$  is the system Hamiltonian,  $\mathcal{H}_B$  is the bath Hamiltonian,  $T_{\rightarrow(\leftarrow)}$  represents the (anti-)time ordering operator. Although we take here the length gauge, the correspondence between the length and the velocity gauge holds exactly in this formulation as we will show in the next section. Equation (4.5.11) includes the dissipation term, the energy shift term, and the gain and loss terms which describe the dynamics of a particle leaving or entering the system. Here, we suppose that a particle that leaves the system loses the information about the acceleration due to the electric fields, and the electric fields do not accelerate the particles in the bath. Under this assumption, the gain and loss terms do not affect the dynamics of  $\rho^{(n)}$  ( $n \neq 0$ ), and therefore, they do not affect the conductivity. Now, we focus on the dissipation term and ignore the energy shift term. Then, Eq. (4.5.11) can be rewritten as

$$\frac{d}{dt} \left( \rho_k^I(t) \right)^{(n)} = -\lambda^2 \int_{t_0}^t ds Re \left[ \left\{ iG_B^I(t-s) \psi_k^{\dagger I}(t) \psi_k^I(s), \rho_k^I(s) \right\} \right]^{(n)}, \quad (4.5.13)$$

where  $G_B^I(t-s) = -iTr_B [\mathcal{B}^I(t) \mathcal{B}^{\dagger I}(s) \rho_B]$  and  $\{O, \rho\} = O\rho + \rho O^\dagger$ .

Now, we use the Markov approximation to simplify Eq. (4.5.13), in which we take the limit  $t_0 \rightarrow -\infty$  and approximate  $\rho_k^l(s) \simeq \rho_k^l(t)$ . The Markov approximation is justified when  $\lambda\tau_B \ll 1$ , where  $\tau_B$  is the relaxation time of the bath and  $G_B(t-s) \propto \exp[-(t-s)/\tau_B]$ . Under the Markov approximation, Eq. (4.5.13) can be rewritten as

$$\frac{d}{dt}\rho_k(t) = -i[\mathcal{H}, \rho_k(t)] - \lambda^2 \left( \int_0^\infty d(t-s) \text{Re} \left[ \{iG_B^l(t-s)\psi_k^\dagger U'(t,s)\psi_k U'^\dagger(t,s), \rho_k(t)\} \right] \right) \quad (4.5.14)$$

$$U'(t,s) = T_{\rightarrow} \exp \left[ -i \int_s^t dt' (\mathcal{H}_0 - q\mathbf{E} e^{i\omega_0 t'} \cdot \mathbf{r}) \right]. \quad (4.5.15)$$

Finally, we consider in what situation we can derive the RTA from Eq. (4.5.14). RTA should be a good approximation to describe transport when the integral in Eq. (4.5.14) becomes time-independent, thus, when  $U'(t,s)$  becomes a function of  $(t-s)$  or is constant. We see that in the DC limit  $\omega_0 \rightarrow 0$  or when the temperature of the bath is infinite and  $G_B(t-s) \propto \delta(t-s)$ , or when  $\omega_0$  is large enough so that  $q\mathbf{E} \cdot \mathbf{r}/\omega_0$  can be ignored, the integral ( $\int d(t-s) \sim$ ) becomes a constant and Eq. (4.5.1) can be derived from Eq. (4.5.14).

After having analyzed the validness of the RTA, we will now directly compare the linear and nonlinear (photogalvanic) optical conductivity calculated by the Green function method with the RDM using the RTA for a simple model. For this purpose, we use a model describing two-dimensional transition metal dichalcogenides (TMD) in which nonlinear optical response has been discussed in the literature [87, 110, 111]. Details about how to perform the numerical calculations is given in Appendix C.6.

The numerical results of the optical conductivity by the RDM method using the RTA and by the Green function method are shown in Fig. 4.1. For the linear optical conductivity, the results of both methods agree with each other over the full frequency range. On the other hand, for the nonlinear optical conductivity, the results only match in the DC limit, and for large frequencies,  $\omega_i \gg \gamma$ , as has been discussed above. We thus find that while RTA is a good approximation for the linear optical conductivity, it leads to severe problems for the nonlinear optical conductivity except in the DC limit and for  $\omega_i \gg \gamma$ . Again, we note that the RTA supposes that all non-equilibrium states decay equally by  $\gamma$ . On the other hand, the Green function method only assumes that the dissipation is constant in the absence of an electric field. The RTA is a more severe approximation, which affects nonlinear responses. We note that the relaxation time in most materials is usually about  $1 \sim 100$  [ps] [112]. Thus, when analyzing a Terahertz laser as input force,  $\omega_i \tau \sim 1$ , and the error of the RTA becomes large.

#### 4.5.4 Gauge invariance with the dissipation in quantum master equation formalism

In this section, we analyze the correspondence between the length gauge and the velocity gauge in the quantum master equation in Eq. (4.5.14) in the main text. By using Eq. (4.5.8), we can describe

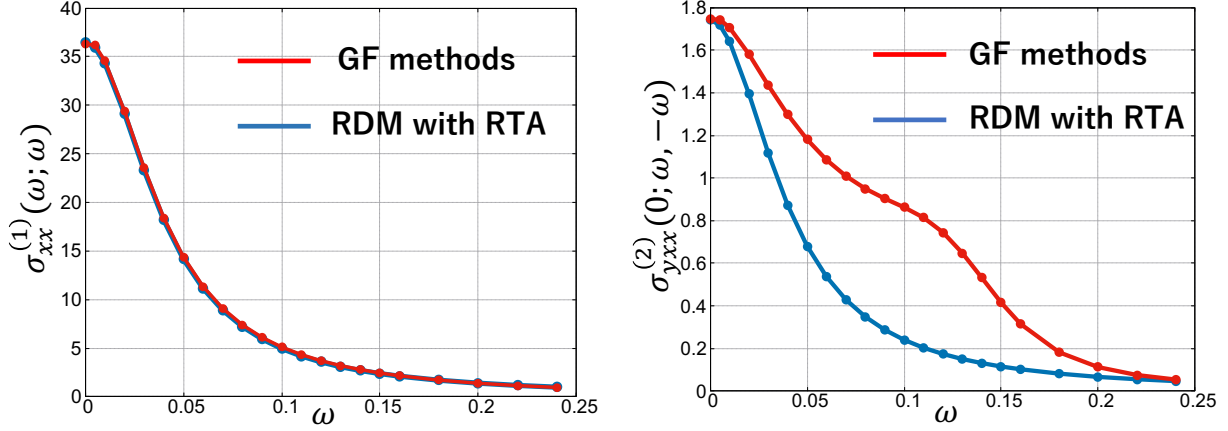


Figure 4.1: Comparison between the RDM method using RTA (blue) and the Green function method (red) for the linear (left panel) and nonlinear (right panel) optical conductivities, which is the photogalvanic effect. The parameters for the monolayer TMD model are  $t = 0.5$ ,  $\mu = 0.7$ ,  $p = 0.7$ ,  $\alpha_1 = 0.08$ ,  $\alpha_2 = 0.06$ ,  $\delta = 0.7$ ,  $\gamma = 0.05$ ,  $T = 0.02$ .

Eq. (4.5.13) under the velocity gauge as

$$\begin{aligned}
& \frac{d}{dt} \rho_{Ak}(t) + i[q\mathbf{E} \cdot \mathbf{r}, \rho_{Ak}(t)] \\
& = -i[\mathcal{H}_0(\mathbf{k} - q\mathbf{A}) - q\mathbf{E} \cdot \mathbf{r}, \rho_{Ak}(t)] \\
& \quad - \lambda^2 \int_{t_0}^t ds \left( \text{Re} \left[ \left\{ iG_B^L(t-s) \psi_k^\dagger \tilde{U}(t,s) \psi_k, \rho_{Ak}(s), \tilde{U}^\dagger(t,s) \right\} \right] \right)^{(n)} \quad (4.5.16)
\end{aligned}$$

$$\tilde{U}(t,s) = T_{\rightarrow} U^{-1}(t) \exp[-i \int_s^t dt' (\mathcal{H}_0 - q\mathbf{E}(t') \cdot \mathbf{r})] U(s) \quad (4.5.17)$$

where  $\{O_1, \rho, O_1\} = O_1 \rho O_2 + O_2^\dagger \rho O_2^\dagger$ . If we can show that  $T_{\rightarrow} \tilde{U}(t,s) = \exp[-i \int_s^t \mathcal{H}_0(\mathbf{k} - q\mathbf{A}(t))]$ , the second term on the right side in Eq. (4.5.16) can be written in the interaction representation in the velocity gauge Hamiltonian and the gauge invariance holds true in the open system. This can

be verified by calculating the  $s$ - and  $t$ -derivative of  $\tilde{U}(t, s)$  as

$$\begin{aligned}
\frac{\partial}{\partial t} \tilde{U}(t, s) &= U^{-1}(t) \left\{ -iq\mathbf{E}(t) \cdot \mathbf{r} - i(\mathcal{H}_0(\mathbf{k}) - q\mathbf{E}(t) \cdot \mathbf{r}) \right\} \\
&\quad \times \exp[-i \int_s^t dt' (\mathcal{H}_0 - q\mathbf{E}(t') \cdot \mathbf{r})] U(s) \\
&= U^{-1}(t) \left( -i\mathcal{H}_0(\mathbf{k}) \right) \exp[-i \int_s^t dt' (\mathcal{H}_0 - q\mathbf{E}(t') \cdot \mathbf{r})] U(s) \\
&= -i\mathcal{H}_0(\mathbf{k} - q\mathbf{A}(t)) \tilde{U}(t, s) \tag{4.5.18}
\end{aligned}$$

$$\frac{\partial}{\partial s} \tilde{U}(t, s) = \tilde{U}(t, s) \left( i\mathcal{H}_0(\mathbf{k} - q\mathbf{A}(s)) \right) \tag{4.5.19}$$

$$\tilde{U}(t, t) = 1. \tag{4.5.20}$$

We use the relation  $U^{-1}(t)\mathcal{H}_0(\mathbf{k})U(t) = \mathcal{H}(\mathbf{k} - q\mathbf{A}(t))$  to derive Eq. (4.5.18) and Eq. (4.5.19). From the equality in Eq. (4.5.18), Eq. (4.5.19), and Eq. (4.5.20), we can identify  $\tilde{U}(t, s) = T_{\rightarrow} \exp[-i \int_s^t dt' \mathcal{H}_0(\mathbf{k} - q\mathbf{A}(t'))]$ . Therefore, the correspondence between the length gauge and the velocity gauge holds true in the quantum master equation, while it is broken when introducing the RTA at finite frequency.

## 4.6 Extension of the reduced density matrix formalism to interacting system

Having derived the Green function method for nonlinear responses, we are able to extend the RDM method to interacting systems, mainly in the DC limit, and reproduce the results of the Green function method. For free electron systems, we use  $\rho_{\mathbf{k}}^{(0)} = \sum_n f(\epsilon_n(\mathbf{k})) |n\rangle \langle n|$ . However, when we consider interacting systems, the pole of the Green function includes the information of the quasi-particle's energy level, and therefore, the density matrix can be written as

$$\rho_{\mathbf{k}}^{(0)} = \int \frac{d\omega}{2\pi i} \sum_n |n\rangle \langle n| \left( G_n^A(\omega) - G_n^R(\omega) \right) f(\omega) \tag{4.6.1}$$

$$= \int \frac{d\omega}{2\pi i} \sum_{\alpha\beta} |\alpha\rangle \langle \beta| \left( G^A(\omega) - G^R(\omega) \right)_{\alpha\beta} f(\omega), \tag{4.6.2}$$

where  $|\alpha\rangle, \langle\beta|$  are states of an arbitrary basis, and  $(\ )_{\alpha\beta}$  represent the elements of the Green function in this basis. We note that we again omit the momentum-dependence of the Green function. Here, we can choose a momentum-independent basis,  $\partial_{\alpha} |\alpha\rangle = 0$ . In this case, the correction of the density matrix by the electric fields only affects the Green function matrices because  $f(\omega)$  does not



depend on  $\mathbf{k}$ . Therefore, the density matrix corrected by  $n$ -th order electric fields can be written as

$$\left(\rho_{\mathbf{k}}^{(n)}\right)_{\alpha\beta} = \int \frac{d\omega}{2\pi i} \sum_{l=0}^n \left( G^{R(l)}(\omega) \left( (G^{R(0)}(\omega))^{-1} - (G^{A(0)}(\omega))^{-1} \right) f(\omega) G^{A(n-l)}(\omega) \right)_{\alpha\beta}. \quad (4.6.3)$$

Although we need the Green function corrected by the  $n$ -th order of the electric field, we can easily derive an equation for this using the RDM method. Here, we note that in Chapter.2[12], we have shown that the dynamics of the matrix elements  $\rho_{\mathbf{k},\alpha}^G(0) = |\mathbf{k}, \alpha\rangle \langle 0|$  corresponds to the retarded Green function  $G^R(\mathbf{k})$ , which reads

$$G_{\alpha\beta}^R(t) = -i\theta(t)\text{Tr}\left[\left(\psi_{\alpha}(t)\psi_{\beta}^{\dagger} + \psi_{\beta}^{\dagger}\psi_{\alpha}(t)\right)\rho_{\mathbf{k}}^{(0)}\right] \quad (4.6.4)$$

$$= -i\text{Tr}\left[\psi_{\alpha}\rho_{\beta}^G(t)\right], \quad (4.6.5)$$

where  $\rho_{\mathbf{k}\beta}^G(0) = \psi_{\beta}^{\dagger}\rho_{\mathbf{k}}^{(0)} + \rho_{\mathbf{k}}^{(0)}\psi_{\beta}^{\dagger} = |\mathbf{k}, \beta\rangle \langle 0|$  and the dynamics of  $\rho^G$  can be described[12] as

$$\frac{d}{dt}\rho_{\mathbf{k}}^{GI}(t) = -\int_{t_0}^t ds i\Sigma^{RI}(t-s)\rho_{\mathbf{k}}^{GI}(s) \quad (4.6.6)$$

$$\frac{d}{dt}\rho_{\mathbf{k}}^G(t) = -i[\mathcal{H}_0 + \mathcal{H}_E, \rho_{\mathbf{k}}^G(t)] - \int_{t_0}^t ds i\Sigma^R(t-s) \left( \sum_{n=0}^{\infty} \frac{(iq(t-s)\mathbf{E} \cdot \mathbf{r})^n}{n!} \right) \rho_{\mathbf{k}}^G(s) \quad (4.6.7)$$

$$\rho_{\mathbf{k}}^{G(n)}(\omega) = \frac{iq\mathbf{E}}{\omega - (\mathcal{H}_0 + \Sigma^R(\omega))} \left\{ \left(1 - \frac{\partial\Sigma^R}{\partial\omega}\right) \nabla \rho_{\mathbf{k}}^{G(n-1)}(\omega) + \sum_{m=2}^{\infty} \frac{1}{m!} \frac{\partial^m \Sigma^R}{\partial\omega^m} (-iq\mathbf{E} \cdot \nabla)^m \rho_{\mathbf{k}}^{G(n-m)}(\omega) \right\}. \quad (4.6.8)$$

To derive Eq. (4.6.7), we approximate  $U'(t, s) \simeq \exp[-i\mathcal{H}_0(t-s)] \exp[-iq\mathbf{E} \cdot \mathbf{r}(t-s)]$  in the dissipation term, which should correspond to ignoring the vertex correction. By using this equation,  $G^{R(1)}(\omega)$  (the first-order correction of an electric field to the single-particle Green function) can be derived as

$$\begin{aligned} \left(G^{R(1)}(\omega)\right)_{\alpha\beta} &= iE^{\mu} \left( G^{R(0)}(\omega) \left(1 - \frac{\partial\Sigma^R}{\partial\omega}\right) G^{R(0)}(\omega) \mathcal{J}_{\mu} G^{R(0)}(\omega) \right)_{\alpha\beta} \\ &= -iE^{\mu} \left( \frac{\partial G^{R(0)}}{\partial\omega} \mathcal{J}_{\mu} G^{R(0)}(\omega) \right)_{\alpha\beta}, \end{aligned} \quad (4.6.9)$$

By inserting Eq. (4.6.9) into Eq. (4.6.3), we can derive the equation for the linear conductivity as given by the path integral method in Eq. (4.2.15). We can also calculate the higher-order DC conductivity in the same way. We note that using the RDM methods might be easier than the path integral methods for higher-order DC conductivities. However, in the AC case, it is hard to derive an equation equivalent to Eq. (4.6.8) so that the path integral method should be used.

## 4.7 Correlation effects on the nonlinear response

Finally, we use the Green function formalism and analyze the effect of renormalization and different lifetimes in different orbitals, which have not been considered in previous studies. We reveal that both effects can enhance the nonlinear conductivity.

### 4.7.1 Renormalization effect

Intuitively, the renormalization effect seems to be a disadvantage for obtaining a large conductivity because it decreases the Fermi velocity. However, as the density of states might be enhanced by the renormalization at the Fermi surface, one should properly analyze how the renormalization affects the linear and the nonlinear conductivities.

First, we analyze the simple case where  $\Sigma^R(\omega) \simeq \Sigma_0^R + \alpha\omega\mathbf{1}$ . Under this approximation, the Green function can be written as

$$\begin{aligned} G^{R-1}(\omega) &= \omega - \mathcal{H}_0 - \Sigma^R(\omega) \simeq (1 - \alpha)\omega - \mathcal{H}'_0 \\ &\equiv G'^{R-1}(Z^{-1}\omega), \end{aligned} \quad (4.7.1)$$

where  $Z^{-1} = 1 - \alpha$ ,  $\mathcal{H}'_0 = \mathcal{H}_0 + \Sigma_0^R$ , and  $G'^{R-1}(\omega) = \omega - \mathcal{H}'_0$ . We can now analyze the effect of the renormalization on the conductivities calculated by the Green function method. By the variable transformation  $Z^{-1}\omega \rightarrow \omega'$  and  $Z^{-1}\omega_i \rightarrow \omega'_i$ , the functions which appear in the linear and nonlinear conductivities change as follows

$$G^{R/A}(\omega) = G'^{R/A}(\omega') \quad (4.7.2)$$

$$f(\omega) \simeq \theta(-\omega) = \theta(-\omega') \simeq f(\omega') \quad (4.7.3)$$

$$\frac{\partial f(\omega)}{\partial \omega} \simeq \delta(\omega) = Z^{-1}\delta(\omega') = \frac{\partial f(\omega')}{\partial \omega'} \quad (4.7.4)$$

$$\frac{\partial G^R(\omega)}{\partial \omega} = Z^{-1} \frac{\partial G^R(\omega')}{\partial \omega'} \quad (4.7.5)$$

$$d\omega = Zd\omega' \quad \frac{1}{\omega_i} = \frac{Z^{-1}}{\omega'_i}, \quad (4.7.6)$$

where the equality in Eq. (4.7.3) and (4.7.4) are justified at zero temperature. By inserting the above equations into Eq. (4.2.14) and Eq. (4.2.16), we can derive  $\sigma^{(2)} = Z^{-1}\sigma'^{(2)}$  in both the AC and the DC case, where  $\sigma'$  is the conductivity described by  $\omega', \omega'_i, G'^{R/A}(\omega')$ , which includes the energy shift by  $\Sigma_0^R$ . We note that we should compare the renormalized conductivity  $\sigma^{(n)}(\omega; \{\omega_i\})$  with  $\sigma'^{(n)}(\omega'; \{\omega'_i\}) = \sigma'^{(n)}(Z^{-1}\omega; \{Z^{-1}\omega_i\})$  in the AC case. In the optical conductivity, the interband contribution becomes large when  $\omega_i \simeq \epsilon_{nm}$ . In order to focus on the same interband transition, we set the frequency  $Z^{-1}\omega$  for the renormalized band. We can generalize this analysis for higher order conductivities and find

$$\sigma^{(n)}(\omega; \{\omega_i\}) \simeq Z^{-(n-1)}\sigma'^{(n)}(\omega'; \{\omega'_i\}). \quad (4.7.7)$$

By remembering that  $Z^{-1} > 1$  holds for correlated systems around the Fermi energy, we conclude that the renormalization effect enhances the higher-order nonlinear conductivity more strongly, while it does not affect the linear conductivity.

Using the Green function technique, we can easily confirm our general discussion above by calculating the linear and the nonlinear optical conductivity for the monolayer TMD model. The results for these calculations using an unrenormalized band ( $Z = 1$ ) and a renormalized band ( $Z = 0.2$ ) are shown in Fig. 4.2. As we have derived analytically, the numerical results confirm that the nonlinear optical response is strongly enhanced by the renormalization effect, while the linear optical response is not enhanced. We note that the renormalized nonlinear optical conductivity is not as strongly enhanced as predicted ( $Z^{-1}\sigma^{(2)}(0; -\omega, \omega)$ ) in Fig. 4.2, which can be attributed to a finite temperature,  $T = 0.02$ , where the Fermi-function does not correspond to the step-function.

## 4.7.2 Different lifetimes in different orbitals

In this section, we analyze the effect of different lifetimes in different orbitals, which is not considered within the RTA. We note that there is the study by Kaplan *et al.* [113, 114], where the authors analyze the effect of different lifetimes on the nonlinear response, assuming that the conventional band-index representation is justified.

When using the RTA, the non-Hermitian (dissipation) term is described by the identity matrix. Therefore, the eigenvectors are the same as that of the Hermitian Hamiltonian. However, when different lifetimes are present in different orbitals, as in a material consisting of strongly correlated electrons coupled to weakly correlated electrons, the eigenvectors are distinct from the Hermitian case. The eigenvectors are then determined by the effective non-Hermitian Hamiltonian, which describes the single-particle Green function. In that case, the conventional band-index representation breaks down, and one should use a non-Hermitian band-index. In this section, we first derive the non-Hermitian band-index and then analyze its effect.

### 4.7.2.1 Band index representation using an effective non-Hermitian Hamiltonian

In this chapter, we suppose that the effective non-Hermitian Hamiltonian can be diagonalized. We note that, in general, there are situations when a non-Hermitian Hamiltonian cannot be diagonalized, which generates novel and interesting phenomena[4, 7, 10, 11, 23, 51]. For a non-Hermitian Hamiltonian, its left eigenstates are different from its right eigenstates, while in the Hermitian case they correspond to each other by Hermitian conjugation. By describing the left and right eigenstates as  $\langle n_L | \mathcal{H} = \epsilon_n \langle n_L |$ ,  $\mathcal{H} | n_R \rangle = \epsilon_n | n_R \rangle$ , the following equations are satisfied:

$$\langle n_L | m_R \rangle = \langle n_R | m_L \rangle = \delta_{nm} \quad (4.7.8)$$

$$\mathbf{1} = \sum_n | n_R \rangle \langle n_L | = \sum_n | n_L \rangle \langle n_R |, \quad (4.7.9)$$

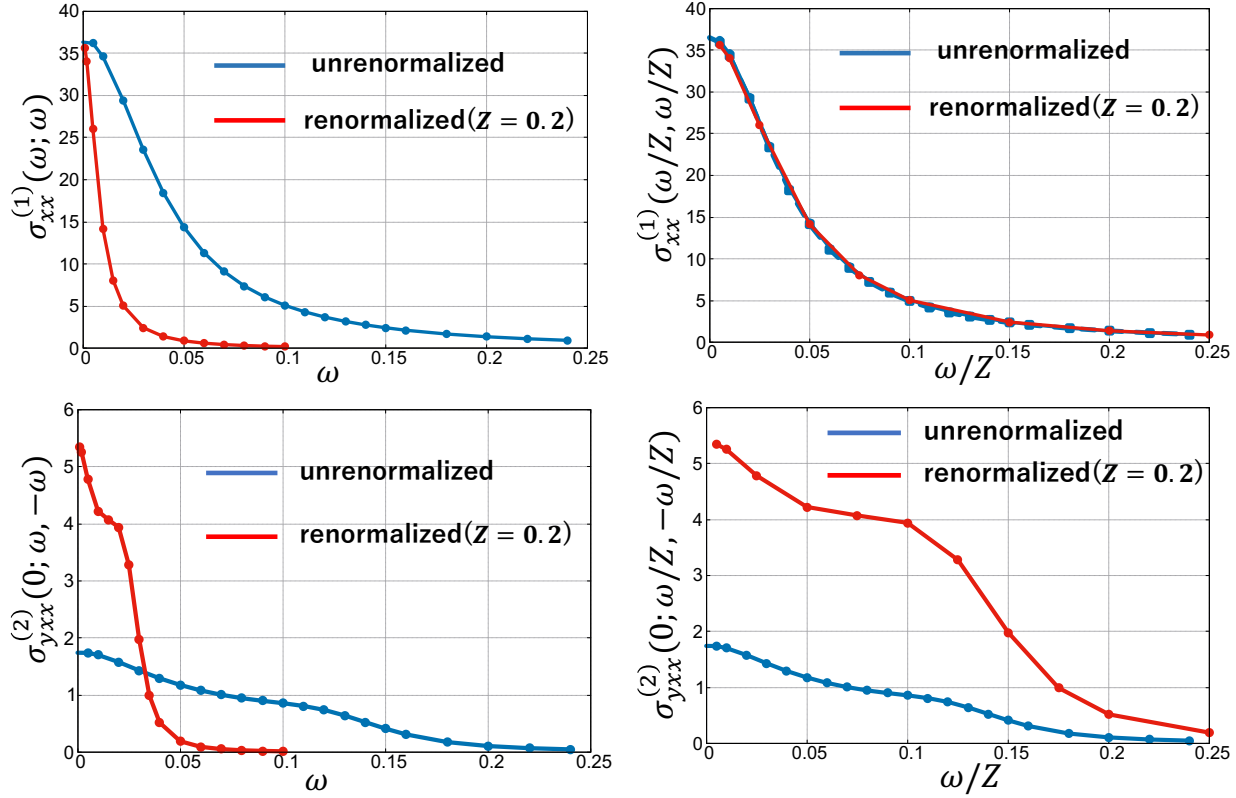


Figure 4.2: Renormalization effect on the linear and nonlinear optical conductivity for the monolayer TMD model – The upper figures show the linear optical conductivity, and the lower figures show the second-order nonlinear optical conductivity (Photogalvanic effect) using an unrenormalized (blue lines) and a renormalized (red lines) band. In the right figures, we use input frequencies normalized by the renormalization factor. The parameters are  $t = 0.5$ ,  $\mu = 0.7$ ,  $p = 0.7$ ,  $\alpha_1 = 0.08$ ,  $\alpha_2 = 0.06$ ,  $\delta = 0.7$ ,  $\gamma = 0.05$ ,  $T = 0.02$ ,  $Z = 1$  or  $0.2$ . The details about how to perform the numerical calculations are written in Appendix C.6.

where  $\langle n_R | = (|n_R\rangle)^\dagger$  and  $|m_L\rangle = (\langle m_L |)^\dagger$ . We note that  $\langle n_R | \neq \langle n_L |$  and  $\langle n_R | m_R \rangle \neq \delta_{nm}$ . In Eq. (4.7.8) and (4.7.9), we can construct the orthonormal basis by the left and right eigenstate, and we represent the Green functions by the band index as

$$\mathcal{H}_{nm}(\mathbf{k}) \equiv \langle n_L | \mathcal{H}(\mathbf{k}) | m_R \rangle = \delta_{nm} \epsilon_m \quad (4.7.10)$$

$$G_{nm}^R(\omega, \mathbf{k}) \equiv \langle n_L | G^R(\omega, \mathbf{k}) | m_R \rangle = \frac{\delta_{nm}}{(\omega - \epsilon_m)} \quad (4.7.11)$$

$$G_{nm}^A(\omega, \mathbf{k}) \equiv \langle n_R | G^R(\omega, \mathbf{k}) | m_L \rangle = \frac{\delta_{nm}}{(\omega - \epsilon_m^*)}, \quad (4.7.12)$$

where  $\mathcal{H} = \mathcal{H}_0 + \Sigma^R$  includes the lifetime of the particles and is thus a non-Hermitian operator. In the following, we consider the effect of non-Hermiticity on the conductivity through the non-Hermitian band-index representation.

#### 4.7.2.2 Non-Hermitian effect on the conductivity

First, we consider the linear conductivity using the non-Hermitian band-index representation, which reads,

$$\begin{aligned} \mathcal{K}_{\alpha\beta}^{(1)}(\omega_1) = & \sum_{n,m} \left\{ \int_{-\infty}^{\infty} \frac{d\omega}{2\pi} \text{Im} \left[ \mathcal{J}_{LR;\alpha\beta}^{nm} G_n^R(\omega) \right] f(\omega) \right. \\ & + \int_{-\infty}^{\infty} \frac{d\omega}{2\pi i} \left[ \mathcal{J}_{LR;\alpha}^{nm} G_m^R(\omega + \omega_1) \mathcal{J}_{LR;\beta}^{mn} G_n^R(\omega) - \mathcal{J}_{RR;\alpha}^{nm} G_m^R(\omega + \omega_1) \mathcal{J}_{LL;\beta}^{mn} G_n^A(\omega) \right. \\ & \left. \left. + \mathcal{J}_{RR;\alpha}^{nm} G_m^R(\omega) \mathcal{J}_{LL;\beta}^{mn} G_n^A(\omega - \omega_1) - \mathcal{J}_{RL;\alpha}^{nm} G_m^A(\omega) \mathcal{J}_{RL;\beta}^{mn} G_n^A(\omega - \omega_1) \right] f(\omega) \right\}, \end{aligned} \quad (4.7.13)$$

where  $\mathcal{J}_{AB;i}^{mn} = \langle m_A | \mathcal{J}_i | n_B \rangle$ . In the DC-limit, this becomes

$$\begin{aligned} \sigma_{DC;\alpha\beta}^{(1)} = & 2 \int_{-\infty}^{\infty} \frac{d\omega}{2\pi} \left( -\frac{\partial f(\omega)}{\partial \omega} \right) \text{Re} \left[ \mathcal{J}_{RR;\alpha}^{nm} G_m^R(\omega) \mathcal{J}_{LL;\beta}^{mn} G_n^A(\omega) \right] \\ & - f(\omega) \text{Re} \left[ \mathcal{J}_{LR;\alpha}^{nm} \frac{\partial G_m^R(\omega)}{\partial \omega} \mathcal{J}_{LR;\beta}^{mn} G_n^R(\omega) \right]. \end{aligned} \quad (4.7.14)$$

In the non-Hermitian band-index representation, four different types of velocity operators appear, which are  $\mathcal{J}_{LL}, \mathcal{J}_{LR}, \mathcal{J}_{RL}, \mathcal{J}_{RR}$ . We note that the conventional velocity operator in the Hermitian case corresponds to  $\mathcal{J}_{LR}$  and  $\mathcal{J}_{RL}$ .  $\mathcal{J}_{LL}$  and  $\mathcal{J}_{RR}$  are unique in the Fermi surface contribution to transport in a non-Hermitian system. In order to compare to the conventional results, we can write  $\mathcal{J}_{LL/RR}$  by  $\mathcal{J}_{LR}$  as

$$\mathcal{J}_{LL}^{nm} = \sum_l \mathcal{J}_{LR}^{nl} \langle l_L | m_L \rangle \quad (4.7.15)$$

$$\mathcal{J}_{RR}^{nm} = \sum_l \mathcal{J}_{LR}^{lm} \langle n_R | l_R \rangle \quad (4.7.16)$$

By using this relation, the Fermi surface term in Eq. (4.7.14) can be rewritten as

$$\begin{aligned}
& \text{Re} \left[ \mathcal{J}_{RR;\alpha}^{nm} G_m^R(\omega) \mathcal{J}_{LL;\beta}^{mn} G_n^A(\omega) \right] \\
&= \text{Re} \left[ \langle n_L | n_L \rangle \langle n_R | n_R \rangle \mathcal{J}_{LR;\alpha}^{nm} G_m^R(\omega) \mathcal{J}_{LR;\beta}^{mn} G_n^A(\omega) \right] \\
&+ \text{Re} \left[ \langle l_L | n_L \rangle \langle n_R | l'_R \rangle \mathcal{J}_{LR;\alpha}^{lm} G_m^R(\omega) \mathcal{J}_{LR;\beta}^{ml'} G_n^A(\omega) \right]. \tag{4.7.17}
\end{aligned}$$

We note that the term including  $\partial f(\omega)/\partial\omega$  is called as "the Fermi surface term." The first term is the conventional term multiplied by the factor  $\gamma_{NH;n} \equiv \langle n_L | n_L \rangle \langle n_R | n_R \rangle$ . We can easily show that  $\gamma_{NH;n} \geq 1$  is always satisfied. (See appendix C.7.) Therefore, we reveal that, when the system is described by a non-Hermitian Hamiltonian, with different lifetimes in different orbitals, the conventional Fermi surface term can be enhanced by the factor  $\gamma_{NH;n}$ . The second term is unique in the non-Hermitian band-index representation, which describes the mixture of eigenstates in the decay dynamics. We call this term "band-coalescent term" in this chapter. For the second-order conductivity, we perform the same analysis and find

$$\begin{aligned}
& \sum_{l,m,n} \gamma_{NH;n} \mathcal{J}_{LR;\alpha}^{nl} \frac{\partial G_l^R(\omega)}{\partial\omega} \mathcal{J}_{LR;\beta}^{lm} G_m^R(\omega) \mathcal{J}_{LR;\gamma}^{mn} G_n^A(\omega) \\
&+ \sum_{l,m,n} \sum_{k,k'(\neq n)} \langle k'_L | n_L \rangle \langle n_R | k_R \rangle \mathcal{J}_{LR;\alpha}^{kl} \frac{\partial G_l^R(\omega)}{\partial\omega} \mathcal{J}_{LR;\beta}^{lm} G_m^R(\omega) \mathcal{J}_{LR;\gamma}^{mk'} G_n^A(\omega), \tag{4.7.18}
\end{aligned}$$

where the first term is the conventional term with non-Hermitian factor and the second term describes the band-coalescent term for nonlinear conductivity. Finally, we numerically check these results and how the non-Hermiticity changes the conventional terms and the band-coalescent terms by explicitly calculating the linear and nonlinear conductivity for two different models, including orbital(sublattice) dependent lifetimes. First, we show the results for the one-dimensional non-Hermitian Rice-Mele model, in which the dissipation depends on the sub-lattice. Here, we note that  $\Gamma$  denotes the difference of the dissipation strength at each sublattice. The upper panels in Fig. 4.3 show the  $\Gamma$ -dependence of the linear and nonlinear DC-conductivity in the non-Hermitian Rice-Mele model. We see that the conventional conductivity with the non-Hermitian factor is dominant for the linear conductivity, while the band-coalescent term is dominant for the nonlinear conductivity. We note that the band-coalescent term can be determined by subtracting the conventional term from the total conductivity.

Next, we analyze the monolayer TMD model with uniaxial strain and spin-dependent scattering rates, where  $\Gamma_{\uparrow/\downarrow} = \pm\Gamma$ . The lower panels in Fig. 4.3 show that the conventional conductivity with the non-Hermitian factor is dominant for the linear conductivity, while the band-coalescent term prevails for the nonlinear conductivity. Notably, the sign of the nonlinear conductivity changes due to the non-Hermitian effect, and the absolute value is strongly enhanced. We note that the small spike in the conventional term of the nonlinear Hall conductivity originates from numerical errors

due to exceptional points. The non-Hermitian band-index is very sensitive in parameter regions, including exceptional points, where the non-Hermitian Hamiltonian cannot be diagonalized.

Although we have analyzed the effect of different lifetimes in orbitals(sublattices) in two specific models, it seems to be clear that the non-Hermitian effect on nonlinear responses is highly model-dependent. Our results, however, suggest that non-Hermiticity due to a difference of lifetimes in orbitals(sublattices) can strongly enhance nonlinear transport. This enhancement of nonlinear responses should also become important for correlated materials, where the self-energy depends on the orbital and atom.

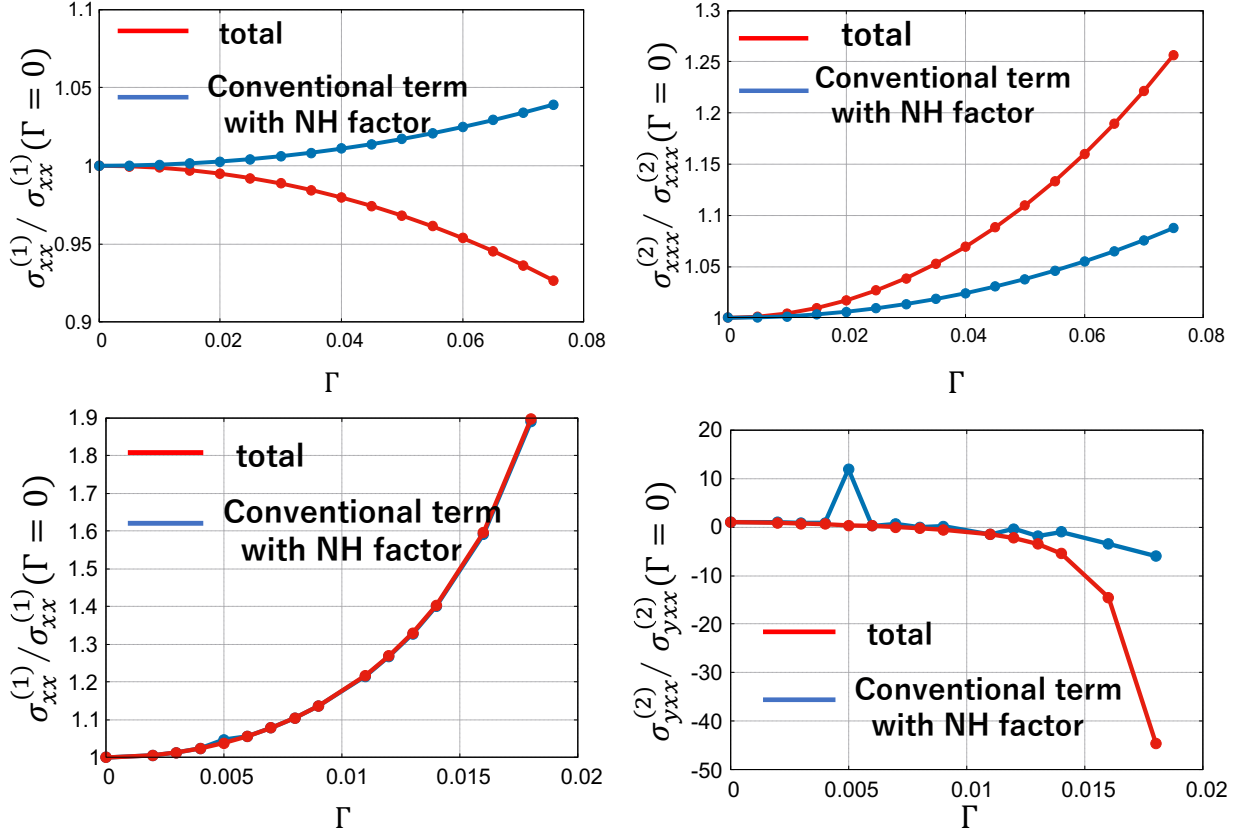


Figure 4.3:  $\Gamma$ -dependence of the linear and non-linear conductivities in the non-Hermitian Rice-Mele model and the the monolayer TMD materials under uniaxial strain – The upper figures show the linear conductivity and the non-reciprocal conductivity in the 1D Rice-Mele model, and the lower figures depict the linear conductivity and the non-linear Hall conductivity in the monolayer TMD model under uniaxial strain. The blue lines represent the original terms (also appearing in the Hermitian model) now modified by the non-Hermitian factor as in Eq. (4.7.18). The red lines describe the total conductivity which is the sum of the conventional term with non-Hermitian factor and the band-coalescent term.. The parameters are  $t = 1.0$ ,  $\delta t = 0.3$ ,  $\Delta = 0.3$ ,  $\eta = 0.05$ ,  $T = 0.02$  for the 1D Rice-Mele model, and  $t = 0.5$ ,  $\mu = 0.7$ ,  $p = 0.7$ ,  $\alpha_1 = 0.08$ ,  $\alpha_2 = 0.06$ ,  $\delta = 0.7$ ,  $\eta = 0.05$ ,  $T = 0.02$  for the monolayer TMD model. The normalization coefficients are  $\sigma_{xx}^{(1)}(\Gamma = 0) = 0.0801$ ,  $\sigma_{xxx}^{(2)}(\Gamma = 0) = -0.0160$  in the Rice-Mele model and  $\sigma_{xx}^{(1)}(\Gamma = 0) = 36.21$ ,  $\sigma_{yxx}^{(2)}(\Gamma = 0) = 1.417$  in the monolayer TMD model.



# Chapter 5

## Conclusion

In this thesis, we have investigated the non-Hermitian physics in strongly-correlated electron systems. We have especially focused on the relationship between OQS and SCES from the non-Hermitian point of view, and the phenomena induced by the unique properties in non-Hermitian systems, such as exceptional points and the non-orthogonality.

In Chapter 2, by analyzing the Hubbard model as an OQS, we have proved that the effective NHH appearing in the context of OQS and equilibrium Green functions are identical. We have demonstrated that the spectral function of a single particle described as an OQS is given by the same non-Hermitian Hamiltonian describing the density matrix of the particle under postselection. Thus, non-Hermitian phenomena that have been analyzed in the dynamics of a system under postselection can also be studied by analyzing spectral functions both in OQS and SCES without postselection. We have also shown that postselection is not necessary to derive a NHH from the spectral function, because off-diagonal elements govern the dynamics of the spectral function, and gain and loss contributions automatically vanish. In the process of deriving the QME for a single particle, we have succeeded in showing that Feynman diagrams, e.g., representing the self-energy, describe the non-Markovian dynamics of a fermionic system coupled to a fermionic bath. This technique might also be applied to other systems, such as QuBits coupled to fermionic baths. Finally, we have demonstrated the importance of non-Markovian dynamics to describe the dynamics in the strongly correlated regime.

In Chapter 3, we have shown a relation between the Kondo temperature and the emergence of exceptional points at the Fermi energy in  $f$ -electron materials. Particularly, we have studied the Kondo insulator and the metallic state with a local hybridization, and the semimetallic state with a  $p$ -wave hybridization in the 2D periodic Anderson model by DMFT/NRG. Around the Kondo temperature,  $f$ -electrons change from localized to itinerant when lowering the temperature. Thus, the emergence of EPs at the Fermi surface is a sign for the crossover between localized and itinerant  $f$ -electrons. We have also shown that the exceptional manifolds have a one more higher dimensional structure when considering the  $\omega$ -dependence of the effective Hamiltonian. For the system with the local hybridization, there are exceptional loops above and below  $\omega = 0$  in the  $(\mathbf{k}, \omega)$ -space

at high temperature, which merge and disappear around the Kondo temperature. For the  $p$ -wave hybridization, there are four exceptional loops each above and below  $\omega = 0$  in the  $(\mathbf{k}, \omega)$ -space at high temperature, which merge and change their topology around the Kondo temperature. Contrary to the system with local hybridization, these exceptional manifolds at the Fermi energy are stable for a wide range of temperatures below the Kondo temperature and these EPs are connected by bulk Fermi arcs.

We can naturally expect that the relation between the emergence of exceptional points at the Fermi energy and the Kondo temperature hold for three-dimensional systems because the DMFT results become more accurate for higher dimensions. Because the band structure of the 3D system can be understood by stacking 2D systems, the 3D f-electron material should host robust exceptional rings in the case of a momentum dependent hybridization and exceptional surfaces in the case of a local hybridization at the Fermi energy.

In Chapter 4, we have constructed a formalism based on the Green functions to calculate the nonlinear response at finite temperature and generally analyze the impact of correlations on nonlinear response. By using a formalism based on the Green functions, correlations and electron scattering can be easily included via the self-energy. Previous studies on nonlinear response mainly focused on noninteracting systems using the semi-classical Boltzmann equation and the reduced density matrix formalism. In these methods, dissipation, which is necessary for the generation of a current, is introduced phenomenologically by the RTA. We reveal that the RTA is justified for nonlinear optical response only in the DC limit and in the free limit  $\omega_i \gg \gamma, \epsilon_{nm}$ , while the RTA seems to be a good approximation for the linear optical conductivity. We note that although Parker *et al.*[102] have also derived the Green function formalism for noninteracting systems, they consider mostly photon decay  $\omega_i \rightarrow \omega_i + i\gamma$  and neglect correlations and electron scattering.

After having established the Green function formalism, we have analyzed the renormalization effect and the impact of different lifetimes in a multi-orbital system as common correlation effects, which are not considered in previous studies. We demonstrate that the enhancement generated by the renormalization effect increases with the order of the nonlinear response. When considering a single-band model, the renormalization coefficient  $z (< 1)$  enhances the  $n$ -th order response by a factor of  $z^{-(n-1)}$ . Thus, the nonlinear response is more strongly increased than linear transport. Finally, we have analyzed systems with different lifetimes, which commonly occur in materials where strongly correlated electrons couple to weakly interacting. The effect of different lifetimes can be analyzed by the band index of the non-Hermitian Hamiltonian. It causes the enhancement of terms that can also be derived in the Hermitian case and the emergence of a new term in which several bands coalesce. We have analyzed these non-Hermitian effects on the conductivity in two specific models. In both models, the conventional term with the non-Hermitian factor is dominant for the linear conductivity, while the band-coalescent term is dominant for the nonlinear conductivity. The non-Hermitian effect can enhance the (non)linear conductivity and can even change the sign, although it depends on the model. Although the non-Hermitian band-index is not well-defined at exceptional points, where the non-Hermitian factor  $\gamma_{NH}$  diverges, different lifetimes

might give rise to novel transport. For example, in photonic crystals, the emergence of exceptional points induces non-reciprocal transport[2, 3, 18, 115]. It should be possible to observe related phenomena in correlated materials. However, these questions are left for future works.



# Appendix A

## Appendix for the Chapter.2

### A.1 Correspondence between the perturbation approach in Nakajima-Zwanzig equation and the diagram approach in the Green function method

In this section, we confirm that the dynamics in Eq. (1.1.16) is described by the self-energy.

First, we confirm this result for the second order perturbation about the interaction  $\mathcal{H}_c$ , which corresponds to a second order process in  $\mathcal{L}$ . We note that any odd order perturbation term disappears because of Eq. (1.1.6). The second order term of  $\mathcal{K}(t)$  reads,

$$\mathcal{K}_2(t, s) = \mathcal{P} \mathcal{L}(t) \mathcal{L}(s) \mathcal{P}. \quad (\text{A.1.1})$$

Applying this to the Hubbard model in the main text, we obtain

$$\mathcal{K}_2(t, s) \rho_S(s) = -\text{tr}_B \left[ \mathcal{H}_c(t), [\mathcal{H}_c(s), \rho_S^I(s) \otimes \rho_B] \right], \quad (\text{A.1.2})$$

which becomes

$$-\int_0^t d\text{str}_B \left[ C_\sigma^\dagger(t) \otimes \mathcal{B}_\sigma(t), [C_\sigma(s) \otimes \mathcal{B}_\sigma^\dagger(s), \rho_S^I(s) \otimes \rho_B] \right] + \text{h.c.}$$

We here have used that the bath is in equilibrium so that  $[\mathcal{H}_B, \rho_B] = 0$  is satisfied. Performing the

commutators in the above expression, we find the following terms

$$\begin{aligned} \left( C_\sigma^\dagger(t) C_\sigma(s) \rho_S^I(s) - C_\sigma(s) \rho_S^I(s) C_\sigma^\dagger(t) \right) &\otimes \text{tr}_B \left[ \mathcal{B}_\sigma(t) \mathcal{B}_\sigma^\dagger(s) \rho_B \right] \\ &= \left( C_\sigma^\dagger C_\sigma \rho_S^I(s) - C_\sigma \rho_S^I(s) C_\sigma^\dagger \right) \otimes \left( i \Sigma_2^T(t-s) e^{i\xi(t-s)} \right) \end{aligned} \quad (\text{A.1.3})$$

$$\begin{aligned} \left( \rho_S^I(s) C_\sigma^\dagger(s) C_\sigma(t) - C_\sigma(t) \rho_S^I(s) C_\sigma^\dagger(s) \right) &\otimes \text{tr}_B \left[ \rho_B \mathcal{B}_\sigma(s) \mathcal{B}_\sigma^\dagger(t) \right] \\ &= \left( \rho_S^I(s) C_\sigma^\dagger C_\sigma - C_\sigma \rho_S^I(s) C_\sigma^\dagger \right) \otimes \left( i \Sigma_2^T(t-s) e^{i\xi(t-s)} \right)^\dagger \end{aligned} \quad (\text{A.1.4})$$

$$\begin{aligned} \left( C_\sigma(t) C_\sigma^\dagger(s) \rho_S^I(s) - C_\sigma^\dagger(s) \rho_S^I(s) C_\sigma(t) \right) &\otimes \text{tr}_B \left[ \mathcal{B}_\sigma^\dagger(t) \mathcal{B}_\sigma(s) \rho_B \right] \\ &= \left( C_\sigma C_\sigma^\dagger \rho_S^I(s) - C_\sigma^\dagger \rho_S^I(s) C_\sigma \right) \otimes \left( i (\Sigma_2^R(t-s) - \Sigma_2^T(t-s)) e^{i\xi(t-s)} \right)^\dagger \end{aligned} \quad (\text{A.1.5})$$

$$\begin{aligned} \left( \rho_S^I(s) C_\sigma(s) C_\sigma^\dagger(t) - C_\sigma^\dagger(t) \rho_S^I(s) C_\sigma(s) \right) &\otimes \text{tr}_B \left[ \rho_B \mathcal{B}_\sigma^\dagger(s) \mathcal{B}_\sigma(t) \right] \\ &= \left( \rho_S^I(s) C_\sigma C_\sigma^\dagger - C_\sigma^\dagger \rho_S^I(s) C_\sigma \right) \otimes \left( i (\Sigma_2^R(t-s) - \Sigma_2^T(t-s)) e^{i\xi(t-s)} \right) \end{aligned} \quad (\text{A.1.6})$$

We note that terms such as  $\text{tr}_B[\mathcal{B}_\sigma(t) \mathcal{B}_\sigma^\dagger(s) \rho_B]$  can be visualized as shown in Fig. A.1 and correspond to the  $\Sigma_2^T(t-s)$  (time-ordered self-energy) in second-order. This correspondence is shown in more detail in S3.

Using

$$\begin{aligned} S_l(t) &= \Sigma^T(t) e^{i\xi t} \\ S_g(t) &= (\Sigma^R(t) - \Sigma^T(t)) e^{i\xi t}, \end{aligned}$$

we can describe the quantum Master equation in second order using the self-energy, which reads

$$\frac{\partial}{\partial t} \rho_S^I(t) = \int_0^t ds \quad (\text{A.1.7})$$

$$\begin{aligned} &\times \left[ \begin{aligned} &-i S_l^r(t-s) [C_\sigma^\dagger C_\sigma, \rho_S^I(s)] \\ &+ i S_g^r(t-s) [C_\sigma C_\sigma^\dagger, \rho_S^I(s)] \\ &+ S_l^i(t-s) \left( \{C_\sigma^\dagger C_\sigma, \rho_S^I(s)\} - 2 C_\sigma \rho_S^I(s) C_\sigma^\dagger \right) \\ &+ S_g^i(t-s) \left( \{C_\sigma C_\sigma^\dagger, \rho_S^I(s)\} - 2 C_\sigma^\dagger \rho_S^I(s) C_\sigma \right) \end{aligned} \right] \end{aligned}$$

$$S_l(t) = S_l^r(t) + i S_l^i(t) \quad (\text{A.1.8})$$

$$S_g(t) = S_g^r(t) + i S_g^i(t). \quad (\text{A.1.9})$$

We also confirm the fourth order term of  $\mathcal{K}(t)$  which corresponds to the fourth order Feynman diagrams. The fourth order term of  $\mathcal{K}(t)$  can be written as,

$$\begin{aligned} \mathcal{K}_4(t) = & \int_0^t dt_1 \int_0^{t_1} dt_2 \int_0^{t_2} dt_3 \left( \mathcal{P} \mathcal{L}(t) \mathcal{L}(t_1) \mathcal{L}(t_2) \mathcal{L}(t_3) \mathcal{P} \right. \\ & \left. - \mathcal{P} \mathcal{L}(t) \mathcal{L}(t_1) \mathcal{P} \mathcal{L}(t_2) \mathcal{L}(t_3) \mathcal{P} \right) \end{aligned}$$

The first term on the right-hand side corresponds to a fourth order Feynman diagram. The other terms can be described by improper Feynman diagrams, such as shown in Fig. A.2. The projection operator,  $\mathcal{Q}$ , in Eq. (1.1.13) removes all improper Feynman diagrams from  $\mathcal{K}$ . Higher order terms,  $\mathcal{K}_n$ , can be described in the same way by higher-order terms of the self-energy. Therefore, we can conclude that the self-energy describes the dynamics of the master equation.

In the main text, we use the dynamical mean field theory to calculate the self-energy, which is then used in the master equation. We calculate  $\Sigma^T$  in dynamical mean field theory by calculating

$$\begin{aligned} & \frac{\sum_{\mathbf{k}', \mathbf{q}} n(\mathbf{k}' + \mathbf{q}, \omega) (1 - n(\mathbf{k}', \omega)) (1 - n(\mathbf{k}_0 + \mathbf{q}, \omega))}{\sum_{\mathbf{k}', \mathbf{q}} (1 - n(\mathbf{k}' + \mathbf{q}, \omega)) n(\mathbf{k}', \omega) n(\mathbf{k}_0 + \mathbf{q}, \omega)} \\ & = \Sigma^T(\omega) / (\Sigma^R(\omega) - \Sigma^T(\omega)) \end{aligned} \quad (\text{A.1.10})$$

Eq. (A.1.10) is satisfied when the equilibrium state of the bath is described by  $\rho_B = \sum_n |n\rangle \langle n| e^{-\beta \epsilon_n} / \sum_n e^{-\beta \epsilon_n}$ .

## A.2 Self-energy in density matrix representation

In this section, we further clarify why  $\text{tr}_B \left[ \mathcal{B}_\sigma(t) \mathcal{B}_\sigma^\dagger(s) \rho_B \right]$  and similar terms arising in Eq. (1.1.13) correspond to the self-energy. The single-particle Green's function  $G_{\mathbf{k}_0}^T(t, s)$  for  $t > s$  is defined as

$$G_{\mathbf{k}_0}^T(t, s) = \text{tr}_{\text{total}} \left[ c_{\mathbf{k}_0}(t) c_{\mathbf{k}_0}^\dagger(s) \rho_{\text{total}} \right], \quad (\text{A.2.1})$$

where  $c_{\mathbf{k}_0}(t) = e^{iHt} c_{\mathbf{k}_0} e^{-iHt}$ . Splitting the Hamiltonian into a free part and the interaction,  $H = H_0 + H_{\text{int}}$ , we can use the interaction representation and write

$$\begin{aligned} e^{-iHt} &= e^{-iH_0 t} \mathcal{S}(t) \\ \mathcal{S}(t) &= T \exp \left[ -i \int_0^t ds H_{\text{int}}(s) \right] \\ e^{iHt} &= \mathcal{S}^{-1}(t) e^{iH_0 t} \\ \mathcal{S}(t, s) &= T \exp \left[ -i \int_s^t ds_1 H_{\text{int}}(s_1) \right] = \mathcal{S}(t) \mathcal{S}^{-1}(s) \\ \mathcal{H}'_B &= \mathcal{Q} H_{\text{int}} \mathcal{Q} \\ \mathcal{H}_c &= \mathcal{P} H_{\text{int}} \mathcal{Q} + \mathcal{Q} H_{\text{int}} \mathcal{P} \\ H_{\text{int}} &= \mathcal{H}'_B + \mathcal{H}_c \\ \mathcal{S}_B(t) &\equiv T \exp \left[ -i \int_0^t ds \mathcal{H}'_B(s) \right]. \end{aligned}$$

By using these relations, we can write

$$G_{\mathbf{k}_0}^T(t, s) = \text{tr}_{\text{total}} \left[ \mathcal{S}^{-1}(t) c_{\mathbf{k}_0}^I(t) \mathcal{S}(t-s) c_{\mathbf{k}_0}^{I\dagger}(s) \mathcal{S}(s) \rho_{\text{tot}} \right] \quad (\text{A.2.2})$$

$$\simeq \int \int ds_1 ds_2 \text{tr}_{\text{total}} \left[ \mathcal{S}_B^{-1}(t) c_{\mathbf{k}_0}^I(t) \mathcal{S}_B(t-s_2) \mathcal{H}_c^I(s_2) \times \mathcal{S}_B(s_2-s_1) \mathcal{H}_c^I(s_1) \mathcal{S}_B(s_1-s) c_{\mathbf{k}_0}^{I\dagger}(s) \mathcal{S}_B(s) \rho_{\text{tot}} \right] \quad (\text{A.2.3})$$

$$= \int \int ds_1 ds_2 G_{\mathbf{k}_0}^{0T}(t, s_2) \text{tr}_B \left[ \mathcal{B}(s_2) \mathcal{B}^\dagger(s_1) \rho_B \right] G_{\mathbf{k}_0}^{0T}(s_1, s) \quad (\text{A.2.4})$$

$$= \int \int ds_1 ds_2 G_{\mathbf{k}_0}^{0T}(t, s_2) \Sigma^T(s_2-s_1) G_{\mathbf{k}_0}^{0T}(s_1, s). \quad (\text{A.2.5})$$

When deriving Eq.(A.2.3) from Eq.(A.2.2), we have used second order perturbation in  $\mathcal{H}_c$ . In this equation,  $\Sigma^T$  is the 0th order term in  $\mathcal{H}_c$ , but exact in  $\mathcal{H}'_B$ . We thus have shown that  $\text{tr}_B \left[ \mathcal{B}_\sigma(t) \mathcal{B}_\sigma^\dagger(s) \rho_B \right]$  in Eq.(9) in the main text corresponds to the self-energy.

### A.3 Spectral function in the case of larger system

When considering a system which includes the Hilbert space spanned by  $c_{\mathbf{k}_0, \uparrow}^{(\dagger)}$  and  $c_{\mathbf{k}_0, \downarrow}^{(\dagger)}$ , additional terms such as  $\frac{U}{N} \sum_{\mathbf{q}} \left( c_{\mathbf{k}_0 \sigma}^\dagger c_{\mathbf{k}_0 + \mathbf{q} \sigma} c_{\mathbf{k} + \mathbf{q} \bar{\sigma}}^\dagger c_{\mathbf{k}_0 \bar{\sigma}} + h.c. \right)$  and  $\frac{U}{N} \sum_{\mathbf{q}} \left( c_{\mathbf{k}_0 \sigma}^\dagger c_{\mathbf{k}_0 + \mathbf{q} \sigma} c_{\mathbf{k}_0 \bar{\sigma}}^\dagger c_{\mathbf{k}_0 - \mathbf{q} \bar{\sigma}} + h.c. \right)$  appear in the coupling Hamiltonian  $\mathcal{H}_C$ . This leads to additional gain and loss modes, which can be described by the two-particle self-energy, which is however ignored in this paper for simplicity. We can write down the quantum master equation for the density operator of the spectral function,

$$\rho^{SF}(t) = a(t) |\uparrow\rangle \langle 0| + b(t) |2\rangle \langle \downarrow|,$$

where  $|0\rangle$  is the unoccupied system and  $|2\rangle = c_{\mathbf{k}_0, \uparrow}^\dagger c_{\mathbf{k}_0, \downarrow}^\dagger |0\rangle$ . The quantum master equation becomes

$$\frac{\partial}{\partial t} \begin{pmatrix} a(t) \\ b(t) \end{pmatrix} = \int_{t_0}^t ds \times \begin{pmatrix} S_{eff}(t-s) + 2S_g^i(t-s) & -2S_l^i(t-s) \\ -2S_g^i(t-s) & S_{eff}(t-s) + 2S_l^i(t-s) \end{pmatrix} \begin{pmatrix} a(s) \\ b(s) \end{pmatrix},$$

Thus, the spectral function is given as

$$\begin{aligned} \frac{\partial}{\partial t} \text{Tr} \left[ C_\uparrow \rho^{SF}(t) \right] &= \frac{\partial}{\partial t} (a(t) + b(t)) \\ &= \int_{t_0}^t ds S_{eff}(t-s) (a(s) + b(s)). \end{aligned} \quad (\text{A.3.1})$$

In this case, the dynamics of  $\rho^{SF}$  originally includes gain and loss modes. However, when calculating the trace for the spectral function, the gain and loss terms disappear. We finally can



derive the spectral function by Fourier transformation

$$A_{\uparrow\uparrow}(\omega) = \frac{1}{\pi} \text{Tr}[C\rho_S^{SF}(\omega)] = i/\pi(\omega - \xi - \Sigma^R(\omega)), \quad (\text{A.3.2})$$

where we use  $a(0) + b(0) = 1$  as initial condition. Therefore, even when we consider a larger system, the gain and loss modes appearing in the dynamics of  $\rho^{SF}$  cancel in the spectral function, whose dynamics is described by an effective non-hermitian Hamiltonian,  $\mathcal{H}_{eff}(\omega) = \mathcal{H}_0 + \Sigma^R(\omega)$ . This statement holds generally in OQS.

## A.4 Spectral function in the steady state of open quantum systems

Here, we verify that gain and loss terms in the quantum Master equation do not affect the dynamics of the spectral function. Therefore, the spectral function can be described by an effective non-hermitian Hamiltonian, which is identical to the effective non-hermitian Hamiltonian in the quantum Master equation under postselection.

We suppose that the density matrix in the steady state is given as  $\rho_{SS} = \sum_n a_n |n\rangle \langle n|$  and that odd powers of the coupling Hamiltonian vanish when tracing out the bath, which can be written as  $\text{Tr}_B[\mathcal{B}^{2m+1}\rho_B] = 0$ .  $\mathcal{B}$  is a fermionic operator of the coupling Hamiltonian on the Hilbert space of the bath. Furthermore, we suppose the absence of gain and loss modes such as  $\psi_\alpha\rho\psi_\beta^\dagger$  ( $\alpha \neq \beta$ ), where  $\alpha$  and  $\beta$  correspond to an internal quantum numbers such as spin or orbital, and  $\psi_\alpha$  is the fermionic annihilation operator of an electron in state  $\alpha$ .

In general, the density matrix of a fermionic system can be written as

$$\begin{aligned} \rho(t) &= \sum_{s_\alpha, s'_\alpha, s_\beta, s'_\beta, \dots = 0,1} D_{s_\alpha, s'_\alpha, s_\beta, s'_\beta, \dots}(t) \\ &\quad \times \psi_\alpha^\dagger(s_\alpha) \psi_\beta^\dagger(s_\beta) \dots |0\rangle \langle 0| \dots \psi_\beta^{(s'_\beta)} \psi_\alpha^{(s'_\alpha)} \end{aligned} \quad (\text{A.4.1})$$

$$= \sum_{n, n'} D_{n, n'}(t) |n\rangle \langle n'|, \quad (\text{A.4.2})$$

where  $n^{(\prime)} = (s_\alpha^{(\prime)}, s_\beta^{(\prime)}, \dots)$  and  $s_\alpha^{(\prime)}$  represents the occupation number of a particle in state  $\alpha$ .

We consider the spectral function  $A_{\alpha\alpha}(t) = \text{Tr}[(\psi_\alpha(t)\psi_\alpha^\dagger + \psi_\alpha^\dagger\psi_\alpha(t))\rho_{SS}]$ , which can be written using  $\rho^{SF} = (\psi_\alpha^\dagger\rho_{SS} + \rho_{SS}\psi_\alpha^\dagger)$ . The density matrix of the spectral function and its initial condition

can be written using  $m = (s_\beta, s_\gamma, \dots)$

$$\rho^{SF}(t) = \sum_m B_m(t) \psi_\alpha^\dagger |m\rangle \langle m| \quad (\text{A.4.3})$$

$$\sum_m B_m(0) = 1 \quad (\text{A.4.4})$$

$$\Rightarrow A_{\alpha\alpha}(t) = \text{Tr} \left[ \psi_\alpha \rho^{SF}(t) \right] = \sum_m B_m(t). \quad (\text{A.4.5})$$

We consider now the contribution to  $\frac{\partial}{\partial t} \sum_m B_m(t)$  from the gain and loss terms  $S_\beta^l(t-s) \psi_\beta \rho^{SF}(s) \psi_\beta^\dagger$  ( $\beta \neq \alpha$ ). It is important to see that the (non-hermitian) counterpart,  $-\frac{1}{2} S_\beta^l(t-s) \{ \psi_\beta^\dagger \psi_\beta, \rho^{SF}(s) \}$ , must exist for each gain and loss term, because of the conservation of probability in the dynamics of the quantum master equation. By defining  $\psi_\alpha^\dagger |m_1\rangle \langle m_1| = \psi_\alpha^\dagger \psi_\beta^\dagger |m_2\rangle \langle m_2| \psi_\beta$ , we can rewrite this part of the master equation for the spectral function as

$$\begin{aligned} & S_\beta^l(t-s) \left[ \psi_\beta \psi_\alpha^\dagger |m_1\rangle \langle m_1| \psi_\beta^\dagger - \frac{\{ \psi_\beta^\dagger \psi_\beta, \psi_\alpha^\dagger |m_1\rangle \langle m_1| \}}{2} \right] \\ &= S_\beta^l(t-s) \left[ \psi_\alpha^\dagger |m_2\rangle \langle m_2| - \psi_\alpha^\dagger |m_1\rangle \langle m_1| \right]. \end{aligned} \quad (\text{A.4.6})$$

If we take the trace,  $\text{Tr}[\psi_\alpha \sim]$ , the contribution of the loss term and the counterpart vanish. The arguments above hold true for any  $(\beta, m)$  and for the gain terms. We note that to derive Eq. (A.4.6), we have to consider the commutation relation between  $\mathcal{H}_c$  and  $\psi_\alpha^\dagger$ .

On the other hand, gain and loss terms including  $S_\alpha^{g(l)}$  vanish because  $\psi_\alpha \rho^{SF} \psi_\alpha^\dagger = \psi_\alpha^\dagger \rho^{SF} \psi_\alpha = 0$  as is written in the main text. The spectral function  $A_{\alpha\alpha}$  is not affected by  $S_\beta^{l/g}$  and can be described only by the non-hermitian term  $S_\alpha^R$ . Therefore, the spectral function of a general fermionic QQS can be described by an effective non-hermitian Hamiltonian without postselection.

Although we here have assumed that gain and loss modes such as  $\psi_\alpha \rho \psi_\beta^\dagger$  ( $\alpha \neq \beta$ ) do not exist, we show in Section. 2.3 that the spectral function in the periodic Anderson model(PAM) is also only described by a non-hermitian Hamiltonian. In the PAM, such gain and loss terms appear due to the hybridization between the conduction- and the  $f$ -electrons.

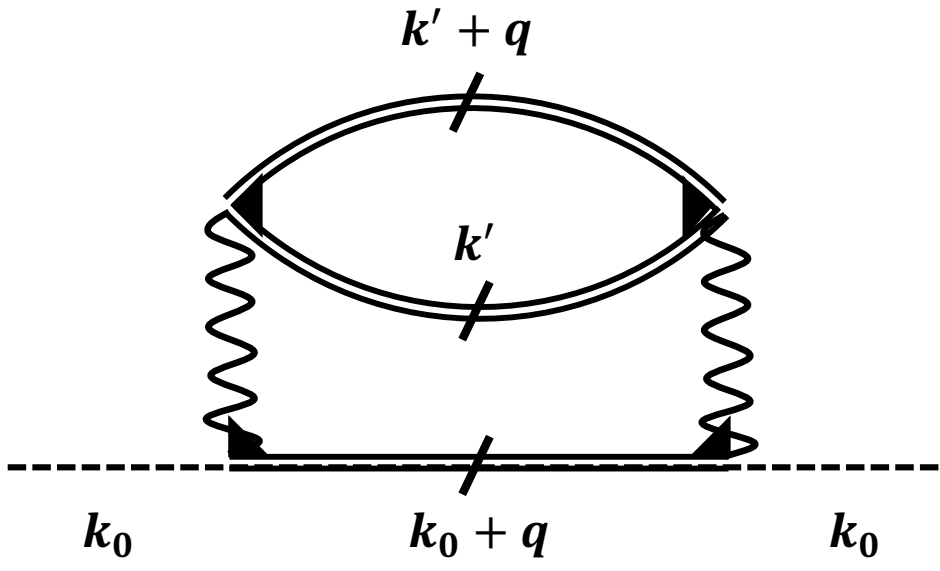


Figure A.1: Second order Feynman diagram

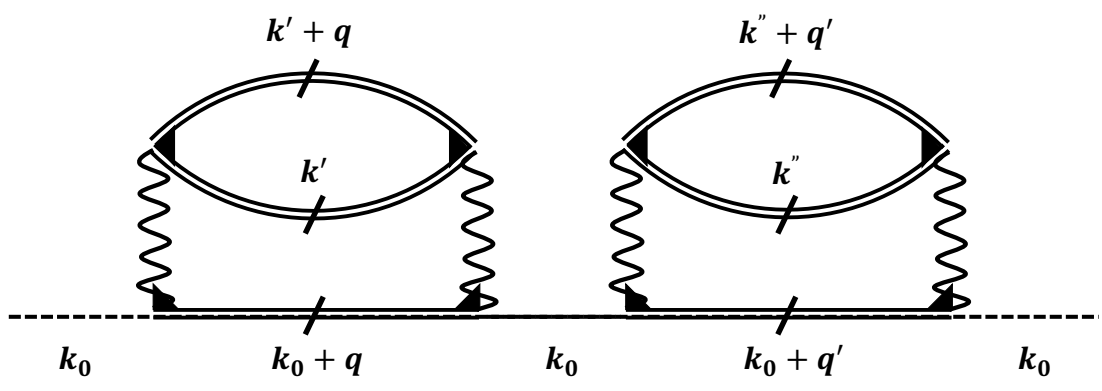


Figure A.2: Improper fourth order Feynman diagram



# Appendix B

## Appendix for the Chapter.3

### B.1 definition of the vorticity in momentum-frequency space

Here, we explain the details of the definition of the vorticity in the  $(\mathbf{k}, \omega)$ -space. In  $(2+1)$  dimensional systems, exceptional points form a loop in the  $(\mathbf{k}, \omega)$ -space. In order to define the vorticity of the exceptional loop, we set up the plane in the  $(\mathbf{k}, \omega)$ -space to which the tangent vector of the loop is the normal vector ( see Fig. B.1). We calculate the vorticity by doing the following line integral in mathematical positive direction,

$$v = \oint_{\text{EP}} \frac{d\mathbf{k}'}{2\pi i} \cdot \nabla_{\mathbf{k}'} \log \det \mathcal{H}_{eff}(\mathbf{k}, \omega), \quad (\text{B.1.1})$$

where  $\mathbf{k}'$  is defined on the plane as shown in Fig.B.1.

However, the sign of the integral still depends on the orientation of the plane, which depends on the direction of the tangent vector. Therefore, we choose the direction of the tangent vector so that the integral in Eq. (B.1.1) becomes  $1/2$ . This uniquely defines a direction for the exceptional loop in the  $(\mathbf{k}, \omega)$ -space, which is shown in Fig. 3.5. To define the vorticity in this way, we need to define a plane perpendicular to the exceptional manifold. Thus, it is necessary that the dimension of the exceptional manifold is  $(d - 2)$ , where  $d$  is the dimension of the  $(\mathbf{k}, \omega)$ -space. By using Eq.(3.1.11) and (3.1.12), we see that exceptional points can merge and disappear only if their tangent vectors are antiparallel, when two loops touch. We note that in systems whose Hamiltonian is described by a larger than 2 by 2 matrix, e.g. a system including more than two orbitals, exceptional points generated by different pairs of eigenvalues can touch with arbitrary direction without merging. Furthermore, we note that a similar definition might be used to analyze 2-dimensional exceptional manifolds in  $(3 + 1)$ -dimensional systems.

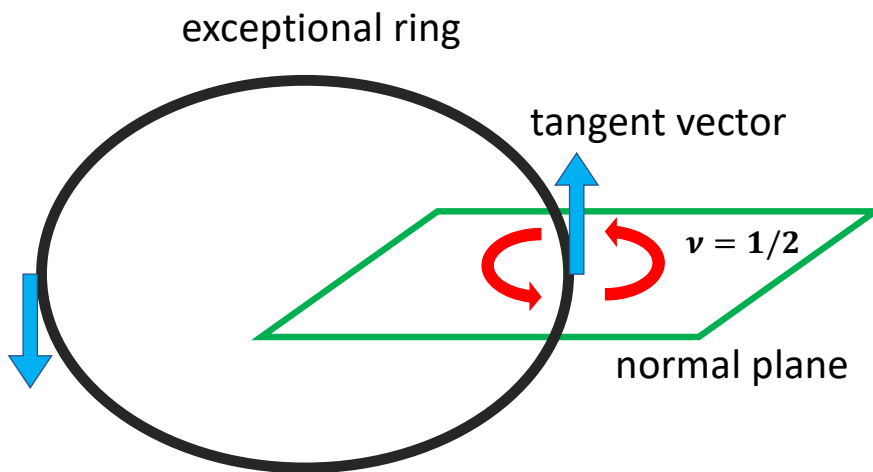


Figure B.1: Visualization of the tangent vector, normal plane, and the vorticity.

# Appendix C

## Appendix for the Chapter.4

### C.1 Derivation of the Matsubara formalism

In this section, we derive the conductivities using Green's function in Eq. (4.2.13) and Eq. (4.2.14) starting from Eq. (4.2.8) and Eq. (4.2.12). The first- and second-order response functions in the imaginary time are written as

$$\begin{aligned} & \mathcal{K}_{\alpha\beta}^{(1)}(\tau, \tau_1) \\ &= \frac{1}{Z[A]} \frac{\delta}{\delta \mathcal{A}^\beta(-i\tau_1)} \frac{\delta}{\delta \mathcal{A}^\alpha(-i\tau)} Z[A]|_{A=0} \end{aligned} \quad (\text{C.1.1})$$

$$\begin{aligned} &= - \langle \bar{\psi}_\mu(\tau) \mathcal{J}_\alpha^{\mu\nu} \psi_\nu(\tau) \bar{\psi}_\lambda(\tau_1) \mathcal{J}_\beta^{\lambda\eta} \psi_\eta(\tau_1) \rangle \\ &+ \langle \bar{\psi}_\mu(\tau) \mathcal{J}_{\alpha\beta}^{\mu\nu} \psi_\nu(\tau) \rangle \delta(\tau - \tau_1) \end{aligned} \quad (\text{C.1.2})$$

$$= -\delta(\tau - \tau_1) \text{Tr} \left[ \mathcal{J}_{\alpha\beta} \mathcal{G}(0) \right] - \text{Tr} \left[ \mathcal{J}_\alpha \mathcal{G}(\tau - \tau_1) \mathcal{J}_\beta \mathcal{G}(\tau_1 - \tau) \right] \quad (\text{C.1.3})$$

$$\begin{aligned} & \mathcal{K}_{\alpha\beta\gamma}^{(2)}(\tau, \tau_1, \tau_2) \\ &= \frac{1}{Z[A]} \frac{\delta}{\delta \mathcal{A}_\gamma(\tau_2)} \frac{\delta}{\delta \mathcal{A}_\beta(\tau_1)} \frac{\delta}{\delta \mathcal{A}_\alpha(\tau)} Z[\mathcal{A}]|_{\mathcal{A}=0} \end{aligned} \quad (\text{C.1.4})$$

$$\begin{aligned} &= \delta(\tau - \tau_1) \delta(\tau - \tau_2) \text{Tr} \left[ \mathcal{J}_{\alpha\beta\gamma} \mathcal{G}(0) \right] \\ &+ \delta(\tau - \tau_1) \text{Tr} \left[ \mathcal{J}_{\alpha\beta} \mathcal{G}(\tau - \tau_2) \mathcal{J}_\gamma \mathcal{G}(\tau_2 - \tau) \right] \\ &+ \delta(\tau - \tau_2) \text{Tr} \left[ \mathcal{J}_{\alpha\gamma} \mathcal{G}(\tau - \tau_1) \mathcal{J}_\beta \mathcal{G}(\tau_1 - \tau) \right] \\ &+ \delta(\tau_1 - \tau_2) \text{Tr} \left[ \mathcal{J}_\alpha \mathcal{G}(\tau - \tau_1) \mathcal{J}_{\beta\gamma} \mathcal{G}(\tau_1 - \tau) \right] \\ &+ \text{Tr} \left[ \mathcal{J}_\alpha \mathcal{G}(\tau - \tau_2) \mathcal{J}_\gamma \mathcal{G}(\tau_2 - \tau_1) \mathcal{J}_\beta \mathcal{G}(\tau_1 - \tau) \right] \\ &+ \text{Tr} \left[ \mathcal{J}_\alpha \mathcal{G}(\tau - \tau_1) \mathcal{J}_\beta \mathcal{G}(\tau_1 - \tau_2) \mathcal{J}_\gamma \mathcal{G}(\tau_2 - \tau) \right] \end{aligned} \quad (\text{C.1.5})$$

where we have used Wick's theorem to derive Eq. (C.1.3) and Eq. (C.1.5) from Eq. (C.1.2) and Eq. (C.1.4). When calculating conductivities for correlated systems, Eq. (C.1.3) and Eq. (C.1.5) are exact except for vertex corrections. Correlations are included via the self-energy in the single-particle Green's function in imaginary time,  $\mathcal{G}$ . We note that physical quantities obtained within the length gauge correspond to those from the velocity gauge when calculating exactly[106]. Therefore, taking the length gauge, we can derive the same results.

After Fourier transformation, we can derive the linear and second-order nonlinear response function in the Matsubara frequency as

$$\begin{aligned} & \mathcal{K}_{\alpha\beta}^{(1)}(i\omega_m; i\omega_m) \\ &= -\frac{1}{\beta} \sum_{\omega_l} \text{Tr} \left[ \mathcal{J}_{\alpha\beta} \mathcal{G}(i\omega_l) + \mathcal{J}_{\alpha} \mathcal{G}(i\omega_l + i\omega_m) \mathcal{J}_{\beta} \mathcal{G}(i\omega_l) \right] \end{aligned} \quad (\text{C.1.6})$$

$$\begin{aligned} & \mathcal{K}_{\alpha\beta\gamma}^{(2)}(i\omega_s (= i\omega_n + i\omega_m); i\omega_n, i\omega_m) \\ &= \frac{1}{\beta} \sum_{\omega_l} \left\{ \frac{1}{2} \text{Tr} \left[ \mathcal{J}_{\alpha\beta\gamma} \mathcal{G}(i\omega_l) \right] \right. \\ & \quad + \left( \text{Tr} \left[ \mathcal{J}_{\alpha\beta} \mathcal{G}(i\omega_m + i\omega_l) \mathcal{J}_{\gamma} \mathcal{G}(i\omega_l) \right] \right. \\ & \quad + \frac{1}{2} \text{Tr} \left[ \mathcal{J}_{\alpha} \mathcal{G}(i\omega_n + i\omega_m + i\omega_l) \mathcal{J}_{\beta\gamma} \mathcal{G}(i\omega_l) \right] \\ & \quad \left. \left. + \text{Tr} \left[ \mathcal{J}_{\alpha} \mathcal{G}(i\omega_n + i\omega_m + i\omega_l) \mathcal{J}_{\beta} \mathcal{G}(i\omega_m + i\omega_l) \mathcal{J}_{\gamma} \mathcal{G}(i\omega_l) \right] \right) \right. \\ & \quad \left. + \left( (\beta, i\omega_n) \leftrightarrow \gamma, i\omega_m \right) \right\}, \end{aligned} \quad (\text{C.1.7})$$

where  $\omega_l = (2l + 1)\pi/\beta$  are Fermionic Matsubara frequencies and  $\omega_m = 2m\pi/\beta, \omega_n = 2n\pi/\beta$  are Bosonic Matsubara frequencies, which originate from the photons.

## C.2 Analytic continuation of the nonlinear response function

We can calculate the (non-)linear response in real frequency by using analytic continuation. By considering the paths in the complex frequency plane shown in Fig. C.1, the (non-)linear response functions can be written as



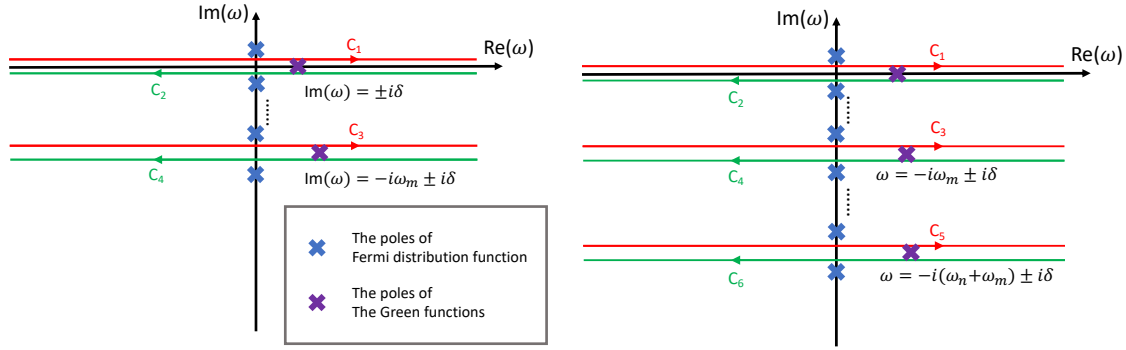


Figure C.1: Paths in the complex  $\omega$ -plane for the analytic continuation of the linear and second-order nonlinear response functions – By constructing the paths, which surround the poles of the Fermi distribution function and avoid the poles of the Green’s functions, we can derive Eq. (C.2.3) and Eq. (C.2.4) from Eq. (C.1.6) and Eq. (C.1.7).

$$\mathcal{K}_{\alpha\beta}^{(1)}(i\omega_m; i\omega_m) = \left( \oint_{up+C_1} + \oint_{C_2+C_3} + \oint_{C_4+low} \right) \frac{d\omega}{2\pi i} f(\omega) \text{Tr} \left[ \mathcal{J}_{\alpha\beta} \mathcal{G}(\omega) + \mathcal{J}_{\alpha} \mathcal{G}(\omega + i\omega_m) \mathcal{J}_{\beta} \mathcal{G}(\omega) \right] \quad (\text{C.2.1})$$

$$= \int_{-\infty}^{\infty} \frac{d\omega}{2\pi i} f(\omega) \left\{ \text{Tr} \left[ \mathcal{J}_{\alpha\beta} \left( G^R(\omega) - G^A(\omega) \right) \right] + \text{Tr} \left[ \mathcal{J}_{\alpha} G^R(\omega + i\omega_m) \mathcal{J}_{\beta} \left( G^R(\omega) - G^A(\omega) \right) \right] \right. \\ \left. + \text{Tr} \left[ \mathcal{J}_{\alpha} \left( G^R(\omega) - G^A(\omega) \right) \mathcal{J}_{\beta} G^A(\omega - i\omega_m) \right] \right\} \quad (\text{C.2.2})$$

$$\Leftrightarrow K_{\alpha\beta}^{(1)}(\omega_1; \omega_1) = \int_{-\infty}^{\infty} \frac{d\omega}{2\pi i} f(\omega) \left\{ \text{Tr} \left[ \mathcal{J}_{\alpha\beta} \left( G^R(\omega) - G^A(\omega) \right) \right] + \text{Tr} \left[ \mathcal{J}_{\alpha} G^R(\omega + \omega_1) \mathcal{J}_{\beta} \left( G^R(\omega) - G^A(\omega) \right) \right] \right. \\ \left. + \text{Tr} \left[ \mathcal{J}_{\alpha} \left( G^R(\omega) - G^A(\omega) \right) \mathcal{J}_{\beta} G^A(\omega - \omega_1) \right] \right\} \quad (\text{C.2.3})$$

$$\begin{aligned}
& \mathcal{K}_{\alpha\beta\gamma}^{(2)}(i\omega_n + i\omega_m; i\omega_n, i\omega_m) \\
&= -\left( \oint_{up+C_1} + \oint_{C_2+C_3} + \oint_{C_4+C_5} + \oint_{C_6+low} \right) \frac{d\omega}{2\pi i} f(\omega) \left\{ \frac{1}{2} \text{Tr} \left[ \mathcal{J}_{\alpha\beta\gamma} \mathcal{G}(i\omega_n) \right] \right. \\
&\quad + \frac{1}{2} \text{Tr} \left[ \mathcal{J}_{\alpha} \mathcal{G}(\omega + i\omega_n + i\omega_m) \mathcal{J}_{\beta\gamma} \mathcal{G}(\omega) \right] + \text{Tr} \left[ \mathcal{J}_{\alpha\beta} \mathcal{G}(\omega + i\omega_m) \mathcal{J}_{\gamma} \mathcal{G}(\omega) \right] \\
&\quad \left. + \text{Tr} \left[ \mathcal{J}_{\alpha} \mathcal{G}(\omega + i\omega_n) \mathcal{J}_{\beta} \mathcal{G}(\omega + i\omega_n + i\omega_m) \mathcal{J}_{\gamma} \mathcal{G}(\omega) + \left( (i\omega_n, \beta) \leftrightarrow (i\omega_m, \gamma) \right) \right] \right\} \quad (\text{C.2.4})
\end{aligned}$$

$$\begin{aligned}
&= - \int_{-\infty}^{\infty} \frac{d\omega}{2\pi i} f(\omega) \sum_k \left\{ \frac{1}{2} \text{Tr} \left[ \mathcal{J}_{\alpha\beta\gamma} (G^R(\omega) - G^A(\omega)) \right] \right. \\
&\quad + \text{Tr} \left[ \mathcal{J}_{\alpha\beta} G^R(\omega + i\omega_m) \mathcal{J}_{\gamma} (G^R(\omega) - G^A(\omega)) + \mathcal{J}_{\alpha\beta} (G^R(\omega) - G^A(\omega)) \mathcal{J}_{\gamma} G^A(\omega - i\omega_m) \right] \\
&\quad + \frac{1}{2} \text{Tr} \left[ \mathcal{J}_{\alpha} G^R(\omega + i\omega_{nm}) \mathcal{J}_{\beta\gamma} (G^R(\omega) - G^A(\omega)) + \mathcal{J}_{\alpha} (G^R(\omega) - G^A(\omega)) \mathcal{J}_{\beta\gamma} G^A(\omega - i\omega_{nm}) \right] \\
&\quad + \text{Tr} \left[ \mathcal{J}_{\alpha} G^R(\omega + i\omega_{nm}) \mathcal{J}_{\beta} G^R(\omega + i\omega_m) \mathcal{J}_{\gamma} (G^R(\omega) - G^A(\omega)) \right. \\
&\quad \quad + \mathcal{J}_{\alpha} G^R(\omega + i\omega_n) \mathcal{J}_{\beta} (G^R(\omega) - G^A(\omega)) \mathcal{J}_{\gamma} G^A(\omega - i\omega_m) \\
&\quad \quad \left. + \mathcal{J}_{\alpha} (G^R(\omega) - G^A(\omega)) \mathcal{J}_{\beta} G^A(\omega - i\omega_n) \mathcal{J}_{\gamma} G^A(\omega - i\omega_{nm}) \right] \\
&\quad \left. + \left[ (\beta, \omega_1) \leftrightarrow (\gamma, \omega_2) \right] \right\} \quad (\text{C.2.5})
\end{aligned}$$

$$\begin{aligned}
&\Leftrightarrow K_{\alpha\beta\gamma}^{(2)}(\omega_1 + \omega_2; \omega_1, \omega_2) \\
&= - \int_{-\infty}^{\infty} \frac{d\omega}{2\pi i} f(\omega) \sum_k \left\{ \frac{1}{2} \text{Tr} \left[ \mathcal{J}_{\alpha\beta\gamma} (G^R(\omega) - G^A(\omega)) \right] \right. \\
&\quad + \text{Tr} \left[ \mathcal{J}_{\alpha\beta} G^R(\omega + \omega_2) \mathcal{J}_{\gamma} (G^R(\omega) - G^A(\omega)) + \mathcal{J}_{\alpha\beta} (G^R(\omega) - G^A(\omega)) \mathcal{J}_{\gamma} G^A(\omega - \omega_2) \right] \\
&\quad + \frac{1}{2} \text{Tr} \left[ \mathcal{J}_{\alpha} G^R(\omega + \omega_{12}) \mathcal{J}_{\beta\gamma} (G^R(\omega) - G^A(\omega)) + \mathcal{J}_{\alpha} (G^R(\omega) - G^A(\omega)) \mathcal{J}_{\beta\gamma} G^A(\omega - \omega_{12}) \right] \\
&\quad + \text{Tr} \left[ \mathcal{J}_{\alpha} G^R(\omega + \omega_{12}) \mathcal{J}_{\beta} G^R(\omega + \omega_2) \mathcal{J}_{\gamma} (G^R(\omega) - G^A(\omega)) \right. \\
&\quad \quad + \mathcal{J}_{\alpha} G^R(\omega + \omega_1) \mathcal{J}_{\beta} (G^R(\omega) - G^A(\omega)) \mathcal{J}_{\gamma} G^A(\omega - \omega_2) \\
&\quad \quad \left. + \mathcal{J}_{\alpha} (G^R(\omega) - G^A(\omega)) \mathcal{J}_{\beta} G^A(\omega - \omega_1) \mathcal{J}_{\gamma} G^A(\omega - \omega_{12}) \right] \\
&\quad \left. + \left[ (\beta, \omega_1) \leftrightarrow (\gamma, \omega_2) \right] \right\}, \quad (\text{C.2.6})
\end{aligned}$$

where *up(low)* means the path in the complex plane surrounding the upper(lower) plane, and  $f(\omega)$  is the Fermi distribution. We use the relation  $\oint_C \frac{d\omega}{2\pi i} f(\omega) A(\omega) = -\frac{1}{\beta} \sum_n A(i\omega_n)$ , where  $\oint_C$  corresponds to the path integral only around the poles of the Fermi distribution function, while avoiding the

poles of  $A(\omega)$ . Using the definitions of the response functions for real frequencies

$$\sigma_{\alpha\beta}^{(1)}(\omega_1; \omega_1) = K_{\alpha\beta}^{(1)}(\omega_1; \omega_1)/i\omega_1 \quad (\text{C.2.7})$$

$$\sigma_{\alpha\beta\gamma}^{(2)}(\omega_1 + \omega_2; \omega_1, \omega_2) = -K_{\alpha\beta\gamma}^{(2)}(\omega_1 + \omega_2; \omega_1, \omega_2)/\omega_1\omega_2, \quad (\text{C.2.8})$$

we can derive Eq. (4.2.13) and (4.2.14) in the main text.

### C.3 DC-limit

In this section, we explicitly perform the DC-limit ( $\omega_i \rightarrow 0$ ) and derive Eq. (4.2.15) and Eq. (4.2.16) starting from Eq. (4.2.13) and Eq. (4.2.14). We thereby show that performing the DC-limit under the velocity gauge does not yield any artificial divergence.

When  $\omega_i$  is small enough, in the sense that  $\beta\omega_i \ll 1$  and  $\tau\omega_i \ll 1$  ( $\tau$  is the inverse of the imaginary part of  $G^{R-1}(\omega)$ ), we can expand the single-particle Green's function as follows:

$$G^a(\omega + \omega_1) \simeq G^a(\omega) + \frac{\partial G^a}{\partial \omega} \omega_1 \quad (\text{C.3.1})$$

$$G^a(\omega + \omega_1 + \omega_2) \simeq G^a(\omega) + \frac{\partial G^a}{\partial \omega} (\omega_1 + \omega_2) + \frac{\partial^2 G^a}{\partial \omega^2} \omega_1 \omega_2 \quad (\text{C.3.2})$$

$$f(\omega + \omega_1) - f(\omega) \simeq \frac{\partial f(\omega)}{\partial \omega} (\omega_1), \quad (\text{C.3.3})$$

where  $a = R, A$  (retarded and advanced Green's function). By using this expansion, Eq. (4.2.13) becomes

$$\sigma_{\alpha\beta}^{(1)}(\omega_1) = \frac{1}{\omega_1} \int \frac{d\omega}{2\pi} \left( A_0(\omega) + A_1(\omega)\omega_1 \right) + \mathcal{O}(\omega_1^2) \quad (\text{C.3.4})$$

$$A_0(\omega) = \int \frac{d\mathbf{k}}{(2\pi)^d} f(\omega) \text{Tr} \left[ \mathcal{J}_{\alpha\beta} \left( G^R(\omega) - G^A(\omega) \right) + \mathcal{J}_\alpha G^R(\omega) \mathcal{J}_\beta G^R(\omega) - \mathcal{J}_\alpha G^A(\omega) \mathcal{J}_\beta G^A(\omega) \right] \quad (\text{C.3.5})$$

$$A_1(\omega) = \int \frac{d\mathbf{k}}{(2\pi)^d} \left\{ \frac{\partial f(\omega)}{\partial \omega} \text{Tr} \left[ \mathcal{J}_\alpha G^R(\omega) \mathcal{J}_\beta G^A(\omega) \right] + f(\omega) \left( \text{Tr} \left[ \mathcal{J}_\alpha \frac{\partial G^R(\omega)}{\partial \omega} \mathcal{J}_\beta G^R(\omega) + \mathcal{J}_\alpha G^A(\omega) \mathcal{J}_\beta \frac{\partial G^A(\omega)}{\partial \omega} \right] \right) \right\}. \quad (\text{C.3.6})$$

We here have used

$$\begin{aligned} & - \int \frac{d\omega}{2\pi} f(\omega) \left( \mathcal{J}_\alpha G^R(\omega + \omega_1) \mathcal{J}_\beta G^A(\omega) - \mathcal{J}_\alpha G^R(\omega) \mathcal{J}_\beta G^A(\omega - \omega_1) \right) \\ & = \int \frac{d\omega}{2\pi} \left( f(\omega + \omega_1) - f(\omega) \right) \mathcal{J}_\alpha G^R(\omega + \omega_1) \mathcal{J}_\beta G^A(\omega) \end{aligned} \quad (\text{C.3.7})$$

to derive Eq. (C.3.6). If  $A_0(\omega)$  would be finite after the integration, the conductivity diverges at  $\omega_1 \rightarrow 0$  even when  $1/\tau > 0$ . However, by using the identity,  $\partial_\alpha G^{R/A}(\omega) = G^{R/A}(\omega) \mathcal{J}_\alpha G^{R/A}(\omega)$ , Eq. (C.3.5) can be rewritten as

$$A_0(\omega) = f(\omega) \int \frac{d\mathbf{k}}{(2\pi)^d} \partial_\beta \left\{ \mathcal{J}_\alpha \left( G^R(\omega) - G^A(\omega) \right) \right\} = 0. \quad (\text{C.3.8})$$

Therefore,  $A_0(\omega)$  becomes zero at  $\omega_1 \rightarrow 0$ , an artificial divergence does not occur, and we can derive Eq. (4.2.15) using  $G^A = (G^R)^*$ .

We perform the same procedure for the second-order conductivity. By using the  $\omega_i$  expansion in Eq. (C.3.1-C.3.3), Eq. (4.2.14) becomes

$$\begin{aligned} & \sigma_{\alpha\beta\gamma}^{(2)}(\omega_1 + \omega_2; \omega_1, \omega_2) \\ &= \frac{1}{\omega_1 \omega_2} \int \frac{d\omega}{2\pi} \left( A_0(\omega) + (A_1(\omega)\omega_1 + A_1'(\omega)\omega_2) + A_2(\omega)\omega_1\omega_2 \right) + \mathcal{O}(\omega_1^2, \omega_2^2, \omega_i^3) \end{aligned} \quad (\text{C.3.9})$$

$$\begin{aligned}
A_0(\omega) &= f(\omega) \int \frac{d\mathbf{k}}{(2\pi)^d} \left\{ \frac{1}{2} \text{Tr} \left[ \mathcal{J}_{\alpha\beta\gamma} \left( G^R(\omega) - G^A(\omega) \right) \right] \right. \\
&\quad + \frac{1}{2} \text{Tr} \left[ \mathcal{J}_\alpha G^R(\omega) \mathcal{J}_{\beta\gamma} G^R(\omega) - \mathcal{J}_\alpha G^A(\omega) \mathcal{J}_{\beta\gamma} G^A(\omega) \right] \\
&\quad + \left( \text{Tr} \left[ \mathcal{J}_{\alpha\beta} G^R(\omega) \mathcal{J}_\gamma G^R(\omega) - \mathcal{J}_{\alpha\beta} G^A(\omega) \mathcal{J}_\gamma G^A(\omega) \right] \right. \\
&\quad \quad \left. + \text{Tr} \left[ \mathcal{J}_\alpha G^R(\omega) \mathcal{J}_\beta G^R(\omega) \mathcal{J}_\gamma G^R(\omega) \right] \right. \\
&\quad \quad \left. - \text{Tr} \left[ \mathcal{J}_\alpha G^A(\omega) \mathcal{J}_\beta G^A(\omega) \mathcal{J}_\gamma G^A(\omega) \right] \right) + (\beta \leftrightarrow \gamma) \left. \right\} \\
&= f(\omega) \int \frac{d\mathbf{k}}{(2\pi)^d} \partial_\gamma \partial_\beta \left\{ \mathcal{J}_\alpha \left( G^R(\omega) - G^A(\omega) \right) \right\} \\
&= 0
\end{aligned} \tag{C.3.10}$$

$$\begin{aligned}
A_1(\omega) &= f(\omega) \int \frac{d\mathbf{k}}{(2\pi)^d} \partial_\beta \text{Tr} \left[ \mathcal{J}_\alpha \frac{\partial G^R(\omega)}{\partial \omega} \mathcal{J}_\gamma G^R(\omega) \right] \\
&\quad + \frac{\partial f(\omega)}{\partial \omega} \int \frac{d\mathbf{k}}{(2\pi)^d} \partial_\beta \text{Tr} \left[ \mathcal{J}_\alpha G^R(\omega) \mathcal{J}_\gamma G^A(\omega) \right] + c.c. \\
&= 0
\end{aligned} \tag{C.3.11}$$

$$A'_1(\omega) = A_1(\omega; \beta \leftrightarrow \gamma) = 0 \tag{C.3.12}$$

$$\begin{aligned}
A_2(\omega) &= \int \frac{d\mathbf{k}}{(2\pi)^d} \left\{ \left( \frac{\partial f(\omega)}{\partial \omega} \right) \left( \text{Tr} \left[ \mathcal{J}_\alpha \frac{\partial G^R(\omega)}{\partial \omega} \mathcal{J}_\beta G^R(\omega) \mathcal{J}_\gamma G^A(\omega) \right] \right. \right. \\
&\quad \left. \left. + \frac{1}{2} \text{Tr} \left[ \mathcal{J}_\alpha \frac{\partial G^R(\omega)}{\partial \omega} \mathcal{J}_{\beta\gamma} G^A(\omega) \right] \right) \right. \\
&\quad - f(\omega) \text{Im} \left( \text{Tr} \left[ \mathcal{J}_\alpha \frac{\partial}{\partial \omega} \left( \frac{\partial G^R(\omega)}{\partial \omega} \mathcal{J}_\beta G^R(\omega) \right) \mathcal{J}_\gamma G^R(\omega) \right] \right. \\
&\quad \left. + \frac{1}{2} \text{Tr} \left[ \mathcal{J}_\alpha \frac{\partial^2 G^R(\omega)}{\partial \omega^2} \mathcal{J}_{\beta\gamma} G^R(\omega) \right] \right) \\
&\quad \left. + (\beta \leftrightarrow \gamma) \right\}
\end{aligned} \tag{C.3.13}$$

In the same way as for the linear conductivity,  $A_0(\omega)$ ,  $A_1(\omega)$ ,  $A'_1(\omega)$  can be written in the form of an integration over a total derivative and thus become zero. Therefore, we can determine  $A_2(\omega)$  as the second-order DC-conductivity.

## C.4 Weak-scattering limit in the Green's function method

When considering the weak-scattering limit where  $G^R(\omega) = 1/(\omega - \mathcal{H} - i\gamma/2)$  and  $\gamma \ll 1/\beta, \omega_1, \epsilon_{nm}$ , we can perform the frequency integration by using

$$\begin{aligned} & \int d\omega A(\omega, \{\omega_i\}\{\epsilon_m\})(G_n^R(\omega) - G_n^A(\omega))f(\omega) \\ & \simeq -2\pi i A(\epsilon_n \pm i\gamma/2, \{\omega_i\}\{\epsilon_m\})f(\epsilon_n \pm i\gamma/2) \\ & \simeq -2\pi i A(\epsilon_n \pm i\gamma/2, \{\omega_i\}\{\epsilon_m\})f(\epsilon_n), \end{aligned} \quad (\text{C.4.1})$$

where  $A(\omega, \{\omega_i\}\{\epsilon_m\})$  is a product of Green's functions and velocities, and the sign takes  $\pm$  when  $A(\omega, \{\omega_i\}\{\epsilon_m\})$  is an analytical function in the upper/lower plane of the complex  $\omega$ -space. The plane is chosen such that  $A(\omega, \{\omega_i\}\{\epsilon_m\})$  is analytic. Other poles than  $\omega = \epsilon_n \pm i\gamma/2$  can be ignored because  $G_n^R(\epsilon) - G_n^A(\epsilon) \simeq 0$  at those due to the assumption  $\gamma \ll 1/\beta, \omega_1, \epsilon_{nm}$ . Then we can derive the linear and nonlinear optical conductivities as

$$\sigma_{\alpha\beta}^{(1)}(\omega_1; \omega_1) \simeq \frac{i}{\omega_1} \sum_k \left\{ \mathcal{J}_{\alpha\beta}^{nm} f(\epsilon_n) + \frac{\mathcal{J}_{\alpha}^{nm} \mathcal{J}_{\beta}^{mn}}{\omega_1 - \epsilon_{mn} + i\gamma} f_{nm} \right\} \quad (\text{C.4.2})$$

$$\begin{aligned} & \sigma_{\alpha\beta\gamma}^{(2)}(\omega_1 + \omega_2; \omega_1, \omega_2) \\ & \simeq -\frac{1}{\omega_1 \omega_2} \sum_k \left\{ \frac{1}{2} \left( \mathcal{J}_{\alpha\beta\gamma}^{nm} f_n + \frac{\mathcal{J}_{\alpha}^{nm} \mathcal{J}_{\beta\gamma}^{mn}}{\omega_{12} - \epsilon_{mn} + i\gamma} f_{nm} \right) + \frac{\mathcal{J}_{\alpha\beta}^{nm} \mathcal{J}_{\gamma}^{mn}}{\omega_2 - \epsilon_{mn} + i\gamma} f_{nm} \right. \\ & \quad \left. + \frac{\mathcal{J}_{\alpha}^{nm} \mathcal{J}_{\beta}^{ml} \mathcal{J}_{\gamma}^{ln}}{(\omega_{12} - \epsilon_{mn} + i\gamma)(\omega_2 - \epsilon_{ln} + i\gamma)(\omega_1 - \epsilon_{ml} + i\gamma)} \right\} + \left( (\beta, \omega_1) \leftrightarrow (\gamma, \omega_2) \right) \end{aligned} \quad (\text{C.4.3})$$

where  $\mathcal{J}^{nm} = \langle n | \mathcal{J} | m \rangle$  and  $G_n^R(\omega) = \langle n | G^R(\omega) | n \rangle = 1/(\omega - \epsilon_n + i/2\tau)$ ,  $\epsilon_{nm} = \epsilon_n - \epsilon_m$ , and  $f_{nm} = f(\epsilon_n) - f(\epsilon_m)$ . We also use the approximation  $(\omega_i - \epsilon_{ni})/(\omega_i - \epsilon_{ni} + i\gamma) \simeq 1$  to derive Eq. (C.4.3). We note that these equations diverge in the DC-limit, where the assumption  $\gamma \ll \omega_i$  is not satisfied. These results correspond to the results by the RDM method with RTA under the velocity gauge. Under the assumption  $\gamma \ll \omega_i$ , we can regard  $(\omega_1 + i\gamma)/\omega_1 \simeq 1$  and derive the same results by the RDM methods under the length gauge from Eq. (C.4.2) and Eq. (C.4.3).

Finally, we analyze the DC-limit by first taking the limit  $\omega_i \rightarrow 0$  and assuming  $\omega \ll \gamma$ . Then

we can derive the DC conductivity as

$$\sigma_{\alpha\beta;DC}^{(1)} = \sum_{\mathbf{k}} \left\{ \tau \mathcal{J}_{\alpha}^{nn} \mathcal{J}_{\beta}^{nn} \left( -\frac{\partial f}{\partial \omega} \right) \Big|_{\epsilon_n} - \frac{\mathcal{J}_{\alpha}^{nm} \mathcal{J}_{\beta}^{mn}}{(\epsilon_{nm} + i\gamma)^2} f_{nm} \right\} \quad (\text{C.4.4})$$

$$\begin{aligned} \sigma_{\alpha\beta\gamma;DC}^{(2)} &= - \sum_{\mathbf{k}} \left\{ \frac{\tau^2}{2} \left( \mathcal{J}_{\alpha}^{nn} \mathcal{J}_{\beta}^{nn} \mathcal{J}_{\gamma}^{nn} \frac{\partial^2 f_n}{\partial \epsilon_n^2} + \mathcal{J}_{\alpha}^{nn} \mathcal{J}_{\beta\gamma}^{nn} \left( -\frac{\partial f(\epsilon_n)}{\partial \epsilon_n} \right) \right) + \frac{i\tau \mathcal{J}_{\alpha}^{nm} \mathcal{J}_{\beta}^{mn}}{(\epsilon_{nm} + i\gamma)^2} \left( \mathcal{J}_{\gamma}^{nn} \frac{\partial f(\omega)}{\partial \omega} \Big|_{\epsilon_n} - \mathcal{J}_{\gamma}^{mm} \frac{\partial f(\omega)}{\partial \omega} \Big|_{\epsilon_m} \right) \right. \\ &\quad + \mathcal{J}_{\alpha}^{nm} \mathcal{J}_{\beta}^{ml} \mathcal{J}_{\gamma}^{ln} \left( \frac{f_l}{(\epsilon_{lm} + i\gamma)^2 (\epsilon_{nl} + i\gamma)^2} + \frac{f_n}{(\epsilon_{nm} + i\gamma)^2 (\epsilon_{nl} + i\gamma)^2} + \frac{2f_n}{(\epsilon_{nm} + i\gamma)^3 (\epsilon_{nl} + i\gamma)} \right) \\ &\quad \left. + \frac{1}{2} \mathcal{J}_{\alpha}^{nm} \mathcal{J}_{\beta\gamma}^{mn} \frac{f_n}{(\epsilon_{nm} + i\gamma)^2} + (\beta \leftrightarrow \gamma) \right\} \quad (\text{C.4.5}) \end{aligned}$$

The first terms, which are proportional to  $\tau$  for  $\sigma^{(1)}$  and proportional to  $\tau^2$  for  $\sigma^{(2)}$ , represent the Drude term. The other terms for the second-order conductivity represent the Berry curvature dipole term and the Fermi sea terms.

## C.5 Semi-classical Boltzmann equation

In the semi-classical Boltzmann treatment, transport phenomena are analyzed by calculating the distribution function for particles near equilibrium[112, 116–118]. The effect of the vector potential is taken into account as

$$\mathcal{H}(\mathbf{p}) \rightarrow \mathcal{H}(\mathbf{k}(\mathbf{p}, t)) = \mathcal{H}(\mathbf{p} - q\mathbf{A}(\mathbf{x}, t)). \quad (\text{C.5.1})$$

By taking the Coulomb gauge  $\mathbf{A}(\mathbf{x}, t) = \mathbf{A}(t)$ , the translational symmetry is preserved, and the following equations are satisfied:

$$\dot{\mathbf{k}} = -q \frac{\partial \mathbf{A}(t)}{\partial t} = q\mathbf{E} \quad (\text{C.5.2})$$

$$\frac{\partial}{\partial p^{\alpha}} = \frac{\partial}{\partial k^{\alpha}}, \quad \frac{\partial}{\partial t} = \dot{\mathbf{k}} \cdot \nabla_{\mathbf{k}} = q\mathbf{E} \cdot \nabla_{\mathbf{k}}. \quad (\text{C.5.3})$$

where  $p$  is the wavenumber of the particle without the electric field,  $E$  the electric field described by the vector potential  $A$ , and  $q$  is the wavenumber under the electric field. Considering the change of the eigenstates and the band velocity induced by the vector potential up to the first order of the

vector potential, we find

$$|n(\mathbf{p})\rangle \rightarrow |\tilde{n}(\mathbf{k}(t))\rangle \simeq |n(\mathbf{p})\rangle - i \sum_{n' \neq n} \frac{|n'(\mathbf{p})\rangle \langle n'(\mathbf{p})| \frac{\partial}{\partial t} n(\mathbf{k}(t))\rangle}{\epsilon_n - \epsilon_{n'}} \quad (\text{C.5.4})$$

$$\begin{aligned} v_{n\alpha}(\mathbf{k}(t)) &= \langle \tilde{n} | \frac{\partial \mathcal{H}}{\partial k^\alpha} | \tilde{n} \rangle \\ &\simeq \frac{\partial \epsilon_n(\mathbf{p})}{\partial p^\alpha} - i \sum_{n' \neq n} \left( \frac{\langle n(\mathbf{p}) | \frac{\partial \mathcal{H}}{\partial q^\alpha} | n'(\mathbf{p}) \rangle \langle n'(\mathbf{p}) | q\mathbf{E} \cdot \nabla_{\mathbf{k}} | n(\mathbf{p}) \rangle}{\epsilon_n - \epsilon_{n'}} - c.c. \right) \\ &= v_{n\alpha}^0(\mathbf{p}) - q \left( \mathbf{E} \times \boldsymbol{\Omega}_n(\mathbf{p}) \right)_\alpha, \end{aligned} \quad (\text{C.5.5})$$

$$\boldsymbol{\Omega}_n(\mathbf{k}) = \nabla_{\mathbf{k}} \times \mathcal{A}_n, \quad \mathcal{A}_n = -i \langle u_{nk} | \nabla u_{nk} \rangle \quad (\text{C.5.6})$$

where  $|n\rangle$  is the eigenstate of the Hamiltonian without the vector potential,  $\epsilon_n(\mathbf{p})$  is the eigenvalue, and  $\mathcal{H}(\mathbf{p}) |n(\mathbf{p})\rangle = \epsilon_n(\mathbf{p}) |n(\mathbf{p})\rangle$  holds. By taking into account the correction of the band velocity, we obtain the semi-classical equation of motion, which reads,

$$\dot{\mathbf{k}}_n = q\mathbf{E}(t), \quad \dot{\mathbf{r}}_n = \frac{\partial \epsilon_n(\mathbf{p})}{\partial \mathbf{p}} - q\mathbf{E}(t) \times \boldsymbol{\Omega}_n(\mathbf{p}) \quad (\text{C.5.7})$$

Finally, the distribution function in the Boltzmann formalism with applied electric field using the relaxation time approximation(RTA) is given by the following equation

$$\frac{df_n(t)}{dt} = \frac{\partial f_n(t)}{\partial t} + \dot{\mathbf{k}} \cdot \nabla_{\mathbf{k}} f_n(t) = -\frac{f_n(t) - f_n^{(0)}}{\tau} \quad (\text{C.5.8})$$

which can be solved as

$$\begin{aligned} f(t) &= f^{(0)}(t) + f^{(1)}(t) + f^{(2)}(t) + \dots \\ &\Rightarrow \tau \frac{\partial f_n^{(m)}(t)}{\partial t} + f_n^{(m)}(t) = -q\tau \mathbf{E}(t) \cdot \nabla_{\mathbf{k}} f_n^{(m-1)}(t), \end{aligned} \quad (\text{C.5.9})$$

where  $f_n^{(0)} = 1/(1 + \exp[\beta\epsilon_n(\mathbf{k})])$  is the Fermi distribution function,  $\beta$  is the inverse of the temperature, and  $f^{(m)}$  represent the  $m$ -th order non-equilibrium perturbative distribution function for the electric field.

The first and second order term of the distribution function become

$$f_n^{(1)}(\omega, \alpha) = \frac{-q\tau}{1 - i\omega\tau} E^\alpha \partial_\alpha f_n^{(0)} \quad (\text{C.5.10})$$

$$\begin{aligned} &f_n^{(2)}((\omega_1, \beta), (\omega_2, \gamma)) \\ &= \frac{-q\tau E^\beta \partial_\beta}{1 - i(\omega_1 + \omega_2)\tau} f_n^{(1)}(\omega_2, \gamma) + \left( (\omega_1, \beta) \leftrightarrow (\omega_2, \gamma) \right) \\ &= \frac{(q\tau)^2 E^\alpha E^\beta \partial_\alpha \partial_\beta f_n^{(0)}}{(1 - i(\omega_1 + \omega_2)\tau)(1 - i\omega_2\tau)} + \left( (\omega_1, \beta) \leftrightarrow (\omega_2, \gamma) \right) \end{aligned} \quad (\text{C.5.11})$$



By combining the recurrence relation in Eq. (C.5.9) with the velocity corrected by the electric field in Eq. (C.5.5), we can derive the second order nonlinear conductivity as

$$\sigma_{\alpha\beta\gamma}^{B(2)}(\omega_1 + \omega_2; \omega_1, \omega_2) = q^3 \sum_{n,k} \left\{ \frac{\partial \epsilon_n}{\partial p^\alpha} \frac{\tau^2 \partial_\beta \partial_\gamma f_0}{(1 - i\omega_{12}\tau)(1 - i\omega_2\tau)} + \frac{\tau}{2(1 - i\omega_2\tau)} \epsilon_{\alpha\beta\mu} \Omega_{n\mu} \partial_\gamma f_0 \right. \\ \left. + \left( (\omega_1, \beta) + \leftrightarrow (\omega_2, \gamma) \right) \right\} \quad (\text{C.5.12})$$

$$\sigma_{DC;\alpha\beta\gamma}^{B(2)} = q^3 \sum_{n,k} \left\{ \frac{\partial \epsilon_n}{\partial p^\alpha} \tau^2 \partial_\beta \partial_\gamma f_0 + \tau \epsilon_{\alpha\beta\mu} \Omega_{n\mu} \partial_\gamma f_0 + (\beta \leftrightarrow \gamma) \right\} \quad (\text{C.5.13})$$

Then, we compare our results with the semi-classical Boltzmann treatment. For the sake of comparison, we set the self-energy in the Green's function as  $G^R(\omega) = 1/(\omega - \mathcal{H} + i/2\tau) = 1/(\omega - \mathcal{H} + i\gamma/2)$ . In this case, the Green's function can be diagonalized with the eigenvalue of the free Hamiltonian, and therefore, the nonlinear conductivity calculated by the semi-classical Boltzmann treatment can be written using Green's functions. First, we focus on the Green's function representation of  $\sigma_{DC;\alpha\beta\gamma}^{B(2)}$  in the DC limit, which reads

$$\sigma_{DC;\alpha\beta\gamma}^{B(2)} = - \sum_{n,m(\neq n),k} \int \frac{d\omega}{2\pi i} \left\{ \frac{1}{2} \mathcal{J}_\alpha^{nm} \left( \frac{\partial G_n^R(\omega)}{\partial \omega} \right) \mathcal{J}_{\beta\gamma}^{nm} G_n^A(\omega) \left( -\frac{\partial f(\omega)}{\partial \omega} \right) \right. \\ + \mathcal{J}_\alpha^{nn} G_n^R(\omega) \mathcal{J}_\beta^{nm} G_n^R(\omega) \mathcal{J}_\gamma^{nm} G_n^A(\omega) \frac{\partial^2 f(\omega)}{\partial \omega^2} \\ + \mathcal{J}_\alpha^n \frac{\partial G_n^R(\omega)}{\partial \omega} \mathcal{J}_\beta^{nm} G_m^R(\omega) \mathcal{J}_\gamma^{mn} G_n^A(\omega) \left( -\frac{\partial f(\omega)}{\partial \omega} \right) \\ \left. + \mathcal{J}_\alpha^{nm} \left( \frac{\partial G_m^R(\omega)}{\partial \omega} \right) \mathcal{J}_\beta^{mn} G_n^R(\omega) \mathcal{J}_\gamma^{nm} G_n^A(\omega) \left( -\frac{\partial f(\omega)}{\partial \omega} \right) + (\beta \leftrightarrow \gamma) \right\}, \quad (\text{C.5.14})$$

where  $\mathcal{J}^{nm} = \langle n | \mathcal{J} | m \rangle$  and  $G_n^R(\omega) = \langle n | G^R(\omega) | n \rangle = 1/(\omega - \epsilon_n + i/2\tau)$ . We use  $q\partial_\alpha \mathcal{J}_\beta^{nm} = \mathcal{J}_{\alpha\beta}^{nm} + (\mathcal{J}_\alpha^{nm} \mathcal{J}_\beta^{mn} + \mathcal{J}_\beta^{nm} \mathcal{J}_\alpha^{mn})/(\epsilon_{nm})$  to derive Eq. (C.5.14). Here, we suppose that  $\beta\gamma$  is small and  $G_n^R(\omega)G_n^A(\omega) = 1/((\omega - \epsilon_n)^2 + \gamma^2/4) \simeq 2\pi\delta(\omega - \epsilon_n)/\gamma$  is justified. Then, doing the frequency integration in Eq. (C.5.14), we can obtain the original result Eq. (C.5.13).

This Green's function representation of the Boltzmann equation Eq. (C.5.14) can be directly derived from the original Green's function method shown in the main text, Eq. (4.2.14), by ignoring the Fermi sea terms and the interband transitions  $\mathcal{J}_{mn}(m \neq n)$  except for the second and third term in Eq. (C.5.14), which is justified when  $\epsilon_{nm}\tau \gg 1$ .

Next, we consider the AC case. We can recover a finite frequency  $\omega_i$  from the DC limit in Eq. (C.5.14), which can be derived from Eq. (4.2.14) under the following assumptions:

- approximate  $\omega_i \simeq \omega_i + i\gamma$  which is justified in the limit  $\omega_i\tau \gg 1$
- approximate  $f(\omega + \omega_i) - f(\omega) \simeq (\partial f(\omega)/\partial \omega)\omega_i$  and  $(\partial f(\omega)/\partial \omega) - (\partial f(\omega - \omega_i)/\partial \omega) \simeq (\partial^2 f(\omega)/\partial \omega^2)\omega_i$  which is justified when  $\beta\omega_i \ll 1$ .

- approximate  $G^R(\omega + \omega_{12}) - G^R(\omega + \omega_2) \simeq (\partial G^R(\omega + \omega_2)/\partial \omega)\omega_1$  and  $1/(\omega_2 - \epsilon_{nm}) \sim 1/(-\epsilon_{nm})$  which is justified when  $\omega_i \ll \epsilon_{nm}$  ( $\epsilon_{nm} = \epsilon_n - \epsilon_m$ ).

Therefore, in the case of AC electric fields, there are severe approximations. Thus, the semi-classical Boltzmann equation is applicable at high temperatures or when the frequency  $\omega_i$  is very small so that the above conditions are satisfied. We note that we can also derive Eq. (C.5.12) from Eq. (4.2.14) by supposing  $\gamma \rightarrow 0$ , which corresponds to the condition  $\omega_i \gg \gamma$  for the RDM method. We note that taking the DC limit in this situation leads to a diverging conductivity. Moreover, the relaxation time in most materials is usually about  $1 \sim 100$  [ps][112]. Thus, when analyzing a Terahertz laser as input force,  $\omega_i \tau \sim 1$ , the conditions are not fulfilled. On the other hand, for a DC electric field in which  $\omega_i = 0$ , the only condition for the semi-classical Boltzmann treatment are  $\epsilon_{nm} \tau \gg 1$  and  $\beta \gamma \ll 1$ .

We note that, by considering higher-order corrections of the eigenstates by the electric field in Eq. (C.5.5), we can derive a more precise semi-classical Boltzmann equation. In this way, it is possible to get rid of the approximation  $\epsilon_{nm} \tau \gg 1$  and to include the Fermi sea terms in the Boltzmann equation. The other approximations listed above, however, remain necessary due to the relaxation time approximation.

## C.6 Details of the numerical calculations

In this section, we write in detail how to numerically calculate the results shown in the figures of the main text. The codes used for the numerical calculations in this paper are published on [https://github.com/YoshihiroMichishita/Test\\_Codes/](https://github.com/YoshihiroMichishita/Test_Codes/).

### C.6.1 Green's function method

Here, we describe the procedure of how to perform the numerical calculation using the Green's function method.

- A tight-binding Hamiltonian,  $\mathcal{H}(\mathbf{k})$ , describing the single-electron part of the model, such as Eq. (4.4.6) or Eq. (4.4.1), must be obtained.
- Starting from this tight-binding Hamiltonian, current operators  $\mathcal{J}_{\alpha\beta\dots}$  can be calculated by Eq. (4.2.4).
- For accounting for correlation effects, self-energies must be calculated. In this paper, we have used the dynamical mean-field theory[71].
- Using  $\mathcal{H}(\mathbf{k})$  and the self-energies, retarded and advanced Green's functions can be calculated.
- Having these Green's functions and current operators, one can use the Green's function formalism to calculate nonlinear response in strongly correlated systems.

To calculate the effect of renormalization of the band structure, we set  $\Sigma^R(\omega) = -(1/Z-1)\omega - \Sigma_0^R$ , where  $\Sigma_0^R$  is the real-part of the self-energy at  $\omega = 0$ . Then, one can analyze the renormalization effects on the linear response and the nonlinear response. We note that, when calculating the optical conductivity for a small input frequency ( $\omega_i$ ), one should do the momentum integration before the frequency ( $\omega$ ) integration. Furthermore, one should use Eqs. (C.3.6), (C.3.10), (C.3.11), and (C.3.12).

## C.6.2 RDM methods using the RTA

When using the RDM for calculating the (non)linear conductivity, one first needs to diagonalize the free Hamiltonian  $\mathcal{H}(\mathbf{k})$ . Using the eigenvectors, one calculates the velocity operators for different bands and calculates the (non)linear conductivity by Eqs. (82) in Ref. [106].

## C.7 Proof that $\gamma_{NH} \geq 1$

The left and right eigenvectors  $\langle n_L|, |n_R\rangle$  can be described as  $|n_R\rangle = (a_1, \dots, a_l)^T$  and  $\langle n_L| = (b_1, \dots, b_l)$ . Then, the following quantity must be larger than zero. Therefore, the non-Hermitian factor  $\gamma_{NH}$  must be larger than one:

$$\begin{aligned}
& \langle n_R|n_R\rangle \langle n_L|n_L\rangle - \langle n_L|n_R\rangle \langle n_R|n_L\rangle \\
&= \left( \sum_s |a_s|^2 \right) \left( \sum_s |b_s|^2 \right) - \left| \sum_s (a_s b_s) \right|^2 \\
&\geq \left( \sum_s |a_s|^2 \right) \left( \sum_s |b_s|^2 \right) - \left( \sum_s |a_s| |b_s| \right)^2 \\
&= \sum_{s,t} (|a_s| |b_t| - |a_t| |b_s|)^2 / 2 \geq 0
\end{aligned} \tag{C.7.1}$$

$$\Leftrightarrow \gamma_{NH;n} = \langle n_R|n_R\rangle \langle n_L|n_L\rangle / \langle n_L|n_R\rangle \langle n_R|n_L\rangle \geq 1 \tag{C.7.2}$$



# Bibliography

- [1] B. Peng, Ş. K. Özdemir, F. Lei, F. Monifi, M. Gianfreda, G. L. Long, S. Fan, F. Nori, C. M. Bender, and L. Yang, *Nature Physics* **10**, 394 (2014).
- [2] J. Doppler, A. A. Mailybaev, J. Böhm, U. Kuhl, A. Girschik, F. Libisch, T. J. Milburn, P. Rabl, N. Moiseyev, and S. Rotter, *Nature* **537**, 76 (2016).
- [3] Z. Lin, H. Ramezani, T. Eichelkraut, T. Kottos, H. Cao, and D. N. Christodoulides, *Phys. Rev. Lett.* **106**, 213901 (2011).
- [4] J. Wiersig, *Phys. Rev. Lett.* **112**, 203901 (2014).
- [5] Z.-P. Liu, J. Zhang, i. m. c. K. Özdemir, B. Peng, H. Jing, X.-Y. Lü, C.-W. Li, L. Yang, F. Nori, and Y.-x. Liu, *Phys. Rev. Lett.* **117**, 110802 (2016).
- [6] H. Hodaei, A. U. Hassan, S. Wittek, H. Garcia-Gracia, R. El-Ganainy, D. N. Christodoulides, and M. Khajavikhan, *Nature* **548**, 187 (2017).
- [7] W. Chen, Ş. K. Özdemir, G. Zhao, J. Wiersig, and L. Yang, *Nature* **548**, 192 (2017).
- [8] H.-K. Lau and A. A. Clerk, *Nature communications* **9**, 4320 (2018).
- [9] Y. Ashida, S. Furukawa, and M. Ueda, *Nature communications* **8**, 15791 (2017).
- [10] R. Hanai and P. B. Littlewood, *Phys. Rev. Research* **2**, 033018 (2020).
- [11] Y. Michishita, T. Yoshida, and R. Peters, *Phys. Rev. B* **101**, 085122 (2020).
- [12] Y. Michishita and R. Peters, *Phys. Rev. Lett.* **124**, 196401 (2020).
- [13] Y. Michishita and R. Peters, *Phys. Rev. B* **103**, 195133 (2021).
- [14] A. Kofuji, Y. Michishita, and R. Peters, *Phys. Rev. B* **104**, 085151 (2021).
- [15] T. Tomita, S. Nakajima, I. Danshita, Y. Takasu, and Y. Takahashi, *Science advances* **3**, e1701513 (2017).

- [16] M. Nakagawa, N. Kawakami, and M. Ueda, Phys. Rev. Lett. **121**, 203001 (2018).
- [17] K. Yamamoto, M. Nakagawa, K. Adachi, K. Takasan, M. Ueda, and N. Kawakami, Phys. Rev. Lett. **123**, 123601 (2019).
- [18] A. Regensburger, C. Bersch, M.-A. Miri, G. Onishchukov, D. N. Christodoulides, and U. Peschel, Nature **488**, 167 (2012).
- [19] M. Liertzer, L. Ge, A. Cerjan, A. D. Stone, H. E. Türeci, and S. Rotter, Phys. Rev. Lett. **108**, 173901 (2012).
- [20] L. Feng, Z. J. Wong, R.-M. Ma, Y. Wang, and X. Zhang, Science **346**, 972 (2014).
- [21] M. Brandstetter, M. Liertzer, C. Deutsch, P. Klang, J. Schöberl, H. Türeci, G. Strasser, K. Unterrainer, and S. Rotter, Nature communications **5**, 4034 (2014).
- [22] T. E. Lee, Phys. Rev. Lett. **116**, 133903 (2016).
- [23] H. Xu, D. Mason, L. Jiang, and J. Harris, Nature **537**, 80 (2016).
- [24] L. Feng, R. El-Ganainy, and L. Ge, Nature Photonics **11**, 752 (2017).
- [25] J. W. Yoon, Y. Choi, C. Hahn, G. Kim, S. H. Song, K.-Y. Yang, J. Y. Lee, Y. Kim, C. S. Lee, J. K. Shin, *et al.*, Nature **562**, 86 (2018).
- [26] T. Yoshida and Y. Hatsugai, Phys. Rev. B **100**, 054109 (2019).
- [27] J. Schindler, A. Li, M. C. Zheng, F. M. Ellis, and T. Kottos, Phys. Rev. A **84**, 040101 (2011).
- [28] M. Ezawa, Phys. Rev. B **99**, 201411 (2019).
- [29] M. Ezawa, Phys. Rev. B **100**, 165419 (2019).
- [30] K. Sone and Y. Ashida, Phys. Rev. Lett. **123**, 205502 (2019).
- [31] L. Yamauchi, T. Hayata, M. Uwamichi, T. Ozawa, and K. Kawaguchi, Chirality-driven edge flow and non-hermitian topology in active nematic cells (2020), arXiv:2008.10852 [cond-mat.soft] .
- [32] K. Sone, Y. Ashida, and T. Sagawa, Nat. Commun. **11**, 5745 (2020).
- [33] K. Adachi, K. Takasan, and K. Kawaguchi, Activity-induced phase transition in a quantum many-body system (2021), arXiv:2008.00996 [cond-mat.stat-mech] .
- [34] N. Hatano and D. R. Nelson, Phys. Rev. Lett. **77**, 570 (1996).
- [35] N. Hatano and D. R. Nelson, Phys. Rev. B **56**, 8651 (1997).

- [36] S. Nakajima, Progress of Theoretical Physics **20**, 948 (1958), provided by the SAO/NASA Astrophysics Data System.
- [37] R. Zwanzig, jcp **33**, 1338 (1960), provided by the SAO/NASA Astrophysics Data System.
- [38] I. Prigogine, *Non-Equilibrium Statistical Mechanics*, Dover Books on Physics (Dover Publications, 2017).
- [39] H.-P. Breuer, F. Petruccione, *et al.*, *The theory of open quantum systems* (Oxford University Press on Demand, 2002).
- [40] V. Gorini, A. Kossakowski, and E. C. G. Sudarshan, Journal of Mathematical Physics **17**, 821 (1976), provided by the SAO/NASA Astrophysics Data System.
- [41] G. Lindblad, Communications in Mathematical Physics **48**, 119 (1976), provided by the SAO/NASA Astrophysics Data System.
- [42] Y. Ashida, Z. Gong, and M. Ueda, Advances in Physics **69**, 249 (2020), <https://doi.org/10.1080/00018732.2021.1876991> .
- [43] A. Ruschhaupt, F. Delgado, and J. G. Muga, Journal of Physics A: Mathematical and General **38**, L171 (2005).
- [44] R. El-Ganainy, K. G. Makris, D. N. Christodoulides, and Z. H. Musslimani, Opt. Lett. **32**, 2632 (2007).
- [45] C. L. Kane and T. C. Lubensky, Nature Physics **10**, 39 (2014).
- [46] S. D. Huber, Nature Physics **12**, 621 (2016).
- [47] M. C. Marchetti, J. F. Joanny, S. Ramaswamy, T. B. Liverpool, J. Prost, M. Rao, and R. A. Simha, Rev. Mod. Phys. **85**, 1143 (2013).
- [48] J. Toner and Y. Tu, Phys. Rev. Lett. **75**, 4326 (1995).
- [49] J. Toner and Y. Tu, Phys. Rev. E **58**, 4828 (1998).
- [50] J. Toner, The Journal of Chemical Physics **150**, 154120 (2019), <https://doi.org/10.1063/1.5081742> .
- [51] H. Shen, B. Zhen, and L. Fu, Phys. Rev. Lett. **120**, 146402 (2018).
- [52] V. Kozii and L. Fu, arXiv preprint arXiv:1708.05841 (2017).
- [53] T. Yoshida, R. Peters, and N. Kawakami, Phys. Rev. B **98**, 035141 (2018).

- [54] Y. Nagai, Y. Qi, H. Isobe, V. Kozii, and L. Fu, *Phys. Rev. Lett.* **125**, 227204 (2020).
- [55] A. MOSTAFAZADEH, *International Journal of Geometric Methods in Modern Physics* **07**, 1191 (2010), <https://doi.org/10.1142/S0219887810004816> .
- [56] A. Mostafazadeh, *Journal of Mathematical Physics* **43**, 205 (2002), <https://doi.org/10.1063/1.1418246> .
- [57] A. Mostafazadeh, *Journal of Mathematical Physics* **43**, 3944 (2002), <https://doi.org/10.1063/1.1489072> .
- [58] Z. Gong, Y. Ashida, K. Kawabata, K. Takasan, S. Higashikawa, and M. Ueda, *Phys. Rev. X* **8**, 031079 (2018).
- [59] N. Okuma, K. Kawabata, K. Shiozaki, and M. Sato, *Phys. Rev. Lett.* **124**, 086801 (2020).
- [60] N. Okuma and M. Sato, *Phys. Rev. Lett.* **126**, 176601 (2021).
- [61] T. Shirai and T. Mori, *Phys. Rev. E* **101**, 042116 (2020).
- [62] T. Mori and T. Shirai, *Phys. Rev. Lett.* **125**, 230604 (2020).
- [63] M. Esposito, U. Harbola, and S. Mukamel, *Rev. Mod. Phys.* **81**, 1665 (2009).
- [64] U. Fano, *Phys. Rev.* **131**, 259 (1963).
- [65] U. Harbola and S. Mukamel, *The Journal of Chemical Physics* **124**, 044106 (2006), <https://doi.org/10.1063/1.2161177> .
- [66] U. Harbola and S. Mukamel, *Physics Reports* **465**, 191 (2008).
- [67] T. Yoshida, R. Peters, N. Kawakami, and Y. Hatsugai, *Phys. Rev. B* **99**, 121101 (2019).
- [68] P. A. McClarty and J. G. Rau, *Phys. Rev. B* **100**, 100405 (2019).
- [69] K. Kimura, T. Yoshida, and N. Kawakami, *Phys. Rev. B* **100**, 115124 (2019).
- [70] T. Matsushita, Y. Nagai, and S. Fujimoto, *Phys. Rev. B* **100**, 245205 (2019).
- [71] A. Georges, G. Kotliar, W. Krauth, and M. J. Rozenberg, *Rev. Mod. Phys.* **68**, 13 (1996).
- [72] R. Bulla, T. A. Costi, and T. Pruschke, *Rev. Mod. Phys.* **80**, 395 (2008).
- [73] R. Peters, T. Pruschke, and F. B. Anders, *Phys. Rev. B* **74**, 245114 (2006).
- [74] J. C. Budich, J. Carlström, F. K. Kunst, and E. J. Bergholtz, *Phys. Rev. B* **99**, 041406 (2019).



- [75] R. Okugawa and T. Yokoyama, *Phys. Rev. B* **99**, 041202 (2019).
- [76] H. Feshbach, *Annals of Physics* **5**, 357 (1958).
- [77] H. Feshbach, *Annals of Physics* **19**, 287 (1962).
- [78] J. C. Petersen, M. D. Caswell, J. S. Dodge, I. A. Sergienko, J. He, R. Jin, and D. Mandrus, *Nature Physics* **2**, 605 (2006).
- [79] L. Zhao, D. H. Torchinsky, H. Chu, V. Ivanov, R. Lifshitz, R. Flint, T. Qi, G. Cao, and D. Hsieh, *Nature Physics* **12**, 32 (2016).
- [80] J. W. Harter, Z. Y. Zhao, J.-Q. Yan, D. G. Mandrus, and D. Hsieh, *Science* **356**, 295 (2017).
- [81] T. Morimoto and N. Nagaosa, *Science Advances* **2**, 10.1126/sciadv.1501524 (2016).
- [82] Y. Tokura and N. Nagaosa, *Nature Communications* **9**, 3740 (2018).
- [83] X. Zhang, X. F. Ma, Y. Jin, T. Lu, E. P. Boden, P. D. Phelps, K. R. Stewart, and C. P. Yakymyshyn, *Applied Physics Letters* **61**, 3080 (1992), <https://doi.org/10.1063/1.107968> .
- [84] C.-K. Chan, N. H. Lindner, G. Refael, and P. A. Lee, *Phys. Rev. B* **95**, 041104 (2017).
- [85] F. de Juan, A. G. Grushin, T. Morimoto, and J. E. Moore, *Nature Communications* **8**, 15995 (2017).
- [86] H. Isobe, S.-Y. Xu, and L. Fu, *Science Advances* **6**, 10.1126/sciadv.aay2497 (2020).
- [87] B. T. Zhou, C.-P. Zhang, and K. Law, *Phys. Rev. Applied* **13**, 024053 (2020).
- [88] L. Wu, S. Patankar, T. Morimoto, N. L. Nair, E. Thewalt, A. Little, J. G. Analytis, J. E. Moore, and J. Orenstein, *Nature Physics* **13**, 350 (2017).
- [89] Q. Ma, S.-Y. Xu, H. Shen, D. MacNeill, V. Fatemi, T.-R. Chang, A. M. Mier Valdivia, S. Wu, Z. Du, C.-H. Hsu, S. Fang, Q. D. Gibson, K. Watanabe, T. Taniguchi, R. J. Cava, E. Kaxiras, H.-Z. Lu, H. Lin, L. Fu, N. Gedik, and P. Jarillo-Herrero, *Nature* **565**, 337 (2019).
- [90] R. Wakatsuki, Y. Saito, S. Hoshino, Y. M. Itahashi, T. Ideue, M. Ezawa, Y. Iwasa, and N. Nagaosa, *Science Advances* **3**, 10.1126/sciadv.1602390 (2017).
- [91] Y. M. Itahashi, T. Ideue, Y. Saito, S. Shimizu, T. Ouchi, T. Nojima, and Y. Iwasa, *Science Advances* **6**, 10.1126/sciadv.aay9120 (2020).
- [92] F. Ando, Y. Miyasaka, T. Li, J. Ishizuka, T. Arakawa, Y. Shiota, T. Moriyama, Y. Yanase, and T. Ono, *Nature* **584**, 373 (2020).

- [93] H. Kishida, H. Matsuzaki, H. Okamoto, T. Manabe, M. Yamashita, Y. Taguchi, and Y. Tokura, *Nature* **405**, 929 (2000).
- [94] H. Liu, Y. Li, Y. S. You, S. Ghimire, T. F. Heinz, and D. A. Reis, *Nature Physics* **13**, 262 (2017).
- [95] H. Rostami, M. I. Katsnelson, and M. Polini, *Phys. Rev. B* **95**, 035416 (2017).
- [96] R. E. F. Silva, I. V. Blinov, A. N. Rubtsov, O. Smirnova, and M. Ivanov, *Nature Photonics* **12**, 266 (2018).
- [97] S. Y. Kruchinin, *Phys. Rev. A* **100**, 043839 (2019).
- [98] Y. Murakami, M. Eckstein, and P. Werner, *Phys. Rev. Lett.* **121**, 057405 (2018).
- [99] N. Tancogne-Dejean, M. A. Sentef, and A. Rubio, *Phys. Rev. Lett.* **121**, 097402 (2018).
- [100] S. Dzsaber, X. Yan, M. Taupin, G. Eguchi, A. Prokofiev, T. Shiroka, P. Blaha, O. Rubel, S. E. Grefe, H.-H. Lai, Q. Si, and S. Paschen, (2018), arXiv:1811.02819 [cond-mat.str-el] .
- [101] T. Morimoto and N. Nagaosa, *Scientific Reports* **8**, 2973 (2018).
- [102] D. E. Parker, T. Morimoto, J. Orenstein, and J. E. Moore, *Phys. Rev. B* **99**, 045121 (2019).
- [103] S. M. João and J. M. V. P. Lopes, *Journal of Physics: Condensed Matter* **32**, 125901 (2019).
- [104] J. E. Sipe and E. Ghahramani, *Phys. Rev. B* **48**, 11705 (1993).
- [105] J. E. Sipe and A. I. Shkrebtii, *Phys. Rev. B* **61**, 5337 (2000).
- [106] G. B. Ventura, D. J. Passos, J. M. B. Lopes dos Santos, J. M. Viana Parente Lopes, and N. M. R. Peres, *Phys. Rev. B* **96**, 035431 (2017).
- [107] D. J. Passos, G. B. Ventura, J. M. V. P. Lopes, J. M. B. L. d. Santos, and N. M. R. Peres, *Phys. Rev. B* **97**, 235446 (2018).
- [108] H. Watanabe and Y. Yanase, *Phys. Rev. Research* **2**, 043081 (2020).
- [109] H. Watanabe and Y. Yanase, Chiral photocurrent in parity-violating magnet and enhanced response in topological antiferromagnet (2020), arXiv:2006.06908 [cond-mat.mtrl-sci] .
- [110] Y. Zhang, J. van den Brink, C. Felser, and B. Yan, *2D Materials* **5**, 044001 (2018).
- [111] X.-Q. Yu, Z.-G. Zhu, J.-S. You, T. Low, and G. Su, *Phys. Rev. B* **99**, 201410 (2019).
- [112] Z. Z. Du, C. M. Wang, S. Li, H.-Z. Lu, and X. C. Xie, *Nature Communications* **10**, 3047 (2019).

- [113] T. Holder, D. Kaplan, and B. Yan, *Phys. Rev. Research* **2**, 033100 (2020).
- [114] D. Kaplan, T. Holder, and B. Yan, Nonvanishing sub-gap photocurrent as a probe of lifetime effects (2020), arXiv:2003.12582 [cond-mat.mes-hall] .
- [115] Y. Choi, C. Hahn, J. W. Yoon, S. H. Song, and P. Berini, *Nature Communications* **8**, 14154 (2017).
- [116] D. Xiao, M.-C. Chang, and Q. Niu, *Rev. Mod. Phys.* **82**, 1959 (2010).
- [117] I. Sodemann and L. Fu, *Phys. Rev. Lett.* **115**, 216806 (2015).
- [118] Z. Z. Du, C. M. Wang, S. Li, H.-Z. Lu, and X. C. Xie, *Nature Communications* **10**, 3047 (2019).
- [119] S. Kanasugi and Y. Yanase, *Phys. Rev. B* **102**, 094507 (2020).

## Acknowledgment

I would like to thank Prof. Robert Peters for his support during my master and doctor courses. I am deeply grateful to him for providing me many opportunities to discuss condensed matter physics, giving me plenty of advice on the direction of my study, and teaching me about desired attitude to establish good researches. Without his guidance, I could not have done this work.

I would like to thank Dr. Kazuaki Takasan, Prof. Masaya Nakagawa and Dr. Hikaru Watanabe, for many fruitful and stimulating discussions and giving me the inspiration for my works.

I would like to thank the faculty in Condensed Matter Theory Group at Kyoto University, Prof. Norio Kawakami, Prof. Ryusuke Ikeda, Prof. Yoichi Yanase, and Prof. Masaki Tezuka, for their support in various academic matters as well as fruitful discussions. I also have greatly benefited from my colleagues in the Condensed Matter Theory Group for everyday discussions on physics and other topics. Especially, I am grateful to Prof. Norio Kawakami for his help with my problems.

I appreciate financial support I have received over the past three years from the Japan Society for the Promotion of Science, and the WISE program, MEXT.

Lastly, I am deeply grateful to my parents Kaoru and Masako, whose encouragement and advice have been a great source of support in learning not only physics but also many other things. I am also grateful to my cousin Ryoya, who enlight the way to live and the way to engage with others.